

My Thesis Title

Philip Gemmell
Oriel College



Computational Biology Research Group
Computing Laboratory
University of Oxford

Define Term

This thesis is submitted to the Computing Laboratory, University of Oxford, for the degree of Doctor of Philosophy. This thesis is entirely my own work, and, except where otherwise indicated, describes my own research.

Philip Gemmell
Oriel College

Doctor of Philosophy
Define Term

My Thesis Title

Abstract

This thesis describes stuff aplenty.

Contents

1	Introduction	I
2	Physiological Background	2
2.1	Structure and Function of the Heart	2
2.2	Structure and Function of the Cardiomyocyte	5
2.2.1	Ion Channel Properties	5
2.3	The Action Potential	8
2.3.1	Excitation-Contraction Coupling	11
2.4	Cardiac Dysfunction	12
2.4.1	Ischæmia	12
	Ischæmic Changes in the AP	13
	Ischæmic Changes in $[Ca^{2+}]_i$	16
	Other Ischæmic Changes	19
2.4.2	Arrhythmogenesis	19
	Delayed & Early After Depolarisations	20
	Alternans	21
	Spiral Waves & Rotors	22
	Re-entry	23
2.5	Experimental & Physiological Variation	24
2.5.1	Action Potential Variation	25
2.5.2	Ion Channel Variation	25
3	Modelling Background	27
3.1	Development	27
3.2	Key Concepts	29
3.2.1	Nernst Potential	30
3.2.2	Hodgkin-Huxley Current	30
3.2.3	Markov Models	31
3.2.4	Mono-/Bi-domain Equations	31
3.3	Computational Modelling of Variability	31
3.3.1	Stochastic Modelling	32
3.3.2	Parameter Sensitivity & Fitting	33
3.3.3	Model Populations	35
4	Computational Methods	36
4.1	Representation of Multi-Dimensional Data	36
4.2	Computational Models & Simulation Techniques	38
4.2.1	Nimrod Distributed Computing Grid	38
4.2.2	Parameter Space Simulations	40
4.2.3	Ischæmia Simulations	41
4.3	Biomarker Calculation	42
5	Parameter Space Exploration	44
5.1	Reproduction of Experimental Variation	44
5.1.1	Comparison with Alternative Methods	45

5.1.2	Caveats	46
5.2	Construction of the Parameter Space	47
5.3	Accuracy of Biomarkers in Defining Model Fit	47
5.4	Defining a Population of Models to Reproduce Physiological Variation	48
5.4.1	Variation within the Population	48
5.4.2	Connectivity within the Parameter Space	55
5.5	Effects of Parameter Variation	55
5.6	Rate Dependence of Biomarkers	60
6	Ischæmic Variation	62
6.1	Variation Within Ischæmia	62
6.2	Population Response to Ischæmia	63
6.2.1	APD_{90}	63
6.2.2	ERP and PRR	65
6.2.3	Other Biomarkers	65
6.3	Model Failure During Ischæmia	65
A	Diffusion	68
A.1	Simple Diffusion	68
A.2	Facilitated Diffusion, Michaelis-Menten Kinetics	68
A.3	Electrodiffusion	69
A.3.1	The Nernst Equation	69

List of Figures

2.1	Structure of a mammalian heart	3
2.2	Structure of myocardial sheets and fibres	3
2.3	Pattern of electrical activation in the heart	4
2.4	Schematic of a cardiac AP	8
2.5	Example of a restitution curve with alternans predicted	10
2.6	Distribution of ischaemic properties in tissue.	14
2.7	Effect of ischaemia on $[Ca^{2+}]_i$	17
2.8	Spatially cordant and spatially discordant alternans in cardiac tissue	21
3.1	Effect of parameter variation on model output.	33
4.1	The dimensional stacking process	37
4.2	Effect of varying $g_{K\text{-ATP}}$ on APD_{90}	42
5.1	Efficacy of biomarkers in determining goodness-of-fit.	49
5.2	Parameter ranges used For ‘Expanded Mahajan’ search.	50
5.3	Model population for the Shannon framework that produces values of both APD_{50} and APD_{90} that fall within the experimentally derived range.	53
5.4	Model population for the expanded Mahajan framework that produces values of both APD_{50} and APD_{90} that fall within the experimentally derived range.	54
5.5	Connectivity within model populations.	56
5.6	Effect of parameter variation on Shannon population.	57
5.7	Effect of parameter variation on Mahajan population.	58
5.8	Rate dependence of biomarkers in the parameter space.	61
6.1	Effect of different degrees of ischaemia on the Shannon and Mahajan model populations.	64
6.2	Effect of $[K^+]_o$ variation with other ischaemic conditions on the Shannon and Mahajan model populations.	66

List of Tables

2.1	Summary of current density results from Szentandrassy et al. (2005).	25
4.1	Models used to train ischæmia conditions	41
5.1	Physiological Ranges for APD ₅₀ and APD ₉₀	49
5.2	Number of parameter sets producing both APD ₅₀ and APD ₉₀ values within the physiological range.	50
5.3	Minimum, mean, and maximum values of all computed biomarkers produced with the physiological parameter sets.	51
5.4	Optimum stack order for APD ₅₀ , APD ₉₀ , and CaT for the Shannon and Mahajan frameworks	59
6.1	Ischæmic environment parameters	63
6.2	Ischæmic Effect on Model Populations	65
6.3	Model failure & ERP prolongation.	67

List of Code Excerpts

4.1	Nimrod/G code: Plan File	39
4.2	Nimrod/G code: Parameter Substitution	39

Acknowledgements

This thesis is the culmination of many year's work and would not have been possible without the help and support of many people.

Notation & Nomenclature

AP	Action Potential
AP_{NRMSE}	Root mean square difference between ‘test’ and ‘training’ data for V_m data
APD_x	Action potential duration to $x\%$ repolarisation
$[\text{Ca}^{2+}]_i$	Free cytosolic Ca^{2+} concentration
g_X	Maximum conductance for current X
$I_{\text{Ca,L}}$	L-type Ca^{2+} current
I_{K1}	Inward rectifying K^+ current
I_{Kr}	Rapidly delayed rectifier K^+ current
I_{Ks}	Slowly delayed rectifier K^+ current
I_{Na}	Na^+ current
I_{NaCa}	Na^+ - Ca^{2+} exchanger current
I_{NaK}	Na^+ - K^+ pump current
I_{stim}	Stimulus current
I_{to}	K^+ transient outward current
$I_{\text{to,f}}$	Fast K^+ transient outward current
$I_{\text{to,s}}$	Slow K^+ transient outward current
V_m	Membrane potential
CaT	Difference between systolic $[\text{Ca}^{2+}]_i$ and diastolic $[\text{Ca}^{2+}]_i$

INTRODUCTION

1

This will be the introduction.

PHYSIOLOGICAL BACKGROUND

*There are more things in heaven and earth, Horatio,
Than are dreamt of in your philosophy.*

(Hamlet, Act 1, Scene 5)

This chapter provides the necessary biological and physiological background for the thesis, and starts by outlining the structure and function of the heart itself. The constituent cell of the heart, the cardiomyocyte, is then described, with the ion channels it contains being outlined. With the physiological means thus outlined, the action potential of the heart itself is outlined, with its link to the mechanical action of the heart being described. Dysfunction of the heart is reviewed, with special focus given to ischaemia. Mention is also given to modes of arrhythmogenesis.

2.1 Structure and Function of the Heart

At the most general level, the heart serves as a pump to transport blood around the body to deliver nutrients and remove waste products. It does this by rhythmic, organised contraction—the rate of this contraction varies depending on species, age, condition of the heart and the activity being undertaken by the organism.

Fig. 2.1 shows the anatomical structure of a mammalian heart—while the size obviously varies widely between mammals, the overall architecture remains constant. It is split into two halves, left and right, by a muscular wall called the *septum*, and then further subdivided into two chambers, the larger, lower chamber being a *ventricle*, and the smaller, upper chamber called an *atrium*.

The passage of blood through the heart follows thus: firstly, deoxygenated blood from the body enters the heart via the superior and inferior/posterior *vena cava*, with superior and inferior representing whether the blood comes from the upper or lower half of the body, respectively. Via this channel, it enters the *right atrium*. Passing through the *tricuspid valve* (also known as the right atrioventricular valve), the blood enters the *right ventricle*, where it is then pumped via the *pulmonary artery* to the lungs, where it is oxygenated. The blood returns to the heart via the *pulmonary vein*, entering the *left atrium*, before moving through the *mitral valve* (also known as the left atrioventricular valve) into the *left ventricle*. The blood is then pumped via the *aorta* to the rest of the body. The valves in the heart serve to ensure the flow of blood is always in the correct direction.

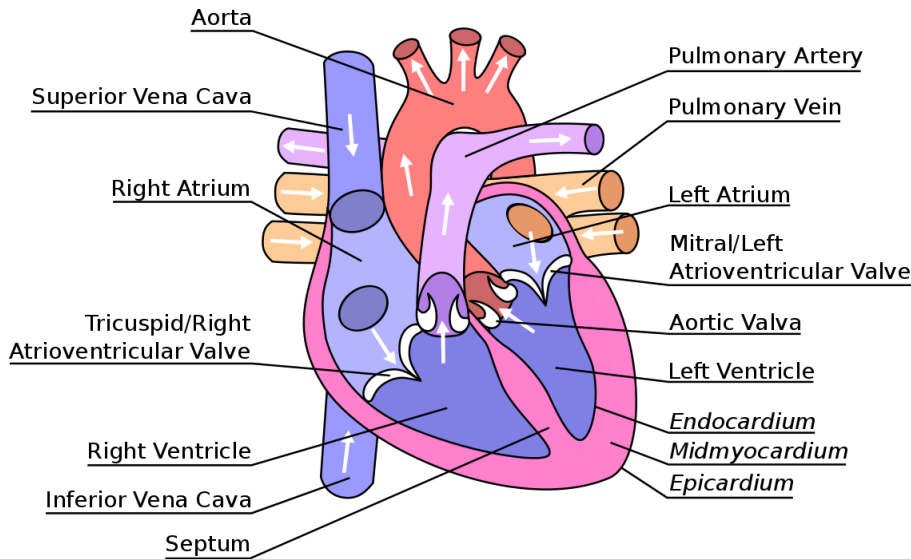


Figure 2.1: Diagram of a longitudinal cross-section of a mammalian heart. The direction of blood flow is shown by white arrows, and all major structural components are labelled.

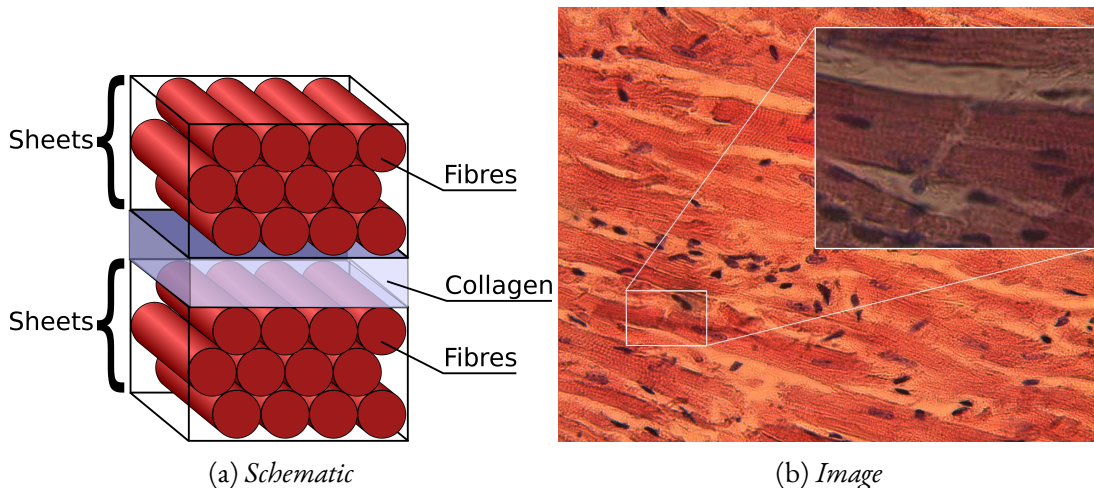


Figure 2.2: (2.2a) Schematic of the structure of myocardial sheets and fibres. (2.2b) Image of cardiomyocytes demonstrating the interconnected nature of the individual myocytes into fibres (Girod and Becker, 2006).

The walls of the heart are mostly composed of muscular tissue known as *myocardium*. The thickness of the myocardium is not constant throughout the heart, being thickest in the left ventricle, which requires the greatest force of contraction to pump the blood from the heart to the rest of the body. The myocardium can be split into three different regimes, as labelled in italics in Fig. 2.1: the *epicardium* is the outermost layer of the myocardium, the *midmyocardium* is the middle layer, and the *endocardium* is the innermost layer. The cells composing these different layers possess different electrophysiological properties; the differences, and the consequences, will be mentioned further in §??.

The structure within the myocardium is shown in Fig. 2.2a: it is composed of a series of sheets of tissue (usually 4 to 6 cells thick) separated by collagen. The myocytes themselves lie longitudinally in these sheets to form fibres, with myocytes connected to each other by intercalated discs spanning the 100 – 200 Å separation between the cells (as opposed to skeletal muscle, which is composed of multinucleated fibres); this structure is seen in Fig. 2.2b. One attribute of these discs is the presence of *gap junctions*, which serve to electrically couple the myocytes by allowing ion flow between neighbouring myocytes. It has been shown that Ca^{2+} ions can cross the gap junctions in a so-called *calcium wave*,

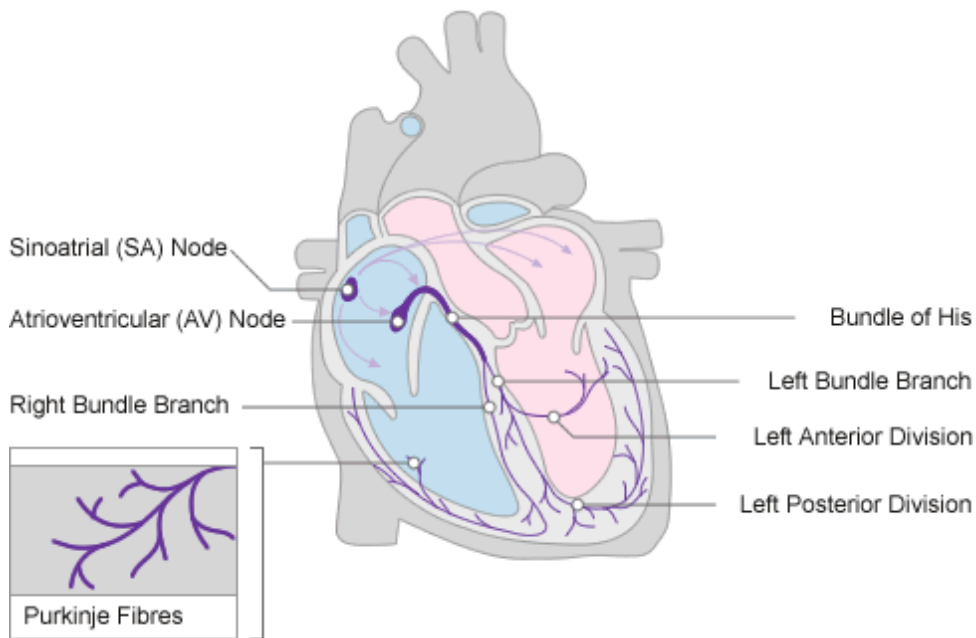


Figure 2.3: Schematic outline of the sequence of electrical activation in the mammalian heart. Image originally downloaded from www.nottingham.ac.uk on 10th December 2012.

triggering activity in neighbouring cells (Miura et al., 1998). This Ca^{2+} -based ‘triggered propagation’ moves more slowly than the Na^+ -dependent action potential (the usual means for conducting the electrical activity through the heart tissue) (Clusin, 2003). It should be noted that the cells are electrically coupled by more than just gap junctions, e.g. ephaptic coupling and K^+ accumulation in the membrane space; for a full review of these coupling methods, see Sperelakis and McConnell (2002).

In the ventricles, each myocyte is electrically coupled to ~ 11 neighbouring myocytes (Smaill et al., 2013). It is known that the conduction velocity is dependent on fibre and sheet orientation, with measured ratios being $\sim 4 : 2 : 1$ between fibre, sheet and transverse directions (?) (though it should be noted that some results indicate uniform connection between ventricular myocytes juxtaposed in side-to-side and end-to-end orientation (Saffitz et al., 1994)). The arrangement of the myocytes into fibres, and the arrangement of these fibres into sheets, allows for ordered contraction in the fibre direction; the fibrous structure also allows the heart to twist as it contracts, leading to a more efficient pumping mechanism.

The conduction pattern of the heart is key to the effective pumping mechanism—by controlling the sequence of electrical events in the heart, the sequence of conduction is similarly controlled. An outline of the conduction pattern of the heart is shown in Fig. 2.3. The sequence of activation starts amongst a complex of self-excitatory cells at the top of the right atrium, called the *sinoatrial node*. This node is electrically isolated from the atria, save for specialised conduction pathways; this both prevents depression of the self-excitation of the node by the hyperpolarising influence of the surrounding atrium, and allows several excitation locations, depending on the condition of the heart (Fedorov et al., 2012). Once the node self-excites, a wave of depolarisation spreads from this node; the depolarisation of the atrial cardiac cells causes the atrium to contract, for reasons detailed in §??. This depolarisation then reaches the *atrioventricular node*—this is the only pathway for electrical excitation to pass from the atria to the ventricles. From the atrioventricular node, the excitation wave passes to the *Bundle of His*, which conducts the electrical stimulus via the left and right bundle branches into the *Purkinje system* near the bottom of the heart, which transmits the stimulus to the ventricular surface; as the stimulus has thus been transmitted directly from the atria to the bottom of the ventricles, the excitation wave thus spreads upwards through the ventricles, allowing the ventricles to contract from the bottom up as required.

2.2 Structure and Function of the Cardiomyocyte

As previously stated, the main rôle of the heart is to serve as a pump to circulate the blood around the body. To do this effectively, it requires coordinated contraction, and this is achieved through the use of coupling the electrical activity of the heart of the mechanical activity (the details of this mechanism will be expanded upon in §??).

Physically, cardiomyocytes are typically $10 - 20\mu\text{m}$ in diameter, and $50 - 100\mu\text{m}$ in length. They are cells bound by a lipid bilayer membrane, separating intracellular space (containing the cytoplasm, nuclei and other organelles) from the extracellular space. The intracellular space has a very different composition to the extracellular space, with the intracellular space containing a high and low concentration of potassium (K^+) and sodium (Na^+) ions respectively; the reverse is true for the extracellular space. These concentration differences are the main reason behind their being an electric potential difference set up across the cell membrane, referred to as the *membrane potential* (V_m); this potential is defined as negative when the intracellular space contains a greater negative charge than the extracellular space. At rest, due to the high K^+ and low Na^+ in the cell, this potential is negative, though the magnitude varies depending upon the location in the heart; a cardiomyocyte in the ventricles typically has a resting potential (V_{rest}) of about -80mV , while the sinoatrial node has a resting potential of between -50 and -60mV .

Embedded within the bilayer are various membrane-bound proteins which serve to transport ions across the membrane, allowing the membrane to be selectively permeable to particular ions, and allowing regulation of this permeability as required. These transporters can be classed as either *channels* (allowing ions to move according to their electrochemical gradient), *pumps* (translocating ions in the opposite direction to their electrochemical gradient by the use of energy) or *exchangers* (translocates a number of ions of one type across the membrane in ‘exchange’ for a number of ions of another type). Most of these transporters are ion-specific, though some are not exclusively selective. Most of these channels are also controlled by, amongst other things, the membrane potential itself (Bezanilla, 2000). The membrane potential causes a conformational change in the ion channel protein, causing it to ‘open’ or ‘close’; that is, to allow ions to be conducted through it or not.

These ion channels are discrete molecular entities, and thus the conformational changes that lead to their open/close state are stochastic; the effects of this stochasticity are discussed in greater detail in §??. However, each type of ion channel possesses its own range of attributes, such as the time it takes to inactivate, the time it takes to reactivate, its permeability to different types of ions, and its susceptibility to other gating factors. Comprehensive summaries of the properties of ion channels are given in Carmeliet and Vereecke (2002); Roden et al. (2002).

Electrically, the heart can be modelled with great success as an analogue to an electrical circuit (Carmeliet and Vereecke, 2002), where the lipid bilayer is represented as a capacitor, and the various ion channels and transporters that span the membrane are represented as resistors, which change their ‘resistance’ depending on their state. By altering the resistance of these channels, ion flow across the membrane is permitted via an ionic current. It is a point of nomenclature that an ‘inward’ current represents the movement of positive ions from the extracellular to the intracellular space, and an ‘outward’ current is the reverse. This definition is based on the movement on electrical charge, and not on the movement of ion flow. This is subtly different to the definition of an inward or outward rectifier current, where an inward rectifier current passes current more easily inward than outward, and vice versa for an outward rectifier current.

2.2.1 Ion Channel Properties

It should be borne in mind that knowledge of ion channel dynamics is not appropriate solely for cell simulations, but is important for the implications of how such changes cascade through the different spatial and temporal scales. Thus, knowledge of how ion channel dynamics affects cellular AP

dynamics leads to knowledge of tissue dynamics implications, and so on (Spach et al., 1988). The emphasis on what follows is on the ion channel dynamics of rabbits—while there are many similarities in these channels between mammalian species, it is important to remember that species differences can be significant (Bassani et al., 1994). For example, I_{to} plays an important rôle in repolarisation in rodents, and thus strongly influences APD, while playing a relatively minor rôle in repolarisation in larger mammals (Rosati and McKinnon, 2004).

I_{Kr} , as the name implies, is the more rapidly activating of the two rectifier K⁺ currents ($\tau \sim 40\text{ms}$ at +30mV), and rapidly activates once V_m increases above -30mV. However, the channel inactivates even more rapidly in a process that precedes voltage-dependent inactivation (Varró and Baczkó, 2011; Spector et al., 1996; Carmeliet, 2006). Due to this, I_{Kr} channels are largely closed during the plateau phase of the AP, only reopening when V_m returns to about 0mV. The transient nature of the current is due to its rapid recovery from inactivation, and subsequent slow deactivation. At slow rates, the contribution of I_{Kr} diminishes further, resulting in a positive feedback loop regarding prolongation of the AP duration (APD) (the same is observed for I_{K1}) (Virág et al., 2009). This same vulnerability of the repolarisation is evident when depolarising factors (e.g. I_{Na} , $I_{Ca,L}$) are augmented or repolarising factors (e.g. I_{Ks} , I_{K1}) diminished.

If the function of I_{Kr} is impaired substantially in some way, APD is measured to be significantly prolonged, both by direct measurement of the membrane potential, and QT interval measurements in electrocardiograms (ECGs) (the QT interval serves as a marker for the time taken for ventricular depolarisation and repolarisation in a clinical setting (Yan and Antzelevitch, 1998)), suggesting especial importance in cellular repolarisation (Varró et al., 2000; Lengyel et al., 2001; Jost et al., 2005). When I_{Kr} is only impaired in a minor way, APD may not necessarily increase due to the action of the repolarisation reserve. I_{Kr} passes via a channel encoded by the human ether-à-go-go related gene (HERG), and is known for being its susceptibility to the effects of drug block, making it of key pharmacological importance (Vandenberg et al., 2001; Haverkamp et al., 2000). It can also be noted that, in spite of what may be predicted by the Nernst potential for I_{Kr} (see §??), increased extracellular K⁺ is known to enhance I_{Kr} (Sanguinetti and Jurkiewicz, 1992; Yang et al., 1997).

I_{Ks} takes longer to activate than its partner (500-1000ms at plateau phase), and deactivates rapidly at negative V_m (Jost et al., 2005; Varró and Baczkó, 2011). It carries a slowly rising current over the duration of the plateau phase. At rapid pacing rates, the current carried by the I_{Ks} channel increases—this is thought to be due to the kinetics of the channel, with an ‘inactivated’ state being intermediate between the open and closed state. At rapid pacing rates, there is less time to transition fully to the closed state, and thus there is a greater proportion of I_{Ks} channels available for immediate opening (Silva and Rudy, 2005). I_{Ks} is also modelled as having a sensitivity to [Ca²⁺]_i, replicating the results of potassium currents’ sensitivity to [Ca²⁺]_i (Meech and Standen, 1975).

Drug block of I_{Ks} causes AP prolongation, but not to the same extent as I_{Kr} ; while direct measurements show a slight increase in APD, there is very little or no change in QT intervals ECG measurements (Varró et al., 2000; Lengyel et al., 2001; Jost et al., 2005). This implies that its amplitude, compared to that of I_{Kr} , during a typical AP is small—this has been confirmed experimentally under normal conditions (Varró and Baczkó, 2011). Combined with its slow activation, there is thus relatively little I_{Ks} active during the AP (Jost et al., 2005). However, its long activation time also means the effect of I_{Ks} block is more pronounced when APD is prolonged, due to (i) the net outward current at long pacing rates is smaller, so the fractional effect of I_{Ks} is greater, and (ii) more channels are activated during a long AP (Carmeliet, 2006). Due to this action, and the response of I_{Ks} to sympathetic stimulation, the current provides a negative feedback for APD prolongation, acting to curtail the increased action of $I_{Ca,L}$ that occurs at longer pacing rates. Thus, while under ‘normal’ circumstances I_{Ks} has limited effect on the repolarisation reserve of the cell, it acts as an effective buffer when APD is longer than normal.

The transmural differences in the expression of I_{Ks} is a large reason behind the transmural variation of APD, and also explains why I_{Kr} block can have a greater or lesser effect, depending on the abundance of the compensatory effect of I_{Ks} ; the scarcity of I_{Ks} can be noted in Purkinje fibres and M-cells, while it is abundant in subepicardial and subendocardial cells (Vandenberg et al., 2001; Carmeliet,

2006). The density of I_{K_s} channels has also been shown to increase in response to sustained I_{Kr} block, demonstrating its importance to the repolarisation reserve (Xiao et al., 2008).

I_{K1} is a strongly inwardly rectifying K^+ current, which means that when V_m is greater than -30mV , the channel is inactivated. Thus it plays a negligible rôle during the plateau phase of the AP, but has a self-reinforcing role in the repolarisation of the cell once V_m decreases to the extent that I_{K1} can be activated. It should be noted that this is not a voltage-dependent activation, but is based on an unblocking of the channel: when $V_m > -30\text{mV}$, the channel is blocked by Mg^{2+} and polyamines which enter the channel from the intracellular side in a voltage-dependent manner. As the current is fully open at V_{rest} , it resists depolarisation caused by either increased pacemaker activity, or Ca^{2+} overload-related delayed afterdepolarisations (DADs). Consequently, I_{K1} may be considered to play an unusual rôle in the repolarisation reserve, and impairment of its function could lead to proarrhythmic effects by making the cell more susceptible to extrasystoles.

I_{to} is actually composed of two separate currents, a rapidly recovering component ($I_{to,f}$) and a slowly recovering component ($I_{to,s}$). As a combined unit, it both activates and inactivates rapidly for $V_m > -20\text{mV}$, and is of greatest importance during the phase 1 repolarisation. As such, it is believed to have little influence directly on the end repolarisation of the cell, but due to its early role, and its consequent effect on the plateau potential, it is believed to have influence on subsequent currents, which lead to great indirect influence. I_{to} is also known for its transmural variation, being greater in epicardial than endocardial tissue.

I_{NaK} is caused due to the Na^+-K^+ pump, which is an electrogenic exchanger, moving 3 Na^+ ions out of the cell in exchange for 2 K^+ ions. It thus works to maintain the concentration gradients and the resting membrane potential, and provides an outward current in support of the repolarisation reserve. It is, however, sensitive to intracellular Na^+ concentration ($[Na^+]_i$), and consequently to the rate of stimulation.

The influence of $I_{Ca,L}$ on the repolarisation of the cell is complex due to its complicated inactivation. It inactivates due to voltage slowly, and thus the main reason for its inactivation is due to Ca^{2+} -induced inactivation, and is thus in response to local Ca^{2+} concentration, which is dynamically changing during the plateau phase. This inactivation is modulated via a protein called calmodulin, and thus can be modulated further. If the AP is extended during the range of activation/inactivation for $I_{Ca,L}$, some $I_{Ca,L}$ channels may reactivate. This resurgence of the inward current can lead to secondary depolarisations or early after-depolarisations (EADs) (Carmeliet, 2006).

It should be noted that $I_{Ca,L}$ is a highly localised current—the responsible channels are not distributed uniformly throughout the sarcolemma, but are instead localised to close proximity to other channels important in the contractile mechanism of the cell, serving to co-ordinate the release of Ca^{2+} throughout the cell; this is explored in greater depth in §??. This localisation is not unique to $I_{Ca,L}$ —it has recently been demonstrated that I_{Na} is also highly localised (Bhargava et al., 2013).

If $I_{Ca,L}$ (or I_{Na}) are augmented and have their activity increased, this serves to make the plateau potential more positive. While at first glance this may indicate that AP may lengthen, it is rather the case that this may serve to enhance activation of outward K^+ currents, thus shortening APD.

The Na^+-Ca^{2+} exchange current (I_{NaCa} , also referred to as I_{NCX}), like I_{NaK} , is an electrogenic exchanger, this time exchanging 3 Na^+ ions for one Ca^{2+} ion. By this process, it is, with the SERCA pump, largely responsible for restoring the low cytosolic Ca^{2+} concentration during diastole; it is the main means for extruding Ca^{2+} from the cell, responsible for 70–90% of the Ca^{2+} efflux (Eisner and Sipido, 2004). Despite this, the activity of I_{NaCa} can be inhibited by 80–90% with cardiac function still being maintained (Henderson et al., 2004)—another example of effective repolarisation reserve. I_{NaCa} depends strongly on V_m and $[Ca^{2+}]_i$ (Clusin, 1983), and thus its magnitude during the AP is difficult to estimate (a problem compounded by the lack a specific inhibitor for the current). It is an outward current at the start of the AP, when V_m and $[Ca^{2+}]_i$ are both low, but then changes to an inward current during the late plateau phase. Due to its sensitivity to $[Ca^{2+}]_i$, in times of Ca^{2+} -overload

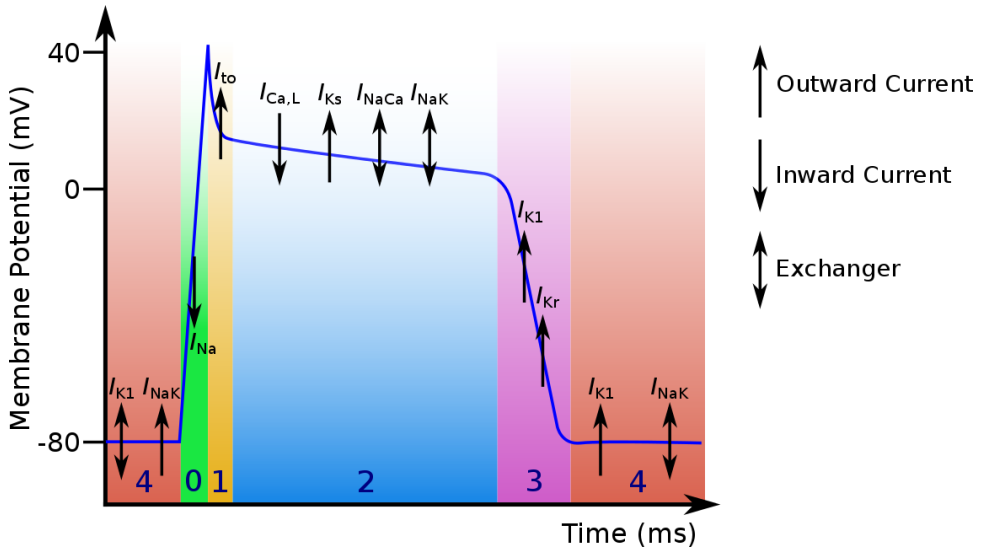


Figure 2.4: Schematic of a ventricular cardiac AP, with the different ‘phases’ of the AP shown, and which key currents are involved in each phase. Upward arrows represent outward currents, inward currents represent inward currents, and double arrows represent exchangers, i.e. where current moves in both an inward and outward direction.

I_{NaCa} can provide a depolarising current, thus increasing the likelihood of DADs and EADs (Clusin, 2003). The density of I_{Na} is also known to depend heavily on $[Ca^{2+}]_i$, decreasing when $[Ca^{2+}]_i$ is high; the gating of the channel is not affected.

These, and other, currents are susceptible to alteration, and demonstrate varying degrees of importance during physiological and pathological conditions; the arrhythmogenic properties of some of these currents will be discussed further in §2.4.2.

2.3 The Action Potential

The changes in internal/external ion concentrations which result from these currents changes V_m . The cyclic, periodic change in membrane potential is referred to as the *action potential* (AP). An example of an action potential, showing the different ‘phases’, is shown in Fig. 2.4.

The AP is considered to consist of 5 different phases, outlined below. The important currents in each phase are mentioned, and greater details are given for a number of these current in §??.

Phase 4: The resting phase. For ventricular and atrial cardiomyocytes, this phase is marked by a relatively constant value for V_m . The negative resting potential is largely achieved by the inwardly rectifying potassium current (I_{K1}) remaining open during this phase. For pacemaker cells, I_{K1} is absent, and thus the resting phase is actually a period of slow depolarisation, until V_m reaches the threshold value for phase 0. There is also an inward current due to the Na^+ - Ca^{2+} exchanger current (I_{NaCa}), which moves 3 Na^+ ions into the cell and one Ca^{2+} ion out at the resting potential.

Phase 0: Period of rapid depolarisation that marks the start of the AP. It is initiated by V_m reaching a threshold value which causes the I_{Na} current to activate, causing a rapid influx of Na^+ into the cell. In response to this, the direction of I_{NaCa} reverses, and this newly outward current brings in Ca^{2+} and removes Na^+ .

Phase 1: Transient repolarisation. The Na^+ channels rapidly deactivate (the process leading to reac-

tivation does not start until the cell repolarises at the end of the AP), and the activation of the transient K⁺ outward current (I_{to} , occasionally referred to as I_{toi}) results in a period of rapid, partial repolarisation. There may also be a contribution from a Ca²⁺-activated Cl⁻ (I_{CaCl} , or I_{to2}). Depending on the strength of this current, this repolarisation may be to the extent that there is a ‘notch’ in the AP, where the cell transiently repolarises beyond the subsequent plateau phase potential. For example, there is a notch in the AP for ventricular epicardial cells, but no notch for ventricular endocardial cells. The characteristics of this phase are also species-dependent (Carmeliet, 2006).

Phase 2: Plateau phase. The membrane potential is sustained at a relatively constant level by a balance of calcium (Ca²⁺) influx via the L-type calcium current ($I_{Ca,L}$), and potassium efflux, through the rectifier K⁺ currents (rapid, I_{Kr} , and slow, I_{Ks}). Despite being a rapidly activated current, I_{Kr} does not carry large current early during this phase, but only peaks at the end. I_{K1} shows a dramatic fall in conductance during this phase. While most I_{Na} is inactivated during phase 1, there is a small contribution from I_{Na} when V_m is in the limited range where activation and inactivation both occur. Late during phase 2, due to the increase in [Ca²⁺]_i, the reversal potential for I_{NaCa} increases to a value greater than V_m , and thus I_{NaCa} returns to being an inward current.

Phase 3: Repolarisation. The L-type Ca²⁺ current channels close, while the I_{Ks} channels remain open, allowing continuing K⁺ efflux resulting in a repolarisation of the cell to the original resting potential. I_{K1} opens during this phase, to remain open during phase 4 to maintain a steady resting potential.

It should be noted that the above description of which currents act during which phase is only an outline. While the upstroke of the AP is due mostly to the action of I_{Na} and the associated rapid influx of Na⁺ ions into the cell, causing the rapid depolarisation, the remaining phases of the AP are more complex, and the failure or part failure of any individual component of the cell mechanism does not necessarily lead to the failure of the whole system. This pseudo-redundancy was first termed *repolarisation reserve* in Roden (1998), and was demonstrated experimentally in Varró et al. (2000). It is essentially the concept that a loss in repolarisation function caused by a reduction or loss of function in one repolarising current can be recovered by increased action of an alternative repolarising current. Such a loss of function can have many possible causes, e.g. loss-of-function mutations in the genotype (Rosati and McKinnon, 2004). Most often, the term repolarisation reserve is applied to K⁺ channels, and specifically for the interaction between I_{Kr} and I_{Ks} (Xiao et al., 2008). Several currents are noted for their rôle in maintaining the repolarisation reserve of the cell, some of which have already been mentioned: I_{Kr} , I_{Ks} , I_{K1} , I_{to} , $I_{Ca,L}$, I_{Na} (Varró and Baczkó, 2011). The repolarisation reserve is not constant, but rather is dynamic with pacing rate, and variable between species and tissues within the heart (Carmeliet, 2006).

It is not just the repolarisation reserve that is dynamic, but the entire action potential itself—most notably, there can be significant variations in the AP morphology between different regions of the heart (caused in turn by different ion channel concentrations) (Giles and Imaizumi, 1988). Beyond this so-called ‘developmental regulation’, it is also possible for the myocyte to adapt to environmental changes, and to ensure the phenotype of the heart is appropriate for the demands placed upon it (‘homeostatic regulation’) (Rosati and McKinnon, 2004).

Even within a particular region of the heart, the AP duration (APD) varies according to the pacing rate. The manner in which the APD varies with pacing rate is often described using a restitution curve, which shows the relation between APD and the *diastolic interval*, which is itself defined according to the quiescent phase of the cell; the sum of APD and DI equals the *cycle length* (CL), i.e. APD + DI = CL. The graphical representation and interpretation of the APD in this manner, with a view to a predicting APD changes after rate changes, was first suggested by Nolasco and Dahlen (1968).

The APD restitution curve describes the duration of the $(i + 1)$ -th APD as a function f of the time since the preceding AP, i.e. the i -th DI. This is typically a monotonically increasing function, and can be expressed as $APD_{i+1} = f(DI_i)$. If we linearise this around the fixed point APD*, and describe

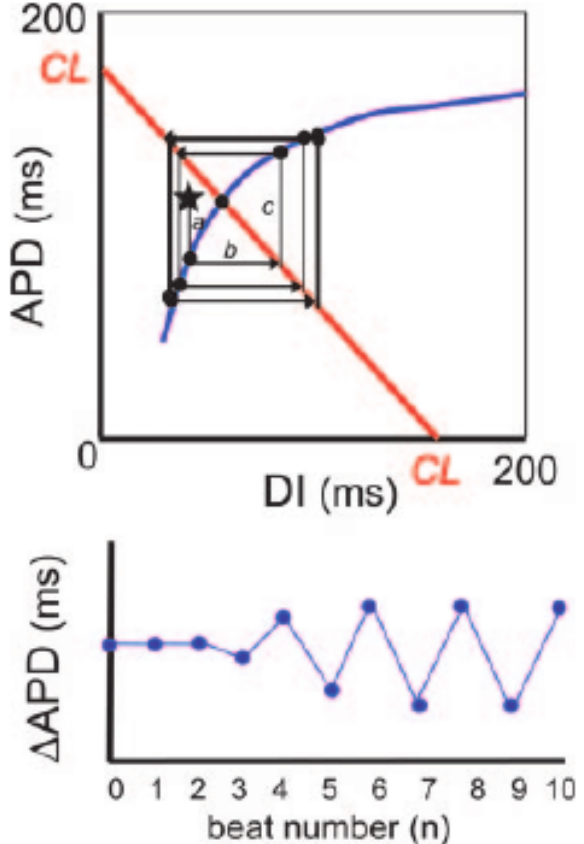


Figure 2.5: Example of a restitution curve with alternans predicted. The blue line represents the restitution curve; pacing at a constant CL can be represented by the red straight line. A small perturbation (represented by the star) from the equilibrium point (represented by the circle) can lead to growing perturbations, that eventually settle to alternans. This instability is due to the equilibrium point existing where the gradient is greater than 1. Figure originally from Weiss et al. (2006).

APD as small perturbations round this point ($\text{APD}_i = \text{APD}^* + \delta\text{APD}_i$), we can obtain the following (also making use of the Taylor expansion of $f(\text{DI}_i)$ and assuming $\mathcal{O}(\delta\text{DI}^2)$ is small):

$$\text{APD}^* + \delta\text{APD}_{i+1} = f(\text{DI}_i) \quad (2.1)$$

$$= f(\text{DI}^*) + f'(\text{DI}^*)\delta\text{DI} + \mathcal{O}(\delta\text{DI}^2) \quad (2.2)$$

$$\approx f(\text{DI}^*) + f'(\text{DI}^*)\delta\text{DI} \quad (2.3)$$

By recalling that $\text{CL} = \text{APD} + \text{DI}$ and $\text{APD}^* = f(\text{DI}^*)$, this becomes further simplified:

$$\delta\text{APD}_{i+1} = -f'(\text{DI}^*)\delta\text{APD}_i \quad (2.4)$$

Based on this, it can be seen that a bifurcation exists (which manifests as alternans) whenever $|f'(\text{DI})| > 1$, due to the amplifying effects of deviations from the fixed point APD^* . This is represented graphically in Fig. 2.5. The gradient of the restitution curve is still of key experimental import, as a steep curve is taken to imply an increased possibility of wave breakup and subsequent fibrillation from tachycardia (Riccio et al., 1999); mechanisms that lead to arrhythmogenesis shall be examined in greater detail in §2.4.2.

However, it should be noted that this approach is limited, as it presents the oversimplification that the APD is dependent purely on the preceding DI. Thus, while the restitution curve can be a useful indicator of a tissue's susceptibility to fibrillation and other disorders, it is by no means the only such indicator (Riccio et al., 1999). Furthermore, it makes no account of the $[\text{Ca}^{2+}]_i$ dynamics—this is discussed further in §2.4.2.

2.3.1 Excitation-Contraction Coupling

Arguably, the complex electrical activity of the AP just described exists for the sole purpose of ensuring the heart acts as an effective mechanical pump. As such, the linking of the electrical activity of the heart to its mechanical contraction is vital, as is referred to as *excitation-contraction coupling*. What follows is a brief summary of the mechanism of this link (the reverse side of this mechanism, termed mechanoelectric feedback, shall not be discussed here). More details of the mechanical aspect of the cardiac cycle, and of the attempts to model it and integrate it with electrical models, can be found in Trayanova et al. (2011). A summary of Ca^{2+} -handling in the cell is provided by Eisner et al. (2000).

For this discussion, the cell may be decomposed into units called calcium release units (CRUs), also known as dyads (Cleemann et al., 1998). These CRUs are spread roughly evenly throughout the cell to allow for a uniform action throughout—the number of CRUs in the cell has been estimated to be between 10,000 and 100,000 (Cleemann et al., 1998; Greenstein and Winslow, 2002). Anatomically, the CRU may be considered to be a section of the cell containing a section of the cell membrane, with some L-type Ca^{2+} channels, and a section of the sarcoplasmic reticulum (SR). The primary rôle of the SR is to sequester and release Ca^{2+} when the required stimulus is given. This release is predominately by *ryanodine receptors* (RyR), but at least one other channel (Inositol triphosphate-activated channels, or IP_3) is known to play a part, and others are reported (Pozzan et al., 1994). This stimulus is the rise in local concentration of Ca^{2+} precipitated by the opening of the L-type Ca^{2+} current channels, and is termed *calcium-induced calcium release* (CICR) (Fabiato, 1992). The result is that a great deal of Ca^{2+} is released into the cytosol of the cell during phase 2 of the AP under ‘normal’ conditions. It can thus be noted that the Ca^{2+} system of the cell is dependent on the AP, which is in turn affected by the Ca^{2+} dynamics (both due to the positive charge associated with Ca^{2+} , and due to Ca^{2+} -sensitive membrane currents, e.g. $I_{\text{Ca,L}}$ (Weiss et al., 2006)). The release of Ca^{2+} from the SR is modulated by means of a Ca^{2+} -binding protein within the SR called calsequestrin (CSQN)—computational modelling of its effects by Restrepo et al. (2008) demonstrate that this is behind the steep load-release relationship exhibited by SR release.

The reason this is vital for ECC is due to the interaction between Ca^{2+} and the contractile units of the cell, called the sarcomere. When the cytosolic concentration of Ca^{2+} ($[\text{Ca}^{2+}]_i$) rises, the free Ca^{2+} binds to a part of the contractile mechanisms of the cell, which then removes the inhibition between the two critical contractile parts of the mechanism, allowing contraction to take place. It should be remembered that the Ca^{2+} transients *precede* contraction, and the upstroke velocity of the transient is faster than the rise in force (Lee et al., 1988).

Subsequent to contraction, the Ca^{2+} released from the SR is recovered by the sarco/endoplasmic reticulum Ca^{2+} -ATPase pumps (referred to as SERCA) (Franzini-Armstrong et al., 2005) (which is inhibited by a protein called phospholamban, among other factors (Talukder et al., 2009; Xu et al., 1993; Eisner et al., 2000)). Further Ca^{2+} is extruded from the cell by I_{NaCa} (Laurita and Rosenbaum, 2008) (it should be noted that I_{NaCa} brings in 3 Na^+ ions for every Ca^{2+} ion extruded, making it an eletrogenic current). Other mechanisms for removing cytosolic Ca^{2+} are negligible (Bassani et al., 1994). At steady state, the influx from $I_{\text{Ca,L}}$ and the efflux from I_{NaCa} are equal. When not in steady state, the value of $[\text{Ca}^{2+}]_i$, influenced by SR Ca^{2+} release (and thus SR Ca^{2+} load), operates to return the system to steady state. This process has been referred to as ‘autoregulation’ (Eisner et al., 2000).

The end $[\text{Ca}^{2+}]_i^{\text{dia}}$ is heavily dependent on this uptake/extrusion process—if there is an inhibition/up-regulation of either process, it can have a significant beat-to-beat effect on $[\text{Ca}^{2+}]_i^{\text{dia}}$. It should be noted that neither the reduction of $[\text{Ca}^{2+}]_i$, nor the involved buffering, are not linear processes. Bers and Berlin (1995) demonstrated a that SERCA demonstrates Michaelis-Menten kinetics in the buffering/sequestration process—this is ideal for the requirements of the system, in that it increases the rate of decay of $[\text{Ca}^{2+}]_i$ when $[\text{Ca}^{2+}]_i$ is increased, i.e. if the Ca^{2+} transient is greater, the cell is able to return $[\text{Ca}^{2+}]_i$ to a diastolic value within a similar amount of time as for a small transient.

There is a long-known association between alternans in the Ca^{2+} -handling mechanisms of the cell and arrhythmias, on the basis of the feedback between the Ca^{2+} system and the AP itself. However, the precise mechanism, and the causal links involved, are still the topic of much debate, and work is ongoing to establish the means by which alternans and arrhythmias are linked (Alvarez-Lacalle et al., 2013; Chen et al., 2009; Restrepo et al., 2008). More details as given in §2.4.2.

2.4 Cardiac Dysfunction

Cardiac dysfunction relates to where the function of the heart is impaired in some way. While this often relates to cardiac disease, it is not always the case that dysfunction requires disease—disease merely imparts a greater disposition to dysfunction.

2.4.1 Ischæmia

A particularly active area of research in cardiac disease is that of *ischæmia*, due to its being one of the main causes of sudden cardiac death (SCD): 80% of those who fall victim to SCD have some form of coronary heart disease. Ischæmia represents a cessation of normal blood flow to an area of tissue, which leads to waste products not being removed, and nutrients not being delivered. This results in a series of changes to the tissue and the surrounding area, which, if left untreated, can lead to irreversible damage to the cells in the tissue and cell death (Carmeliet, 1999). At the tissue/organ level, this process can lead to subsequent fibrillation, arrhythmia and the failure of the pump action of the heart (Harris et al., 1954).

As such, investigation into the effects and possible treatments of ischæmia is of high value. Due to the difficulty of gathering human data, especially during an ischæmic event, animal experiments have moved to fill the gap where possible. To that end, rabbit data has been shown to reproduce many of the salient features of human data (Giles and Imaizumi, 1988; Barrett et al., 1997; Panfilov, 2006), and many metrics can be adapted according to a body mass relation (Noujaim et al., 2007). Computational models are also of vital importance, as they allow probing of questions that, due to the rapidity of the evolution of acute ischæmia and the difficulties of getting transmural experimental data, are currently untenable to be answered experimentally.

As has been discussed previously, ion channels are the key determinant for many of the mechanisms of the cell that relate to its pump action, notably the membrane potential and the concurrent change in $[\text{Ca}^{2+}]_i$ that leads to cardiac contraction. Changes to these channels thus have a profound effect on the action of the cardiomyocyte, and thus the heart itself; drug block has already been mentioned as one means for changing the action of these channels. Under conditions of ischæmia, however, the key changes come from changes in the extra- and intra-cellular concentrations of ions and metabolites. From the Nernst potential, for example, one can plainly see that changing concentrations will impact on the action of channels. During ischæmia, however, it is more than just ion concentrations that change. With pumps such as the Na-K pump, changes in the concentrations of ATP and ADP drastically affect the response.

Studies have shown that, in some drug trials intended to treat arrhythmic effects, the drug actually had a delitrious effect (Ch'en et al., 1998), emphasising the complicated nature of these pathological conditions.

As with all computational modelling of complex biological systems, it is necessary to determine what are the salient features of a system, and aim to model only those changes: it is unnecessary to model every known aspect of a system. In this thesis, the focus is on the acute initial phase of ischæmia (phase 1A), which is considered as the first ~ 10 minutes following the onset of ischæmic conditions. For a summary of the changes involved in phase 1A acute ischæmia, and how these changes can be effectively

modelled computationally, the reader is referred to (Rodríguez et al., 2006). It is noted that there is much work done on ischaemia beyond this stage, in terms of (a) reperfusion, (b) longer infarct times and (c) cardiac remodelling, but these studies are not addressed in detail here as beyond the remit of this work.

Ischaemic Changes in the AP

The ischaemic changes in AP are well-documented, and are an increase in V_{rest} , and a decrease in APD, AP amplitude, and the maximum rate of membrane depolarisation ($(dV_m/dt)_{max}$) (Carmeliet, 1999; Weiss and Shine, 1982; Weiss et al., 1992; Kléber et al., 1987b; Barrett et al., 1997; Janse et al., 2001). These changes are not minor— V_{rest} is increased by 15mV, APD₉₀ is reduced by approximately 50%, and AP amplitude is reduced from ~ 120mV to ~ 90mV (Rodríguez et al., 2002). As a result of these changes, and other underlying changes, ischaemic tissue is known for its arrhythmogenic properties—3 to 9 min after occlusion, APD alternans can be observed in the ventricles, which can then degenerate into spontaneous fibrillation (Downar et al., 1977). Computer models of ischaemia have also noted the importance of increased heterogeneity within the tissue (Avitall, 1979; Behrens et al., 1997).

Under normal conditions, in well-oxygenated myocardium, the cell recovers its excitability almost simultaneously with its repolarisation. As such, the APD is a good indicator of the *effective refractory period (ERP)*, defined as the minimum length of time a cell requires before another AP can be elicited (Huang et al., 2004). However, with ischaemic conditions leading to the impaired recovery of I_{Na} , the cell recovery is also impaired, and the ERP lengthens beyond the APD; the difference between the two is referred to as the PRR period. Some work has shown an initial decrease in ERP during early acute ischaemia (Downar et al., 1977), while other work has shown a consistent increase (Sutton et al., 2000) during the first three minutes of ischaemia. In both cases, however, the correlation between APD and ERP breaks down, leading to an increase in PRR.

Simulations have demonstrated that the changes in the AP can be reproduced by simulating the effects of three changes of ischaemia (Shaw and Rudy, 1997b,a; Ferrero et al., 1996; Rodríguez et al., 2004): the removal of oxygen from the environment (*anoxia*), and the increase in extracellular potassium (*hyperkalæmia*), and the increase in intracellular and extracellular pH (*acidosis*); it should be noted that some simulations of ischaemia simulate a partial block of the flow of oxygen instead of the complete block: this is referred to as *hypoxia*. Furthermore, studies have shown that each of these conditions are required for ‘successful’ ischaemia—individually applied, the conditions present different pathologies (Rodríguez et al., 2006; Sharma et al., 1983). The time course of each of these separate pathologies during ischaemia is poorly defined (Niederer, 2013).

The key methods of simulating these changes is explained in more detail below, but briefly, these are:

Anoxia: Activation of I_{K-ATP} channels.

Hyperkalæmia: Increase in extracellular K⁺ concentration ([K⁺]_o).

Acidosis: Decrease in peak conductance of I_{Na} and $I_{Ca,L}$ by 25%.

While simulation of these three conditions as described has been shown to reproduce the changes in the AP, it must be remembered that the ischaemic milieu is complicated: these changes offer the most efficient means of reproducing the AP effects of ischaemia. However, one may also reproduce ischaemia using alternative formulations, or include other aspects. A common method is to model the changes as a direct response to the changing concentrations of ATP and ADP. Another important consideration can be the inhibition of I_{NaK} caused by anoxia. This, coupled with the decrease in [Na⁺]_o caused by the lack of perfusion, leads to an increase in [Na⁺]_i and an inhibition of I_{NaCa} . Finally, recent research has shown the I_{to} downregulation caused by hypertrophy could have significant implications for AP repolarisation (Verkerk et al., 2011).

It should be noted that the ischaemic conditions described here are correct for fully ischaemic tissue. In reality, however, it is rarely the case that fully ischaemic tissue arises in isolation, and instead there

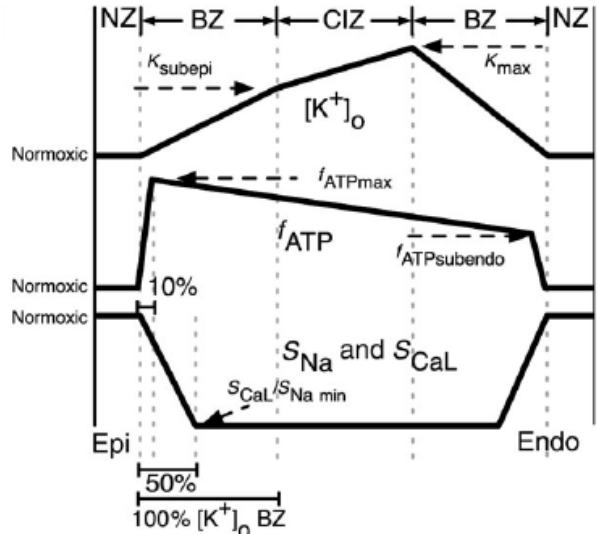


Figure 2.6: Distribution of hyperkalaemia, anoxia and acidosis in a transmural ischaemic tissue simulation. In non-transmural tissue, there is no gradient of $[K^+]$ _o and f_{ATP} values within their respective ischaemic zones. This figure demonstrates the different ranges of border zones for the different components of ischaemia. Figure originally from Tice et al. (2007).

are three distinct areas of concern: normal tissue, the central ischaemic zone, and the so-called *border zone*, which is the interface between normal and ischaemic tissue. This border zone experiences varying degrees of anoxia, acidosis and hyperkalaemia over different spatial ranges. There are several very important consequences of this spatial heterogeneity, which have been examined in depth in the literature: what follows is a brief outline of the relevant points for this thesis, whose focus is not specifically on the effects of spatial heterogeneity. However, the heterogeneities mentioned here may also be found to be due to parameter variation, which is the focus of this thesis.

An example model of the spatial distribution of anoxia, acidosis and hyperkalaemia is presented in Tice et al. (2007). The used spatial variation is shown in Fig. 2.6, and demonstrates that the individual components of ischaemia do not vary uniformly across the defined border zone. This sets up the stage for heterogeneity in tissue responses. One key feature of this is the evolution of APD and ERP: in both the central ischaemic zone (CIZ) and border zone (BZ), APD decreases. However, due to the anoxic conditions with normal $[K^+]$ _o in the border zone, there is no concurrent increase in ERP in the border zone, while the ERP increases as described above ~ 6 minutes post-occlusion in the CIZ (Tice et al., 2007; Coronel et al., 2012). A further important heterogeneity is that of APD between the CIZ/BZ and the normal zone (NZ): due to the difference in repolarisation state, there can be a current flow from tissue with late repolarisation to tissue with early repolarisation (CIZ/BZ to NZ). This current flow causes depolarisation of the NZ; if this depolarisation reaches the threshold value, a spontaneous, ectopic beat is generated, in what is referred to as *phase 2 reentry* (Coronel et al., 2009; Lukas and Antzelevitch, 1996; Coronel et al., 2012).

It should be remembered that the BZ is not a simple ‘buffer’ between the CIZ and the NZ: Experimental data have also shown that a majority of extrasystoles occur in the peri-infarct zone, corresponding here with the BZ, *i.e.* these data imply that the conditions in the BZ, and not just in the CIZ, promote arrhythmogenesis (Chou et al., 2007). This may be due in part to the difference in conditions between the CIZ and the NZ leading to a sharp heterogeneity present in the BZ, which then gives rise to arrhythmogenic conditions (more detail is given in §2.4.2). Furthermore, it has been shown that the heterogeneity within the BZ is not uniform, by which it is meant that the concentration gradients of different ions are not the same across the BZ (Niederer, 2013).

Anoxia represents the loss of oxygen from the ischaemic milieu, and is not directly modelled in most simulations, but is instead modelled by the effect on cellular respiration and the consequent decrease in ATP availability and increase of APD concentration. This change in ATP concentration is mainly felt through the activation of the I_{K-ATP} channel, which is the single greatest contributor to the shortening of the AP. This shortening of the AP, along with the increased inexcitability and shift of V_{rest} , works to protect the cell by avoiding excessive K^+ loss (Carmeliet, 1999).

Two important different formulations of this channel have been developed: the first was originally by Ferrero et al. (1996), and has been subsequently used by Trénor et al. (2007), while the second was

originally shown in Michailova et al. (2005), and has been implemented in Terkildsen et al. (2007) and Michailova et al. (2007). Both are dependent on both the ATP and ADP concentrations, and also $[K^+]$ _i. The Ferrero implementation was used in a Luo-Rudy model, which can be considered as a general mammalian model, but much of its components are derived from guinea pig data. It includes dependency on the intracellular concentrations of Na^+ and Mg^{2+} . The Michailova model was originally implemented in a canine model, was subsequently adapted for a rabbit ventricular model, and lacks the sensitivity to Na^+ and Mg^{2+} .

Activation of the I_{K-ATP} channels is achieved by decreasing $[ATP]$ _i and increasing $[ADP]$ _i. However, experimental data on the channel itself demonstrated that full activation of the channel in the cell would require a change in concentrations that are significantly greater than actually observed. It is thus currently thought that only minimal activation of the I_{K-ATP} channels is required to effect the changes in ischaemia; under this ‘spare channel’ hypothesis (Cook et al., 1988), activation has been postulated as being ~ 0.8% (Rodríguez et al., 2002; Weiss et al., 1992; Ferrero et al., 1996; Trénor et al., 2007; Ferrero et al., 2003b). This small degree of activation allows for a very finely balanced activation of the channel to achieve the desired effect: consequently, it has been noted that the degree of activation of this channel is important for determining the vulnerability of the tissue/organ to reentry in regional ischaemia (Ferrero et al., 2003a; Trénor et al., 2005). However, within the ischaemic tissue, the activation of I_{K-ATP} is usually modelled as a linear increase of activation until it reaches maximum activation at 10 minutes post-occlusion (Trénor et al., 2007; Tice et al., 2007).

The onset of hyperkalæmia is known to follow a biphasic pattern: a rapid rise for the first ~ 10 minutes of ischaemia, followed by a plateau phase (changes later in time are not discussed here) (Wilde et al., 1988). This rise is partly caused by the efflux of K^+ from the cell caused by activation of I_{K-ATP} , but this impact is negligible on its own—simulations have demonstrated that the increase requires the coordinated action of I_{K-ATP} with both inhibition of I_{NaK} and activation of an inward Na^+ -pump, I_{NaS} (Rodríguez and Ferrero, 2001b,a; Rodríguez et al., 2002; Terkildsen et al., 2007).

The rate of increase, and final plateau level, of $[K^+]$ _o has been shown to be rate-dependent, with values of $[K^+]$ _o ranging from 12 – 17 mM reached within 10 – 15 min (Rodríguez et al., 2002; Coetze and Opie, 1987). However, most simulation models take the time to plateau to be 10 min, and the plateau concentration to be ~ 12 mM, though higher values have also been used in simulation (Ferrero et al., 2003a; Trénor et al., 2007). Research indicates that hyperkalæmia (with $[K^+]$ _o greater than 12.5 mM) is vital to the development of reentry, with its absence precluding reentry (Ferrero et al., 2003b).

The hyperkalæmia is secondary to I_{K-ATP} in shortening the APD (Gasser and Vaughan-Jones, 1990)—its main effect is to affect the excitatory properties of the cell/tissue. For the first few minutes of ischaemia, the rise in $[K^+]$ _o and its attendant rise in V_{rest} brings the cell closer to the activation threshold, and thus facilitates an increase in conduction velocity in tissue. However, once $[K^+]$ _o rises beyond 8mM, the process of reactivation of I_{Na} is inhibited by the increase in V_{rest} . This reduces the number of I_{Na} channels available at the start of the AP, and this reduction in I_{Na} magnitude is reflected in a reduction in the rate of depolarisation of the cell (a reduction in $(dV_m/dt)_{max}$); it has been shown that the recovery of $(dV_m/dt)_{max}$ and the *h.j* inactivation gates of I_{Na} are similar (Shaw and Rudy, 1997b). In severe ischaemia (10-12 minutes after onset), this can lead to a biphasic upstroke (Barrett et al., 1997): the first phase corresponds to the reduced activation of I_{Na} , and the second phase corresponds to the activation of $I_{Ca,L}$ that completes the depolarisation. It should be noted that $(dV_m/dt)_{max}$ is proportional as the square root to conduction velocity in tissue, so changes in cellular $(dV_m/dt)_{max}$ correlates with changes in tissue restitution properties (Kléber and Rudy, 2004; Walton and Fozard, 1983; Tasaki and Hagiwara, 1957)—ischaemia is known to lead to a reduction in conduction velocity in tissue (Caldwell et al., 2007), though this is likely partly due to electrical uncoupling of the cells in ischaemic tissue (Kléber et al., 1987a).

The reduction in availability of I_{Na} channels is also one of the main causative agents behind ischaemic *post-repolarisation refractoriness* (PRR), and changes in myocardial excitability generally (Coronel et al., 2012).

The acidosis inherent in ischaemia is due mostly to the accumulation of CO_2 that arises due to the

cessation of blood flow, with a lesser rôle being played by the accumulation of lactate (Ichihara et al., 1984). The concentration of hydrogen ions that is represented by the pH is normally a tightly regulated feature of the cell, with small changes being responsible for major cellular dysfunction (Ch'en et al., 1998). During the first 10 minutes of ischæmia, intra- and extra-cellular pH drop linearly with time, with a ~ 1 pH unit drop after 10 minutes (Shaw and Rudy, 1997b; Neely et al., 1975; Mohabir et al., 1991)¹.

Prior work in computational modelling has shown the key importance of the impact this has on the ion flow through the I_{Na} and $I_{\text{Ca,L}}$ channels. It is postulated that acidosis is one of the key factors behind reduced uptake of Ca^{2+} into the SR during ischæmia (Krause and Hess, 1984). The ischæmic pH drop reduces I_{Na} maximum conductance by 25% (as well as shifting its voltage-current dependence by 3.4 mV) (Kagiyama et al., 1982). For guinea pig ventricular cells, a sigmoidal decrease in maximum conductance of $I_{\text{Ca,L}}$ has been noted (with a 50% reduction at pH 6.6). In computational models of ischæmia, the effect of acidosis is thus modelled as a linear reduction in maximum conductance of I_{Na} and $I_{\text{Ca,L}} \sim 5$ minutes after the onset of ischæmia, until a 25% reduction is reached after 10 minutes (Trénor et al., 2007); this corresponds to a pH of ~ 6.4 (Ferrero et al., 2003b). This, combined with the previously mentioned effects of hyperkalæmia, leads to a marked decrease in cell excitability and $(dV_m/dt)_{\text{max}}$, leading to a decrease in membrane excitability conduction velocity in tissue (Shaw and Rudy, 1997b).

The ischæmic suppression of I_{NaK} (Dhalla et al., 1988) has been shown to be due to acidosis, which linearly affects I_{NaK} (Severi et al., 2002).

Ischæmic Changes in $[\text{Ca}^{2+}]_i$

However, it should be noted that changes during ischæmia are not limited to changes in the action potential—notable changes also occur in $[\text{Ca}^{2+}]_i$ and the contractile mechanisms of the cell (for a more detailed discussion of ischæmic changes in other ion concentrations, the reader is referred to Carmeliet (1999); Niederer (2013)). Immediately post-occlusion, there is an increase in $[\text{Ca}^{2+}]_i$ until ~ 2 min post-occlusion, followed by a decline (possibly to pre-occlusion levels), followed by a secondary increase at 5–15 min post-occlusion (see Fig. 2.7) (Lee et al., 1988; Mohabir et al., 1991; Camacho et al., 1993). The increase in $[\text{Ca}^{2+}]_i$ can be described more fully as

- Elevation of $[\text{Ca}^{2+}]_i^{\text{sys}}$,
- Elevation of $[\text{Ca}^{2+}]_i^{\text{dia}}$,
- Broadening of systolic Ca^{2+} peak (indicative of reduced SR uptake function),
- Increase in net amplitude of the Ca^{2+} transient (though this is not always observed (Camacho et al., 1993)).

Results indicate that the increase in $[\text{Ca}^{2+}]_i$ is due mostly to the effects of acidosis, but other mechanisms are required in addition to explain the initial increase (Bers and Ellis, 1982; Mohabir et al., 1991). It has been hypothesised that the initial increase may be due to reduced SR uptake. The later increase may be augmented due to increased activation of $I_{\text{Ca,L}}$ caused by the increase in V_{rest} , though Niederer (2013) concluded that the increase in $[\text{Ca}^{2+}]_i^{\text{dia}}$ is due primarily to inhibition of I_{NaK} .

The increase in $[\text{Ca}^{2+}]_i$ could be in small part be responsible for the increase in V_{rest} due to the action of Ca^{2+} -activated cation channels (Colquhoun et al., 1981). The increase in $[\text{Ca}^{2+}]_i$ also occurs for low-flow ischæmia, *i.e.* it is also likely to be present in the border zone to ischæmic tissue (Camacho et al., 1993).

¹It should be noted that the value of pH falls approximately linearly (see Fig. 10 in Mohabir et al. (1991)), and not the concentration of “

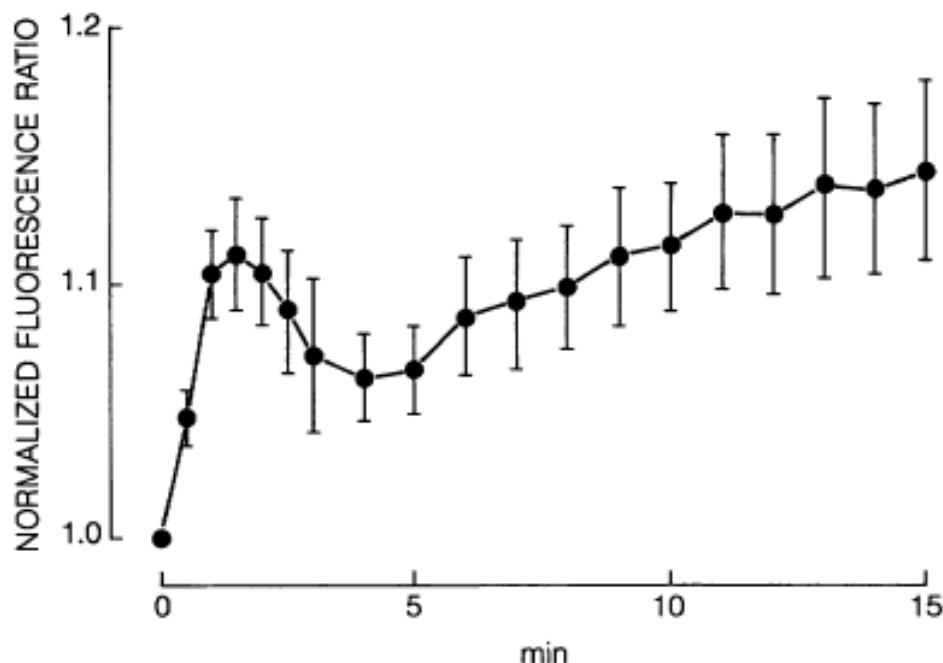


Figure 2.7: Mean systolic fluorescence ratio for rabbit hearts under ischemic conditions, normalised to pre-ischemic values. Data obtained using whole rabbit hearts loaded with indo-1, a cell-permeant fluorescent indicator for Ca^{2+} , and demonstrate an initial increase in $[\text{Ca}^{2+}]_i$, followed by a marginal decrease at 5–10 min post-occlusion, before increasing further. Figure originally from Mohabir et al. (1991).

The secondary increase coincides with pH_i increasing to a ‘tipping point’ at which changes in $[\text{Ca}^{2+}]_i$ are noted in purely acidic conditions, thus implying that this secondary increase is due entirely to decreasing pH_i .

There is a large body of evidence that the time constant of $[\text{Ca}^{2+}]_i^{\text{dia}}$ decline increases during ischaemia (Allen and Orchard, 1983; Camacho et al., 1994; Lee et al., 1988) (though not during hypoxia (Silverman et al., 1991)). This may be achieved via a change in either Ca^{2+} uptake to the SR, or via reduced extrusion of Ca^{2+} via I_{NaCa} ; evidence indicates that there is minimal change in Ca^{2+} -uptake from the extracellular space during ischaemia (Bourdillon and Poole-Wilson, 1982).

For a fuller summary of the changes in SR function during ischaemia, both in terms of uptake (SERCA) and release (RyR), the reader is referred to Mubagwa (1995). Other details of changes in Ca^{2+} handling during ischaemia are given in Talukder et al. (2009). Note that possible changes in mitochondrial Ca^{2+} handling are not considered in this thesis, as the consensus is that Ca^{2+} pathophysiology is mainly due to changes in the SR (Fauconnier et al., 2013).

Kinetic studies have demonstrated a decrease in action of SERCA with no change in Ca^{2+} sensitivity, i.e. there is a change in the number, not properties, of active SERCA. There is a large body of evidence for impaired SERCA action during ischaemia (Dhalla et al., 1988; Temsah et al., 1999; Lee et al., 1967; Toba et al., 1978; Kaplan et al., 1992). Krause and Hess (1984) present results indicating SERCA becomes more sensitive to $[\text{Ca}^{2+}]_i$ as pH_i decreases, with a reduction in maximal velocity. However, while a decrease in maximal velocity was also seen in Kaplan et al. (1992), there was no observed change in dissociation constant, representing Ca^{2+} sensitivity. Antibody assays indicate a reduction in the number of active SERCA channels (Levitsky et al., 1989). As such, these results indicate that the conditions reduce the open probability of the SERCA channel. The reduction in SERCA action may be caused by ATP deficiency (Camacho et al., 1993), accompanied by other acidic effects (Krause and Hess, 1984). It has been suggested that free radicals are the means by which SERCA is impaired (Temsah et al., 1999; Wang et al., 2013; Xu et al., 1997; Zweier, 1988). The decrease in SERCA function

persists after treatment for assays and the like, thus indicating that the causative agent in the change is not $[Ca^{2+}]_i$, and the recovery of SERCA action after reperfusion indicates SERCA is not denatured. It is of note that results indicate that expression of SERCA and phospholamban are altered during cardiac remodelling post-infarct (Sun et al., 2005).

It is unclear if release from the SR is also affected during ischaemia (increased loss would have a similar effect to reduced gain), with conflicting results. For example, Feher et al. (1989) used RyR blockers during ischaemia to achieve a reduction in rate of Ca^{2+} uptake, indicating an influence of RyR in the process, and Fauconnier et al. (2011) demonstrated an increase SR leak (though this is likely a reperfusion effect). However, other results do not indicate a change in release (Kaplan et al., 1992), and others indicate RyR action is actually decreased (RyR channels are inhibited by NADH (Wang et al., 2013), which increases during ischaemia (Esumi et al., 1991)).

The rôle of I_{NaCa} during ischaemia is unclear—that it transiently reverses direction is not in doubt, but it is considered unlikely that this is a permanent feature of the ischaemic milieu (Noble, 2002; Rodríguez et al., 2006); the reverse action of I_{NaCa} brings about the exact conditions required to return the exchanger to its normal operation, indicating that, at most, there is a reduction in I_{NaCa} during ischaemia. This inhibition is brought about not just due to the changes in Ca^{2+} concentration—it is also driven by the changing Na^+ gradient, with a decrease in $[Na^+]_o$ caused by lack of perfusion, and an inhibition of I_{NaK} caused by anoxia. Noble (2002) used simulations to demonstrate the requirement of this increase in $[Na^+]_o$ to be modelled to account fully for the increase in $[Ca^{2+}]_i$, driven by the reduction in action of I_{NaCa} .

The reduction in I_{NaCa} hypothesis has been used computationally (Pollard et al., 2002), with peak I_{NaCa} reduced by 80% for simulation of Phase 1B ischaemia. Tani and Neely (1989) demonstrated that the decrease in pH led to an rapid initial increase in $[Na^+]_i$ (via the -Na^+ exchanger), which then correlated with an increase in $[Ca^{2+}]_i$, and Cross et al. (1998) demonstrated a correlation in male mice between increased I_{NaCa} and declined ischaemic recovery. Furthermore, inhibitor of I_{NaCa} has been shown to have cardioprotective properties.

Opposing this increase in $[Ca^{2+}]_i$, there is a counter-intuitive decrease in contractile strength of the myocyte (Lee et al., 1988; Kaplan et al., 1992), accompanied by an increase in diastolic tension (Mubagwa, 1995). There are many suggested mechanisms to explain this decline in contractile strength, despite the increase in $[Ca^{2+}]_i$. Mohabir et al. (1991) postulated competitive inhibition by Ca^{2+} in the troponin-C complex (Blanchard and Solaro, 1984), and thus the ischaemic decline in pH_i is responsible. Alternatively, Camacho et al. (1993) suggests the increase in inorganic phosphate (P_i) also attendant to ischaemia is responsible. However, against this fact is that contractile strength is reported to increase under hypoxic conditions (Kihara et al., 1989).

Another way to explain the decrease in contractile strength is to appeal to the ‘garden hose effect’, which is that the contractile strength of the myofilaments are reduced if the preceding relaxation is reduced (Camacho et al., 1993; Kléber et al., 1987a; Kléber, 1987; Vogel et al., 1982) (though some findings dispute such a mechanism *in vivo* (Zhao et al., 1988)). As such, while an increase in $[Ca^{2+}]_i^{\text{sys}}$ might indicate an increase in contractile strength, it is the increase in $[Ca^{2+}]_i^{\text{dia}}$, preventing relaxation, that is more influential by this hypothesis. Of note for this hypothesis is the increase in the time constant for decline in left ventricular pressure (Serizawa et al., 1981; Applegate et al., 1987; Serizawa et al., 1987; Isoyama et al., 1987).

At 2-3 min post-occlusion, $[Ca^{2+}]_i$ alternans develops. This is likely due to the function of the sarcoplasmic reticulum, rather than APD alternans: the smaller transient follows a higher diastolic $[Ca^{2+}]_i$, indicating reduced SR release due to reduced SR sequestration. This is not to say that the SR release is impaired; rather it is a consequence of the steep-load relation of the SR previously mentioned (Shiferaw et al., 2003; Restrepo et al., 2008).

Other Ischaemic Changes

It has also been shown that $[Na^+]_i$ and $[Na^+]_o$ change during ischaemia, although the degree of this change is subject to some debate. Carmeliet (1999) provides a comprehensive review of the available literature at the time regarding changes that occur during ischaemia, concluding that there is a sustained monotonic increase in $[Na^+]_i$ during ischaemia, leading to a two- to five-fold increase (leading to values of 20–25 mM 15–20 min after ischaemia). However, within the realm of acute ischaemia which concerns this thesis, the increase is more often noted as ~ 50% (Malloy et al., 1990; Pike et al., 1993; van Echteld et al., 1991; Tani and Neely, 1989).

Noble (2002) obtained good agreement with experimental data regarding the changes in $[Ca^{2+}]_i$ by modelling a ~ 30% decrease in $[Na^+]_o$, coupled with a threefold increase in $[Na^+]_i$.

Results from Coetze and Opie (1987) indicate that (mainly as a result of hypoxia), ischaemia reduces the incidence of DADs in guinea pigs, which would ordinarily be expected to increase in conditions of increased $[Ca^{2+}]_i$.

2.4.2 Arrhythmogenesis

One of the key reasons for studying ischaemia, as mentioned previously, is due to the cost of sudden cardiac death, and the rôle ischaemia plays in sudden cardiac death. As such, one of the key areas of research is how ischaemia can lead to sudden cardiac death, and thus the study of ischaemic arrhythmogenesis is vital.

Studies have been conducted to establish the means by which ischaemic conditions can provide the substrate for arrhythmogenesis, and how it can lead to sustained arrhythmias. It should be emphasised at this point that arrhythmogenesis is not the preserve of ischaemia—arrhythmias can develop for any number of reasons, ischaemia being just one of them. It is of note that increasing susceptibility to arrhythmias is a consequence of something as harmless as aging, due to the increasing heterogeneity presented by certain breakdowns in the heart structure that occur naturally (Spach et al., 1988). Furthermore, it is not the case that tissue will ‘become’ arrhythmic, and then, inevitably, arrhythmia will occur. Rather, tissue changes dynamically, and while it may have greater arrhythmogenic properties, this does not necessarily guarantee arrhythmia (Weiss et al., 2006).

Fibrillation in ventricular tissue can be initiated and maintained by several different mechanisms, including:

- Ectopic beats (Haïssaguerre et al., 1998; Tobón et al., 2010; Zhang et al., 2011);
- Spiral/scroll waves and rotors (Jalife, 2003, 2009; Pandit and Jalife, 2013);
- Stable points of reentry (Mandapati et al., 2000; Allessie et al., 1977);
- Unidirectional block (Allessie et al., 1976; Gough et al., 1985);
- Vortex formation (Cabo et al., 1996).

Ischaemia has been shown to provide the substrate for all of these mechanisms. Furthermore, research has demonstrated that structural heterogeneities, another potential side-effect of ischaemia, can increase incidence of arrhythmia and other atypical electrical activity, e.g. early after-depolarisations (EADs) (Auerbach et al., 2011).

This increase in dispersion of electrophysiological properties is a key area for investigation for its arrhythmogenic properties (Kuo et al., 1983). Recently, there has been increased awareness of the importance of multiple different factors simultaneously for the development of arrhythmias in ischaemic tissue. While ischaemia is well known to increase the vulnerability to ectopic beats (Zhang et al., 2011), the ‘width’ of the vulnerability window (the range of coupling intervals at which an ectopic beat will

lead to sustained arrhythmias) does not increase throughout the onset of ischaemia, *i.e.* arrhythmogenic risk does not increase linearly with duration of ischaemia (Tice et al., 2007; Romero et al., 2009b; Barrett et al., 1997). Furthermore, the properties of the tissue play a profound rôle in arrhythmogenesis. For example, it is insufficient to only have unidirectional block in tissue for a sustained arrhythmia: an interaction between the coupling interval, the unidirectional block, the restitution properties of the tissue, the scale of the block, and the conduction velocity in the tissue are all required (Coronel et al., 2009; Cherry et al., 2012). As a consequence, there is a minimum size of tissue for which arrhythmias can be maintained, though this size can vary depending on the circumstances of the tissue (Adeniran et al., 2011). This is not to say that increased dispersion, evident on the cellular scale, is meaningless—quite the opposite. Rather, the dispersion can provide the underlying properties that, given the correct interaction, leads to dangerous tissue properties.

As has previously been noted, the cardiac system is an inherently dynamic one—multiple different currents interact in a time- and voltage-dependent manner with each other, and other complicating factors, to produce the complete AP and associated cardiac contraction. These interactions vary depending on the condition of the heart, and the environment the heart is found in. This dynamic nature is true not only for the normal, ‘healthy’ conditions, but also for the pathological conditions such as arrhythmia and ischaemia. As such, with the consideration that the key thrust of this thesis is concerned with variability in ion channel properties and its correlation with experimentally observed variation, it is necessary to consider the ionic bases that exist for arrhythmias, and how these manifest in arrhythmia.

What follows is a brief summary of some pertinent ion channel mutations, their possible effects, and how these electrical alterations can lead to arrhythmia; I do not pretend to present a comprehensive compilation of the possible mutations, for the simple fact that they are legion, and it is beyond the remit of this thesis to discuss them.

Delayed & Early After Depolarisations

Delayed after depolarisations (DADs) refer to a spontaneous depolarisation of the cell after cellular repolarisation with no external stimulus. Along with early after depolarisations (see next section), these can provide the source for ectopic beats, which lead to reentry. DAD frequency is sensitive to increases in $[Ca^{2+}]_i$. The underlying mechanism by which the $[Ca^{2+}]_i$ overload can occur is usually attributed to changes in $I_{Ca,L}$, but can also be due to alterations in CICR (a mechanism which can also result in EADs) (Volders et al., 1997). Due to the increased $[Ca^{2+}]_i$, this activates I_{NaCa} , which due to its electrogenic properties, depolarises the cell, causing a DAD (Clusin, 2003).

The occurrence of DADs is reduced during ischaemia (though not in the border zone or otherwise partly ischaemic tissue), mostly due to the action of hypoxia, but DAD amplitude increases after reperfusion of the ischaemic tissue (Coetzee and Opie, 1987; Ferrier et al., 1985).

Early after depolarisations (EADs) are spontaneous, premature depolarisations that occur before the original cellular repolarisation is completed, and usually occur under situations when the AP is prolonged. There are many possible ionic causes for EADs: the most commonly muted ionic bases for EADs are changes in $I_{Ca,L}$ and I_{Na} : I_{Na} mutations resulting in reduced inactivation work to prolong the action potential (Clancy and Kass, 2005; Hashambhoy et al., 2011; Hiraoka et al., 1992). If the Ca^{2+} concentration near the sarcolemmal surface remains high during the AP, an EAD may also be initiated by I_{NaCa} (Volders et al., 1997). The upstroke of an EAD is often slower than the usual AP upstroke, due to the fact that it is based on $I_{Ca,L}$, rather than I_{Na} (the lack of repolarisation means the I_{Na} current is still deactivated) (Clusin, 2003).

In addition to defects in the currents regulating repolarisation causing EADs, it is also possible for defects in the Ca^{2+} -handling system to be responsible. Moreover, it has been demonstrated that the stochastic effects within each of these systems can increase the likelihood of the development of EADs (Tanskanen et al., 2005; Sato et al., 2009; Heijman et al., 2013).

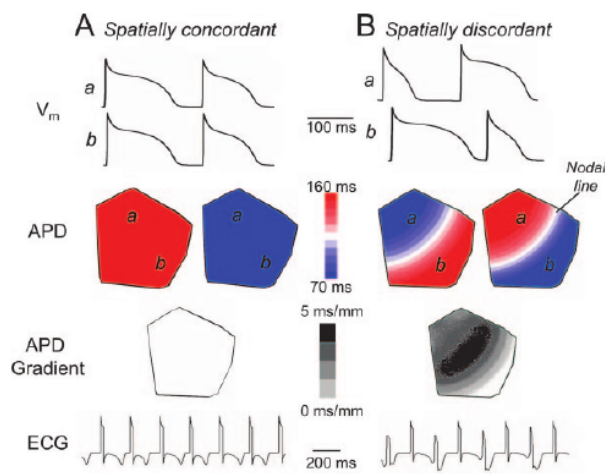


Figure 2.8: Spatially cordant (left column, A) and spatially discordant (right column, B) alternans in cardiac tissue. The top panel shows the AP and $[Ca^{2+}]_i$ data for two separate locations in the tissue. The second panel shows the APD during each beat, with the third panel showing the APD gradient resulting from such distributions. The bottom panel shows the simulated ECG for each tissue. These simulations were performed using a modified Luo-Rudy model from Qu et al. (2000). Figure originally from Weiss et al. (2006).

There are clinical similarities between EADs and the presentation of LQTS, but the rôle has not been confirmed (Clusin, 2003).

The mode of transmission from the occurrence of DAD/EAD to arrhythmia is complicated, especially in connexion with the effects of cell coupling, but recent research is beginning to unravel the substrate requirements for an after depolarisation event to graduate to an arrhythmogenic event (Tanskanen et al., 2005).

Alternans

Alternans is a phenomenon wherein the AP or $[Ca^{2+}]_i$ alternate properties from beat to beat. Usually (and for the majority of the following discussion), this is defined in terms of the duration of the AP alternating between long/short duration and the $[Ca^{2+}]_i$ transient alternating between large/small magnitude, respectively. However, it should be remembered that alternans of the AP amplitude also exists, and may reflect the inability of I_{Na} to fully recover between beats. Such a process could lead to a reduction in plateau amplitude, which in turn could lead to $[Ca^{2+}]_i$ alternans (Clusin, 2003). AP amplitude and APD alternans are not exclusive of each other.

In tissue, alternans can be either spatially concordant or spatially discordant (Fig. 2.8). Qian et al. (2001) demonstrated that Ca^{2+} alternans ‘self-organises’ into regions of tissue with the same phase, and hypothesised that this was due to movement of Ca^{2+} across gap junctions to neighbouring cells allowed some degree of synchronisation.

It is a consequence of spatially discordant alternans that, between the out-of-phase regions there is a region where no alternans is present (referred to as the *nodal line*). It is this region that, due to the APD/ $[Ca^{2+}]_i$ gradients being steepest here, is most predisposed to develop unidirectional conduction block—a region with long APD remains inexcitable when a region with short APD is excited, with the resulting AP being blocked initially, forming a reentrant circuit (Laurita and Rosenbaum, 2008). As concordant alternans does not demonstrate this dispersion of properties, it is less arrhythmogenic than discordant alternans. It has been shown that heterogeneity is not required for spatially discordant alternans to occur—due to the dependence of conduction velocity on diastolic interval (conduction velocity restitution), rapid pacing can induce spatially discordant alternans in homogeneous tissue (Watanabe et al., 2001). It should be noted that the ischaemic reduction in I_{Na} availability increases the DI range over which CV varies, and thus increases the risk of this phenomenon. Ectopic beats have also been shown to induce spatially discordant alternans in homogeneous tissue.

There is no firm evidence as to whether APD alternans drives Ca^{2+} alternans or vice versa, but mounting evidence indicates the latter to be the case. Evidence for this is varied. Lee et al. (1988) demonstrated that, when APD alternans and Ca^{2+} alternans were both present (and recorded simultaneously), there

was no variation in the APD until after the Ca^{2+} transient had reached its peak—it was only after this that the APD alternans manifested. Chudin et al. (1999) were able to induce Ca^{2+} alternans without APD alternans at rapid pacing rates in cell (demonstrating an instability in the Ca^{2+} system independent of the AP). Similar results have been achieved *in vivo* (Astrup et al., 2006) and *in silico* (Sato et al., 2006).

Research is ongoing to determine the mechanisms behind Ca^{2+} alternans. A simple hypothesis is that, at rapid pacing rates, there is simply not enough time for the SR to resequester the Ca^{2+} it has previously expended. Thus, the subsequent Ca^{2+} release from the SR is smaller, leaving more time for a complete resequestration of the Ca^{2+} by the SR. Mechanistically, Shiferaw et al. (2003) were able to reproduce Ca^{2+} alternans at rapid pacing rate without APD alternans by including a steep release-load relation for the Ca^{2+} sequestered in the SR. On a molecular level, evidence indicates that alternans prone regions express significantly less SERCA2a and RyR—this indicates responsibility lies with both SR uptake and release. Research is ongoing to find methods to protect these functions in ischæmia/reperfusion therapy (Wang et al., 2013).

The coupling between APD and Ca^{2+} alternans can be either positive or negative, *i.e.* a long APD corresponds with a large $[\text{Ca}^{2+}]_i$ transient, or with a small $[\text{Ca}^{2+}]_i$ transient. Which of these relations predominates depends on the dominant current—a large $[\text{Ca}^{2+}]_i$ transient enhances both I_{Ks} and inactivation of $I_{\text{Ca,L}}$ (which would shorten the APD, *i.e.* negative coupling), but this process also enhances the activity of the exchanger I_{NaCa} (which would prolong the APD, *i.e.* positive coupling) (Shiferaw et al., 2005). Whether positive or negative coupling predominates suggests which mechanism is the primary. Positive coupling is the more common of the two (Laurita and Rosenbaum, 2008), but negative coupling has been noted in ischæmia (Lee et al., 1988).

The question can be asked: is it APD alternans that leads to Ca^{2+} alternans, or vice versa? Mounting experimental evidence indicates that the onset of APD alternans is caused by instability in the cellular $[\text{Ca}^{2+}]_i$ dynamics, rather than by a steep APD restitution curve (Goldhaber et al., 2005; Pruvot et al., 2004). There are also expected spatial differences in the nodal line distributions depending on whether the alternans are AP or Ca^{2+} driven (Weiss et al., 2006).

While the restitution curve can provide a useful indication of when tissue is at risk of developing alternans (when the gradient is greater than 1), it must be remembered that this assumes that the APD depends entirely on the preceding DI—this is not the case. It has been observed that alternans can occur when the restitution curve is flat, and no alternans when it is steep (Shiferaw et al., 2005). Part of the reason for these anomalies is the influence of $[\text{Ca}^{2+}]_i$. It is of note that ischæmia has been observed to flatten the restitution curve (Taggart et al., 1996) while the occurrence of alternans is increased (Qian et al., 2001). Much work has been conducted to try and determine the mechanisms behind Ca^{2+} alternans (Shiferaw et al., 2003; Weiss et al., 2006).

Spiral Waves & Rotors

Spiral/scroll waves and rotors are a key area of research in arrhythmias, and consist of a curved wave-front and curved wavetail that meet each other at a ‘phase singularity’ (Fitzhugh, 1960, 1961; Gray et al., 1998). This singularity processes around an excitable core, with this core able to be either stationary or mobile. Not only do spiral waves represent a local source of activation within ventricular tissue, they are also liable to break-up, leading to fibrillation (Riccio et al., 1999).

Of the previously discussed ion channels, three are known to have an effect on rotor dynamics: I_{Na} , I_{K1} and $I_{\text{Ca,L}}$. Block of $I_{\text{Ca,L}}$ has been shown to stabilise reentry, but its exact rôle is still unclear (Jalife, 2003, 2009). I_{Na} is of note due to its impact on the conduction velocity of the AP, and thus affects the speed (and thus dominant frequency) of the spiral wave. Reducing I_{Na} also increases the meander of the core of the rotor. I_{K1} mediates the electrotonic interactions between the unexcited core and the immediate surroundings. It also stabilises reentry due to its ability to shorten APD and reduce

conduction velocity near the core, thus preventing wavefront-wavetail interactions that could destabilise and breakup the rotor. Furthermore, by decreasing the resting membrane potential, it facilitates the reactivation of I_{Na} (Pandit and Jalife, 2013). I_{Kr} has been shown to accelerate the rotor, but not to a degree comparable to the effect of I_{K1} . While I_{Ks} does not in itself change the rotor dynamics, it is important in determining post-repolarisation refactoriness and wave break formation, and thus important for the transition from tachycardia to fibrillation. It is also interesting to note that regional cooling of a rotor decreases its frequency and increases the rotor's meander, causing it to collide with a boundary and extinguish (Yamazaki et al., 2012).

Re-entry

Generally speaking, *re-entry* refers to the mechanism by which the electrical activity of the heart does not complete its 'normal' circuit, but instead enters a process whereby it self-excites itself (hence the term)—the process has also been termed 'circus movement'. Such a process can occur in many forms, as spiral waves (§??) or figure-of-eight patterns (Ferrero et al., 2003b) to name but two. Modes of re-entry are often associated with tachycardia, and can subsequently lead to fibrillation and other forms of arrhythmogenesis.

It must be noted that ectopic beats are not required to initiate reentry—dispersion of electric properties in the tissue are sufficient (Xie et al., 2007). An example is the case where there are two regions with different effective refractory periods (ERPs), one of which is greater than the CL, the other where it is less. The region with $ERP > CL$ is thus unexcitable when the wavefront is incident, and conduction block occurs at this region. However, the region with $ERP < CL$ is excitable, and thus the wavefront progresses through this region, and subsequently may excite the previously blocked region in a figure-of-eight reentry pattern (Weiss et al., 2006).

Cardiac disease is a costly condition for Western countries. In the UK, cardiovascular disease (CVD) was the biggest killer in 2010, with 180,000 people dying and 46,000 of those deaths being premature; 80,000 of these deaths were from coronary heart disease. This costs the UK health system £8.7 billion, and the economy as a whole £19 billion (Townsend et al., 2012). On a global scale, the World Health Organisation estimates CVD is responsible for ~30% of deaths worldwide, equating to ~17.3 million people in 2008 (Alwan et al., 2011).

However, the pathology of CVD can often be complicated. In-depth analysis of the mechanisms for disease is vital in determining how to treat diseases at a more fundamental level than symptomatically. As such, research has demonstrated many causal links between the cellular mechanisms, such as ion channels and their links to pacing rate, etc., and pathologies (Inoue et al., 2006; Kurz et al., 1993; Rodríguez et al., 2006; Dumaine et al., 1996; Nattel et al., 2010; Jurkat-Rott and Lehmann-Horn, 2005; Biagetti and Quinteiro, 2006).

Using the multi-parameter matrix regression method mentioned in §??, it is possible to simulate the effects on the model output of the known changes in input parameters in disease conditions. The data from the effect matrix B can then be used to determine which of the parameter changes causes which effect on the output, and to what degree (Sarkar et al., 2012).

As with computational modelling in general, the importance of the possible effects of variation are coming into focus in disease modelling as well. The focus in this dissertation thus far has been on the importance of modelling variation to gain insight into the mechanics underlying cellular processes, and the different methods that have been used in this goal thus far. However, one key area of work is not just to understand variability under normal conditions, but under pathological conditions—it has already been established that variation can have significant, meaningful effects to the outcome of pathological conditions, either by exacerbating or ameliorating the condition (Sarkar et al., 2012; John et al., 2012). For example, a particular variation can lead to either an increase or a reduction in the repolarisation reserve. The possible consequences of the changes that this variation could lead to are significant, not least due to providing a key to understanding the differing responses to different therapies, including the effects of drug block.

A leading area of research to that effect has been on drug-induced Long QT Syndrome (diLQTS). Drug-induced or not, LQTS represents a condition where repolarisation is extended; the name derives from the prolongation of the QT interval on an ECG. The most common genetic form of LQTS (Type 1) is caused by a mutation in one of the subunits of the I_{K_s} channel, which works to delay the channel activation (Jons et al., 2011; Hoefen et al., 2012; Jou et al., 2013), though other forms have also been determined with mutations in the I_{Na} channel (Hashambhoy et al., 2011). Where LQTS is drug-induced, the most common causative drug action is to block the action of I_{Kr} (in the literature, this may also be referred to as HERG block, named after the gene that produces the channel). However, not only is the response to I_{Kr} -blocking drugs variable (Kannankeril et al., 2010), but the degree of response appears uncorrelated with baseline ECG recordings. The causes for these differences are only beginning to be elucidated, but it has been theorised that it may be due to differing repolarisation reserves (Varró and Baczkó, 2011), which in turn may be due to variation—variation which may be amenable to computational modelling (it should be noted that drug effects are subject to variation at many levels, and the variation that has been the subject of this dissertation—ion channel variation—is only one). Novel work has been performed in Sarkar and Sobie (2011) to investigate the link between different input parameter values and the resulting change in output when drug block is simulated.

It is of note that the ‘opposite’ condition, Short QT Syndrome (SQTS), is also a clinically recognised phenomenon, and instead of being anti-arrhythmic, is also pro-arrhythmic (Adeniran et al., 2011). This serves to underline how the AP, while adaptive, is also tightly constrained, with alterations of properties in either positive or negative manner leading to subsequent loss of stability.

2.5 Experimental & Physiological Variation

As stated, variation exists at all scales, both temporally and spatially: from individual ion channels, to the level of the cell, to tissue, to organ, and to organism. At the scale of ion channels, variation has been noted in the mRNA concentrations that are translated to functional ion channels (Gaborit et al., 2007). While it has been noted that mRNA levels do not translate directly to ion channel concentrations for numerous reasons (Edelman and Gally, 2001; Nattel et al., 2010), a link has still been demonstrated between mRNA levels and observable effects on the AP (Walmsley et al., 2013). There is also a substantial body of evidence for notable variation in cellular processes—in neuronal studies, maximal conductance of ion channels has been shown to vary substantially (Marder and Taylor, 2011; Goaillard et al., 2009; Schulz et al., 2006), both in theoretical and experimental studies.

As has previously been commented upon, there are notable differences in cellular APs depending the the spatial location on the cell—this is evident from variation between ventricular and atrial (and other) cardiac cells (Carmeliet and Vereecke, 2002), to transmural variation (Antzelevitch et al., 1991). Furthermore, temporal variation is also a common phenomenon (Walmsley et al., 2010). At the organ level, numerous factors have been cited as having notable effects on the AP (Taylor and Lipsitz, 1997). At the organismal level, different individuals react differently to different therapies (Kannankeril et al., 2010). After considering all these changes, there are still notable differences that can be attributed to gender, age, and experimental method (Yang and Clancy, 2012; Kurokawa et al., 2012).

A complete and comprehensive discussion of experimental variation is beyond the scope of this dissertation. However, mention shall be made for the experimentally observed variation that is of note for the models and experiments contained within this thesis. The complete gamut of experimental values is almost impossible to find—rather, some measure of the experimental range can be ascertained from the literature by the error values given, which represent the standard deviation of the results from the presented mean value.

Current	Location	Value (pApF ⁻¹)	Percentage Variation
I_{to}	Apex	29.6±5.7	±19.3%
	Base	16.5±4.4	±26.6%
$I_{K_s,\text{peak}}$	Apex	5.61±0.43	±7.7%
	Base	2.14±0.18	±8.4%
$I_{K_s,\text{tail}}$	Apex	1.65±0.21	±12.7%
	Base	0.85±0.19	±22.4%
$I_{\text{Ca,L}}$	Apex	-5.85±0.76	±13.0%
	Base	-7.17±0.63	±8.8%

Table 2.1: A summary of the results for the current densities of basal and apical ventricular tissue in human and canine myocytes and tissue, obtained from Szentandrásy et al. (2005).

2.5.1 Action Potential Variation

Collaborators from the University of Szeged have been able to obtain AP traces for ventricular tissue at pacing rates of 600ms and 1,000ms. These preparations are internally consistent—the trace for each preparation comes from a single sample (although the electrode recording the potential occasionally lost contact, and thus had to be reapplied, thus leading to the recording not necessarily coming from the same individual myocyte). These valuable data allow assessment of the intra-preparation variation in AP, and inter-preparation variation. Using data for APD₉₀ (arguably the most common AP metric), these data suggest an intra-preparation variability of ∼ 3.5%, and an inter-preparation variability of ∼ 10%.

However, these data come from a single laboratory—a full literature review provides a much greater range of values. From these results, it is possible to generate a range of APD₉₀ values that can be regarded as physiologically realistic. While many of these values come from tissue preparations, preliminary experiments with the Mahajan model suggest that there is little difference between cellular and tissue results for APD₉₀. The results of such a literature search gives the physiological range for APD₉₀ to be 142 – 185ms for a CL of 400ms, 160 – 220ms for a CL of 600ms, and 167 – 230ms for a CL of 1,000ms (Biagetti and Quinteiro, 2006; Szigligeti et al., 1996; Yan et al., 2001; Jung et al., 2011; Goldhaber et al., 2005; Wu et al., 2011, 2008b,a; Chen et al., 2006; Kirchhof et al., 2003; Eckardt et al., 1998; Zabel et al., 1997b,a; Kurz et al., 1993; McIntosh et al., 2000). Subsequent to these ranges being established and the populations being derived (see Chapter 5), further literature was discovered that could expand these ranges further, but not to such an extent that it was felt that the population would change dramatically (Wu et al., 2006).

2.5.2 Ion Channel Variation

Many experiments, aware of the added variation associated with differences in gender and age, pick the experimental test subjects to be as homogeneous as possible. Even with that, notable variations can be found. Fülöp et al. (2004) used experimental data to determine properties of $I_{\text{Ca,L}}$, and found (amongst other details) that the density of peak $I_{\text{Ca,L}}$ in human ventricular myocytes was $-5.5 \pm 0.4 \text{ pApF}^{-1}$ (±7.27%). Similar values were obtained by Li et al. (1999), with even greater variation reported for plateau $I_{\text{Ca,L}}$ (up to 18.2%). In the work of Fink et al. (2008), by fitting to experimental data, g_K was determined to be $0.5871 \pm 0.0503 \text{ pApF}^{-1} \text{ mV}^{-1}$.

Notable work has also been carried out in Szentandrásy et al. (2005), which examined the amplitude (and time constants) of several ion channel currents in human and canine tissue to study the inhomogeneities between basal and apical ventricular tissue—a summary of these results is given in Table 2.1. It can be seen that the individual results demonstrate significant variation, and variation between apical and basal values is often noteworthy.

The effect of gender is addressed in humans in Verkerk et al. (2005), and in rabbits in Sims et al. (2008), which also examines the effect of age. The data for humans is not statistically significant, but still shows consistent bias. For example, $I_{Ca,L}$ density in female ventricular myocytes is consistently greater than in male at all voltages (*e.g.* 129% at 0mV) and for I_{to} , female I_{to} density at 50mV is 84% of the male. The individual measurements in Sims et al. (2008) show up to 9.4% variation in individual measurements, but the gender difference can be far greater—from 22% in prepubertal rabbit ventricular myocytes, to 32% in adult myocytes extracted from the base of the ventricle.

MODELLING BACKGROUND

I can't be as confident about computer science as I can about biology. Biology easily has 500 years of exciting problems to work on. It's at that level.

(Donald Knuth, *Computer Literacy Bookshops Interview*)

Computational Modelling Literature Review Summary

3.1 Development

What follows is a summary of the progression and development of computational cardiac models. For further details of the models themselves, the reader is referred to the original papers, and for more in depth summaries of the development, the reader is referred to the reviews given in Noble and Rudy (2001); Noble et al. (2012); Noble (2011); Puglisi et al. (2004); Rudy and Silva (2006); Niederer et al. (2009).

The precursor to all computational models of cardiac cells was the model developed in Hodgkin and Huxley (1952). This model described the electrical activity of a giant squid axon. It described the ionic currents required to explain the change in membrane potential, using a model for each current of a series of activation and inactivation gating variables (details given in §??). This model was able to sufficiently model the AP of the neuron using only three ionic currents: a K^+ current, a Na^+ current, and a ‘leak’ current of other ions. It was further developed by Fitzhugh (1960), which even then recognised that, while the ‘truth’ of the model was not universally accepted, the model nonetheless was successful in reproducing experimental results. However, FitzHugh was able to demonstrate that, with the correct adaptations of the model equations, the output could be altered to reproduce the longer APs of cardiac cells.

The Hodgkin-Huxley model was hugely successful, and paved the way for the extension of the computational modelling approach to cardiac cells. Preliminary work was shown in Hutter and Noble (1960); Noble (1960), which presented an adaptation of the Hodgkin-Huxley model for the AP of cardiac pacemaker cells. The same 3 currents were used, with adaptations in I_K to reproduce the longer AP of cardiac cells. The model was subsequently refined and expanded to reproduce the AP of Purkinje fibre cells (Noble, 1962), taking into account experimental data demonstrating the existence of at least two K^+ currents (labelled I_K and I_{K1}) with the resulting change in K^+ permeabilities of the cell membrane (Hutter and Noble, 1960; Carmeliet, 1961; Hall et al., 1963).

This model was followed by a model designed to reproduce the AP of a ventricular myocyte (Krause et al., 1966). The Noble and Krause models were both based on the Hodgkin-Huxley model, with the Noble model being used as the seed for future developments in the computational cardiac modelling field. The next major refinement of the model came with that proposed by McAllister et al. (1975). In response to experimental data, this model greatly expanded the number of ion channels that were being modelled—the previous 4 ODEs of the Noble model were now replaced with 10. This included modelling the components of I_K separately as I_{Kr} and I_{Ks} , as well as incorporating a Ca^{2+} current based on experimental recordings from patch clamp experiments. This model, despite its success in reproducing experimental data, also contained an impressive flaw, in that it posited the slow conductance changes near the resting potential to an outward current, activated by depolarisation. In fact, the change was due to an inward current activated by hyperpolarisation (the so-called ‘pacemaker current’ (I_F)). Despite this flaw, the overall model remained sound, and iterations of the current continued through to DiFrancesco and Noble (1985), which was the first model to incorporate a formulation for the $\text{Na}^+ \text{-K}^+$ exchanger, and made most intracellular ion concentrations dynamics. It also managed to model SR Ca^{2+} release, and demonstrated the stoichiometry of the $\text{Na}^+ \text{-Ca}^{2+}$ exchanger had to be 3:1, not 2:1 as had previously been supposed—consequently, the resulting current from this exchange (I_{NaCa}) was incorporated into future models.

While this progress was still being made in the modelling of Purkinje fibre APs, a new focus was found in modelling the AP of ventricular myocytes. While this had already been achieved to some extent in Krause et al. (1966), the first widely used ventricular model was that proposed in the work of Beeler and Reuter (1977). This model was also the first to make more explicit mention of the internal calcium dynamics of the cell, by simulating the Ca^{2+} release from the sarcoplasmic reticulum. Of particular note in the further development of the field is the so-called Luo-Rudy model, first published in Luo and Rudy (1991). This model was originally designed to study arrhythmias in guinea pig ventricular cells, but has been subsequently developed for a wide variety of different tasks, and key components have been adapted into other models for other species (Shaw and Rudy, 1997a,c; Wagner et al., 1999; Viswanathan and Rudy, 1999; Garfinkel et al., 2000; Shannon et al., 2004; Mahajan et al., 2008). Specifically, the model was further adapted in two papers (Luo and Rudy, 1994b,a) to include dynamic intracellular ion concentrations, and $I_{\text{Ca,L}}$ was reformulated. Significantly, I_K was separated into the two constituent currents of I_{Kr} and I_{Ks} in Zeng et al. (1995), based on experimental evidence for this separation (Sanguinetti and Jurkiewicz, 1990). The Luo-Rudy model was also adapted to be able to model ischaemia by the incorporation of $I_{K\text{-ATP}}$ (Shaw and Rudy, 1997b) (further details of the modelling of ischaemia can be found in §2.4.1). A further significant advance came with Clancy and Rudy (1999), which for the first time incorporated Markov modelling into a cell model (Markov modelling is described in greater detail in §??).

Stern (1992) noted a short-coming of the Luo-Rudy model by its inability to reproduce the graded relationship between $I_{\text{Ca,L}}$ and the SR Ca^{2+} release—this was due to what was termed the ‘common pool’ model for Ca^{2+} . This can be overcome by introducing a compartmentalised system to model Ca^{2+} dynamics. This allowed for modelling of not only graded Ca^{2+} release (local $I_{\text{Ca,L}}$ influx causes local SR Ca^{2+} release, which spreads across the cell in a Ca^{2+} wave), but also predicted the phenomenon of Ca^{2+} sparks, which were observed experimentally in Cleemann et al. (1998). The model was subsequently revised and expanded by Shiferaw et al. (2003) to include SR load-release dependence, although on a purely phenomenological basis. This model has been used as the basis for more elaborate models, incorporating greater biophysical details, including 3D cellular architecture (Restrepo et al., 2008; Chen et al., 2009).

It should be noted that almost all currents in the models described above still use the same basic model form as that given in Hodgkin and Huxley (1952)—details and nuances have been added to some equations, and other equations have been formulated using entirely different methods (e.g. Markov modelling), but the underlying modelling philosophy has remained rather steady, and been found sufficient to the present day.

It is through this evolution of models from relatively humble beginnings that we have reached the point where we are today—computational models of cardiac systems can be used to model anything

from the subcellular to the full organ level, with specialisations depending on species, location and situation. In this thesis, focus is mainly devoted to the models presented in Shannon et al. (2004) and Mahajan et al. (2008). These are both models for rabbit ventricular myocytes, with the latter model being itself based on the former—they are both in turn based in large part on the Luo-Rudy model. However, it should not be thought that it is a direct step from the Luo-Rudy model to the Shannon model to the Mahajan model—there are numerous intervening steps (Zeng et al., 1995; Puglisi and Bers, 2001; Bassani et al., 2004).

Further developments in modelling are constantly being made. Work is also now being increasingly focused on tissue and organ simulations, and the pathologies that one encounters under such situations (Pitt-Francis et al., 2009; Arevalo et al., 2007). Such higher order simulations are computationally far more expensive, and some work has been conducted to investigate the specific effect of tissue level effects (Viswanathan and Rudy, 2000). Molecular simulations are being conducted, but due to their computational intensity, they are limited to ion channel investigations (Nekouzadeh and Rudy, 2011). Work is also ongoing on using bioenergetic considerations to model the system (Niederer, 2013). On a purely practical level, work is also increasingly being performed to standardise the computational tools used for simulation, to support reuse of code and replicability of results (Pitt-Francis et al., 2009; Mirams et al., 2013), and advances in the techniques used to perform the simulations are ongoing (Dangerfield et al., 2012).

3.2 Key Concepts

The model's purpose defines what variables are considered, and how these variables are determined. Some models (*e.g.* Restrepo et al. (2008)) define a certain section of the cellular mechanism as of interest, and thus the output is defined accordingly. However, most models are trained according to the membrane potential, and thus that is considered the primary output. In modelling the cell as an electrical circuit with the membrane considered as a capacitor, the instantaneous change in membrane potential is calculated according to

$$\frac{dV_m}{dt} = -\frac{1}{C_m}(I_{ion} + I_{stim}), \quad (3.1)$$

where C_m is the membrane capacitance, I_{ion} is the sum of all ionic currents in and out of the cell, and I_{stim} is the stimulus current, if applied, to initiate an AP. In experiments and simulation, the value of I_{stim} can vary, but it is usually at least 1.5 times the minimum value required to initiate activation (the activation threshold) (Sutton et al., 2000; Riccio et al., 1999; Ferrero et al., 2003b).

It should be noted that the membrane potential method can also be calculated according to an 'algebraic method', based on the charge conservation principle and the charge-voltage relation of a capacitor; identical results are produced by both methods (Hund et al., 2001; Rudy and Silva, 2006).

In biophysically detailed models of electrically excitable cells, most ionic currents are modelled according to:

$$I_X = g_X(\mathbf{x})(V_m - E_X), \quad (3.2)$$

where I_X represents the ionic current being modelled, $g_X(\mathbf{x})$ represents the conductance of the channel and E_X represents the Nernst potential, also known as the reversal potential of the cell. This is the potential at which there is no net ion flow through the channel, *i.e.* there will be no ionic current. The general form of E_X is explained in §???. $g_X(\mathbf{x})$ is current-dependent variable, and can be modelled as varying with time, voltage, extra-/intracellular ion concentration, *etc..*

3.2.1 Nernst Potential

Of key importance in mathematical modelling of electrically active cells is the *Nernst equation*. A full derivation is given in the appendix, but the key result is thus:

$$E_X = \frac{RT}{z_X F} \ln \frac{[X]_o}{[X]_i} \quad (3.3)$$

In the above equation, R represents the gas constant, z_X represents the valence of ion X , F represents the Faraday constant, and $[X]_o$ and $[X]_i$ represent the extracellular and intracellular concentrations of X respectively. The quantity of interest, E_X is the *Nernst potential* or *reversal potential*, and represents the value of V_m required to maintain the intra-/extracellular concentration ratio constant, *i.e.* to make the net ionic flux across the cell membrane zero.

When a channel is entirely selective, the reversal potential (which can now be thought of as the potential at which there will be no net flux of ions) is given by the Nernst equation for the specific ion. However, some ion channels are permeable to more than one type of ion, in which case their reversal potential for channel α is given by the *Goldman-Hodgkin-Katz equation*:

$$E_\alpha = \frac{RT}{F} \ln \frac{\sum_i^N P_{A_i^+} [A_i^+]_o + \sum_j^M P_{B_j^-} [B_j^-]_i}{\sum_i^N P_{A_i^+} [A_i^+]_i + \sum_j^M P_{B_j^-} [B_j^-]_o} \quad (3.4)$$

The above equation describes the situation for N different monovalent positive ionic species and M monovalent negative ionic species; different valencies complicate matters further. In it, E_α represents the reversal potential for the channel, *i.e.* the potential at which, with the given ion concentrations, no net electric flow will occur. The permeability of the membrane is given by P_X ; as with the concentrations, the terms have been split into positive (A_i^+) and negative (B_j^-) ionic terms.

3.2.2 Hodgkin-Huxley Current

As previously stated, the seminal work presented in Hodgkin and Huxley (1952) modelled currents as being composed of one or more activation/inactivation gates. It should be noted that the original paper was at pains to emphasise that this was not intended as a description of the actual, physical channel, but was to be used as is: as a mathematical equation that provides a fidelity to the experimental data. It is of note, however, that it is the case that the structure of the K^+ channel does consist of four identical subunits, which does correspond with the four gating variables required in the Hodgkin-Huxley formulation of the current.

Within the Hodgkin-Huxley framework, the current conductance can be modelled according to

$$g_X = \bar{g}_X m^a h^b, \quad (3.5)$$

where \bar{g}_X represents the maximum conductance through the channel, a and b are constants, m represents the activation gate and h the inactivation gate. In Hodgkin and Huxley (1952), a physical basis was given to m and h by describing them as proportions of ‘activating molecules’ and ‘inactivating molecules’, respectively—the conductance through the channel is thus proportional to the proportion of these molecules that are within and outwith the cell. The change in these variables are described according to

$$\frac{dm}{dt} = \alpha_m(1 - m) - \beta_m, \quad (3.6)$$

where α_m and β_m are functions of V_m . It can be noted that this is often expressed as

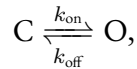
$$\frac{dm}{dt} = \frac{m_\infty - m}{\tau_m} \quad (3.7)$$

where $m_\infty = \frac{\alpha_m}{\alpha_m + \beta_m}$ and $\tau_m = \frac{1}{\alpha_m + \beta_m}$, and are the steady state value of m and the time constant, respectively.

3.2.3 Markov Models

The Hodgkin-Huxley formulation is computationally efficient, but does not represent a physical reality of the channel state. As such, it is poorly suited to model state specific processes, such as mutation effects or stochasticity (Adeniran et al., 2011). It also relies on the independence of the activation and inactivation processes—the formulation assumes these depend only on V_m . However, this assumption is not always valid: inactivation of I_{Na} has a greater probability of occurring when the channel is open (Bezanilla and Armstrong, 1977; Armstrong and Bezanilla, 1977).

To address these limitations, *Markov modelling* can be used (it should be noted that in the formalism presented here, it is not suited to modelling stochastic processes, but can be adapted to do so). Markov modelling works by assuming that the channel can exist in any one of n discrete states, *i.e.* it attempts to directly model the ion channel state. These states can be open, closed or inactivated, and there can be multiple types of each state. The simplest form is a two state system, such as



where k_{on} and k_{off} represent the transition rates between these two states—in cardiac modelling, these transition rates typically depend only on the membrane potential. The key requirement for a Markov model is the *Markov property*, which states that the transition to the next state depends only on the current state, and there is no cumulative history of the system that influences its future. Thus, if $x_i(t)$ represents the proportion of channels in state i at time t , and k_{ij} represents the transition rate from state i to state j , the transition rates for a system containing m different states may be modelled according to

$$\frac{dx_i}{dt} = \sum_{j=1}^m (k_{ji}x_j - k_{ij}x_i). \quad (3.8)$$

The conductance of the channels for a particular current is thus calculated by multiplying the maximum conductance by the proportion of the channels that currently exist in an open state. It should be noted that, when the transitions between states are independent, the Markov formulation devolves to the Hodgkin-Huxley formulation—for further details, see Rudy and Silva (2006).

3.2.4 Mono-/Bi-domain Equations

3.3 Computational Modelling of Variability

It is a handicap that is only recently being overcome that, in constructing cell models, the focus has been on fitting the model output to one particular value, whether this is the mean or some other measure. As such, these models are often poorly equipped to reproduce the variation that is seen in the original experimental data.

When modelling variation, it must be remembered once again that models are only useful up to the point of answering the question posed to them—taking a model further than its original purpose is useful only when this new purpose does not stray irrevocably from the original, and the original models assumptions and approximations remain valid. As such, reproduction of variation using existing computational models is fraught with difficulties when translating the results to the real system. For

example, Davies et al. (2012) showed that by allowing parameters describing peak ion channel conductance to vary, a wide range of possible values could be made to fit experimental AP, with peak conductance varying by factors of 0.1 to 7.43 of the original model's peak conductance value. However, this demonstrates one possible problem in simply fitting parameters: numerically, it may well be entirely accurate, but it may not represent physiological reality (experimental data for conductance variation implies a variation of as much as threefold (Schulz et al., 2006)).

As a tangent to this problem of maintaining the link between reality and model, it has been shown that, under particular conditions, a computational model can produce identical AP traces while using two vastly different input parameter sets. However, these models can then differ in other important regards; Sarkar and Sobie (2010) used two parameter sets for the same model to produce near identical AP traces, but very different data for $[Ca^{2+}]_i$. Obviously, if the model is required only to reproduce the AP, both models are entirely adequate. However, the problem is demonstrated further in Cherry and Fenton (2007) in a comparison between two different canine ventricular models: while both produce APs of similar morphologies, there are significant underlying differences, and these are reflected in different responses to certain conditions. Similar conclusions have been reached in Romero et al. (2011), and work has been made in finding some way of curating models according to their differences in response (Terkildsen et al., 2008; Cooper et al., 2011).

It is generally felt that a ‘good’ model should be able to reproduce a wide range of data. If a biophysically detailed model can reproduce a wide range of data, it gives us greater confidence that the underlying details of the model can be said to represent reality. By combining a consideration of the model response to different conditions with data regarding the model response to variation, a model’s accuracy and efficacy may be assessed, and new experimental directions suggested to either determine which of certain models’ hypotheses regarding cell mechanics is accurate, or to elucidate other questions raised.

Methods of determining the sources of variability in computational models can be divided into two arenas: stochastic variation, by which it is meant that stochastic, random properties are introduced into the model, and deterministic variation, by which it is meant that known variation is applied to the model to observe the resulting effect. These arenas are not mutually exclusive, and it is perhaps more useful to consider both methods as tools: the former is adapted for recreation of the actual physical environment, and the latter is adapted for mapping the input/output parameter space. For the purposes of this thesis, they will be discussed separately below.

3.3.1 Stochastic Modelling

Increasing effort has been focused of late on incorporating stochasticity into computational models, and using this to reproduce experimentally observed variation. Previously, the requirement for multiple simulations to determine the statistical properties of the model prohibited large scale use of such methods, but this restriction has diminished with increasing computational power. It should be noted at this point that stochasticity may be introduced to a model in more than one way—the two most common manners are to introduce stochastic differential equations to the model, or to introduce stochastic state transitions to a Markov model (if one is present). Heijman et al. (2013) were able to demonstrate that the latter approach produces results that more closely correlate with experimentally observed short and long term variability.

Tanskanen et al. (2005) introduced stochastic gating to Ca^{2+} dynamics, and were able to demonstrate the important implications of stochastic events in observable phenomena, in their case the occurrence of early after-depolarisations (for details of this pathology, see §??). Further work in Sato et al. (2009) demonstrated that inclusion of stochastics in I_{Ks} was able to reproduce chaotic occurrence of EADs (though it should be noted that this paper also demonstrated that many seemingly random events relating to EADs could rather be explained by model sensitivity to initial conditions leading to chaotic outcomes). Pueyo et al. (2011) and Lemay et al. (2011) showed that stochastic variation in ion channels, both in terms of channel conductances and channel numbers, has a measurable effect on APD

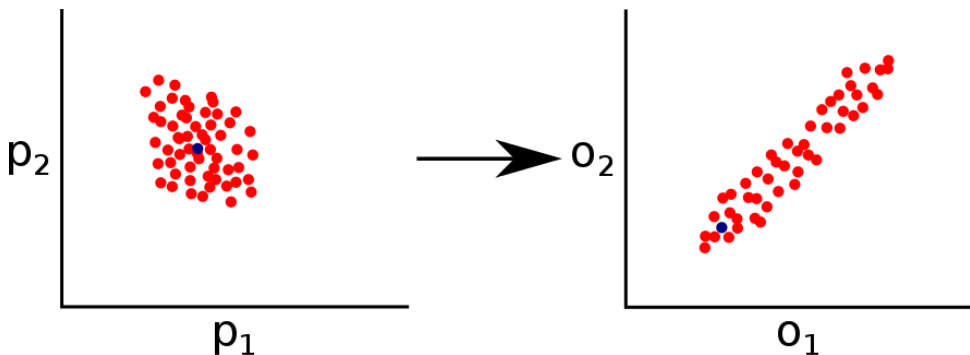


Figure 3.1: Illustration of the effect of possible parameter variation on model output. In this example, two given input parameters (p_1 and p_2) have a complicated effect on two measured outputs of the model (o_1 and o_2); one possible example data point is highlighted in blue. Based on a figure from Sarkar et al. (2012).

variation. However, in contrast to this, Sato et al. (2010) appear to demonstrate that the main cause behind APD variation is chaotic variation, and not stochasticity (though it is admitted that stochasticity could be a potentiating factor).

While such effects are masked by inter-cellular electrotonic interactions in tissue (Zaniboni et al., 2000; Heijman et al., 2013), the effects could become more noted under some pathological conditions, e.g. intercellular uncoupling due to acidosis. It should also be noted that there is a spatial scale beyond which the ‘smoothing’ effects of tissue electrotonic interactions are reduced (Xie et al., 2007; Sato et al., 2009). However, both experimental and computational studies of sino-atrial node cells indicate that stochastic fluctuations remain important for observed variation in beat rate (Ponard et al., 2007).

3.3.2 Parameter Sensitivity & Fitting

The interplay between input parameters and output parameters is decidedly non-linear, and the effects of changes in one, or many parameters, cannot easily be predicted (Sarkar et al., 2012); an example of these problems is shown in Fig. 3.1. The previous modelling paradigm has been to consider the model as occupying a single point in the input/output parameter space—this is represented by the blue point in the figure. However, it is becoming increasingly prevalent to consider variation in both input and output parameter space, represented by the cloud of red points in the figure. However, the mapping between the input and output spaces is non-linear, and there is no guarantee that a point in the middle of the input cloud translates to a point in the middle of the output cloud, or even if the clouds are the same shape (as shown in the figure). This point is worth restating: due to the complicated interactions between input components, the effect of a specified change in one input parameter may produce an entirely different effect if other input parameters are altered. Furthermore, the problem increases in complexity as one considers more input parameters and output metrics.

There are many different ways to try and elucidate this input/output mapping. One method is *parameter sensitivity analysis*, which varies one individual input parameter at a time to elucidate the effect this parameter has on a given set of output metrics, and expressing this effect in a quantitative manner (e.g., $\Delta_{\text{output}}/\Delta_{\text{parameter}}$).

The initial step in this process (and with all following processes) is to define the range over which the sensitivity of a parameter is to be assessed. There are numerous ways to define this range. In some cases, a range based on available values from the literature is appropriate, and sufficient data are available for a range to be estimated. When such an approach is not appropriate, an arbitrary range can be defined, often in terms of a percentage range, e.g., $\pm 15\%$. Alternatively, a log-normal distribution can be used (the range will equally represent halving and doubling the parameter). These three options represent the most common methods, but other methods are possible.

This work successfully indicates which parameters are most directly responsible for which output

metric (Nygren et al., 1998; Romero et al., 2009a, 2010; Corrias et al., 2011; Romero et al., 2011). This method (and many of the following methods) has obvious extensions to computational predictions for pharmacological ion channel block.

However, biophysically detailed cell models are highly inter-connected, through membrane channel currents' dependence on V_m , ion concentrations *etc.*, and the resulting non-linear interactions are often missed by a single dimensional parameter sensitivity analysis. Thus, with increasing computational power available, more work is being conducted to examine the multi-dimensional parameter effects within a model.

However, as the number of parameters being varied increases, the size of the space increases exponentially. As such, to minimise the computational cost, it is common to survey a sample of the parameter space. There are many ways to extract such a sample, the simplest being a simple random sampling technique. Alternative methods include stratified sampling and Latin hypercube sampling, which attempt to ensure that the parameter space is evenly tested (McKay et al., 1979).

An elegant method to extract the required data from this multi-dimensional sample was demonstrated in Sobie (2009). For a parameter space surveying the effects of p parameters, a sample of size n parameter sets (where the complete size of the space can be represented by N parameter sets) is selected. Models using these parameter sets are simulated, and the result of these models is recorded according to m output metrics (*e.g.*, APD₉₀, [Ca²⁺]_i^{syst}, *etc.*). Before further analysis, the data are mean-centred and normalised by the standard deviation, *i.e.* $x_{\text{new}} = (x_{\text{orig}} - \mu_x)/\sigma_x$, where x_{new} and x_{orig} are the new and original data values, and μ_x and σ_x are the population mean and standard deviation for the data, respectively.

The data are now organised into matrices: the input parameter data are organised into an input $n \times p$ matrix (\mathbf{X}), and the output metric data are organised into a $n \times m$ output matrix (\mathbf{Y}). Each column thus represents one of the input parameters/output metrics, and each row represents one of the parameter sets simulated, and the resulting output. Multivariable regression analysis is then used to derive the effect matrix \mathbf{B} such that

$$\mathbf{XB} = \hat{\mathbf{Y}} \approx \mathbf{Y}, \quad (3.9)$$

where $\hat{\mathbf{Y}}$ is a close approximation of \mathbf{Y} . The result of this analysis is the $p \times m$ matrix of regression coefficients, and has been utilised as each row representing the effect of a given input parameter on the numerous output metrics, and each column representing the effect of various input parameters on a particular output metric. This has been shown to be successful in predicting the output of a new parameter set (Sobie, 2009), implying the underlying assumption that the relations remain linear is relatively well-founded while ion concentrations are not varied too much (Sobie, 2009; Sarkar and Sobie, 2010). The method has also been used to replicate the results of the original parameter sensitivity analysis, *i.e.* to demonstrate the effect of a series of input parameters on a given output metric. This method has been used to investigate the effect of such variability on the repolarisation reserve (Sarkar and Sobie, 2011), and also to investigate the possible range of variability in a given set of parameters given the experimentally observed variation in certain output metrics by reversing the regression analysis (*i.e.* calculating \mathbf{B} such that $\mathbf{X} \approx \hat{\mathbf{X}} = \mathbf{YB}^{-1}$) (Sarkar and Sobie, 2010).

This method is an elegant method of investigating the effect of multiple parameter variation on multiple model outputs. However, it should be noted that this method still, to some degree, reduces the multi-dimensional parameter variation to a single-dimensional result. The interactions are still tested, and are thus present in an intrinsic sense in the resulting matrix \mathbf{B} . Extracting these interactions in an explicit manner is not so simple, and thus the results of the multi-dimensional parameter variation are, in effect, reduced to the result of a single-dimensional parameter variation.

Despite this apparent limitation, the conclusions reached by this method are often robust. Furthermore, the methodology has been shown to be adaptable to stochastic simulations—Heijman et al. (2013) used the methodology to examine variation in maximal conductance in ion channels when stochasticity was also included. This was used to determine effects that were not apparent when single ion channel stochasticity was tested.

An alternative method is to take advantage of so-called genetic algorithms to tune models to given experimental data. This has been used to provide single parameter sets, and adapt models to new data (Kherlopian et al., 2011). It has also been successfully adapted to find multiple parameter sets that reproduce experimental data, where the parameter sets are not considered part of a continuum of models, with minor variations accounting for the different sets (Achard and De Schutter, 2006; Syed et al., 2005). While that work reproduced a single set of experimental data, it is not unreasonable to expect this method to be easily adapted to reproduce a range of experimentally observed values.

The effects of multiple parameter variation can also be addressed via a comprehensive parameter sweep (this approach has also been referred to as a database method). The guiding principle of such a method is to comprehensively examine a given parameter space—for example, if the effect of variation in p different parameters is being investigated, the model is simulated for every single possible combination of these parameters. If there are q different possible values for each parameter, this leads to p^q different simulations that would be run, unless measures are taken to limit this by some means (such as by taking advantage of experimentally demonstrated correlations between parameters (Schulz et al., 2006)). While this method can be computationally expensive, such a parameter search is also often embarrassingly parallel, and thus can be performed rapidly in real-time using such facilities as the Nimrod computing system (Abramson et al., 2000, 1997, 2009, 2010).

The parameter sweep method was first used in Prinz et al. (2003), which applied variation to eight maximal conductances in a model of a lobster stomatogastric neuron to generate a database of about 1.7million different models, and then classified these models according to their activity pattern. This database could then be searched for different models that satisfied a prescribed set of criteria. Similar work has been carried out to investigate CICR (Sobie and Ramay, 2009). Indeed, there is increasing traction for replacing the previous paradigm of a single parameter set with a single model with a parameter ‘space’ for a model, leading to a population of models (Davies et al., 2012; Taylor et al., 2009; Prinz et al., 2003; Marder and Taylor, 2011). Indeed, one of the most notable works in relation to this thesis is the work of (Britton et al., 2013), where a possible population was defined for study. To reduce the computational load, Latin hypercube sampling was used to sample from this parameter space, producing a population of $\sim 10,000$ models, which was then compared to experimental data to refine this to a population of 213 models that matched experimental data. This population was then able to successfully reproduce the effects of I_{Kr} drug block.

It is of note, and one of the topics addressed in this thesis, that the progress in investigating parameter variation is in its infancy, and thus it is not surprising that some aspects are not readily addressed. Specifically, while model populations have been used to recreate experimental variation, little investigation has been done on the population itself, *i.e.* what relations exist between the parameters involved in these individual models. Furthermore, while work has shown how the effects of disease and other pathological conditions can be recreated by simultaneous variation of input parameters, this has not yet been linked to the variation already in evidence under physiological conditions. This may be considered the main thrust of this DPhil thesis: to bridge the gap between recreation of physiological evidence, and the investigation of the changes inherent in disease states.

3.3.3 Model Populations

COMPUTATIONAL METHODS



Though this be madness, yet there is method in 't.

(Hamlet, Act 2, Scene 2)

This chapter presents the computational methods that are used throughout this dissertation—it provides both a summary of those techniques that are used generally throughout this thesis, and also those techniques that are specific to particular chapters. The background to the representation of multidimensional data will be given, with the techniques used explored. The computational models and frameworks used will be expanded upon, and techniques used in their simulation will be mentioned. Details will be given regarding model adaptation to ischaemic conditions. The tools used in exploring the parameter space will be explained, and their integration with other models commented upon. Methods used to calculate particular biomarkers used in this dissertation are given. This chapter serves to collate the computational methods used in this dissertation, and analysis based on these methods is found in other chapters.

4.1 Representation of Multi-Dimensional Data

Comprehensive investigation of the effect of variation into multiple different parameters in a model can be thought of as an investigation into a multi-dimensional parameter space: each parameter corresponds to a single dimension. A key problem to be overcome when examining multi-dimensional parameter spaces is how to represent the associated data in a manner that is both meaningful and comprehensible. It is only possible to ‘directly’ map the effect of up to two dimensions on a given marker using a contour plot. As such, to visually represent higher dimensional spaces, without losing any of the data in the space, may be thought of as finding a way to represent these spaces in only two dimensions. The method used here is called *clutter-based dimension reordering*, and has been employed in studying the effect of variation on the electrophysiology of neurons (LeBlanc et al., 1990; Peng et al., 2004; Peng, 2005; Taylor et al., 2006).

The key aspect of this is the method used to render higher dimensional spaces in two dimensions, which can be thought of as a form of linear projection. Linear projection, from n dimensions to one or two dimensions, is a relatively simple affair with finite data sets, by rearranging the data, and giving each point in the n dimensional a unique point in a 2 dimensional space that has the same number of points contained within it. This is much like slicing a cube, and placing the resulting squares sequentially next to each other. Here, however, the ‘slices’ can exist in higher dimensions, but

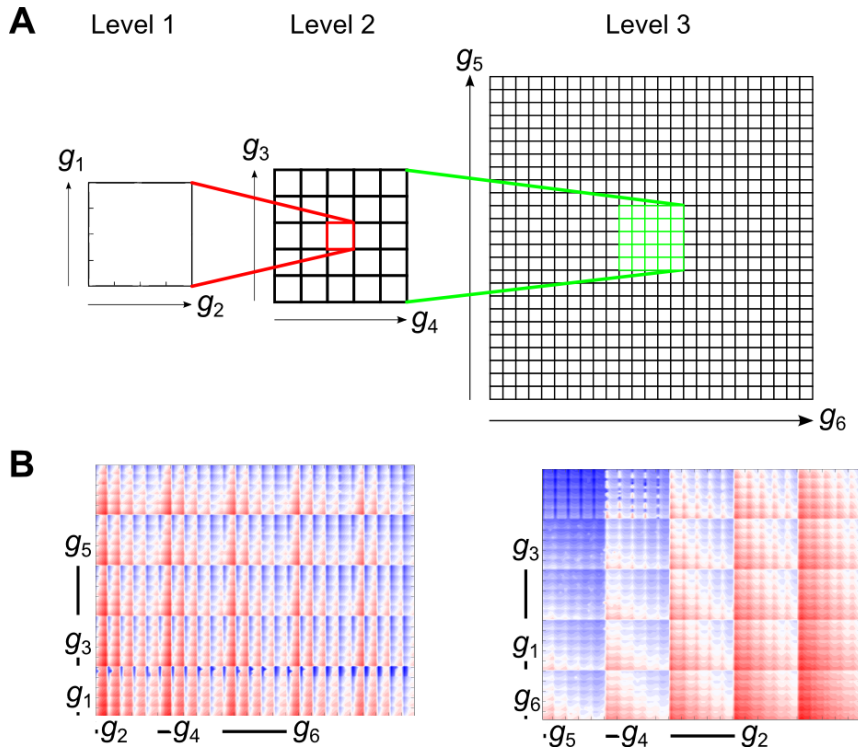


Figure 4.1: (A) The effect of two ‘low order’ conductances (g_1 and g_2) are plotted in a contour plot, with all other conductances set to their control values. This plot is then embedded in a larger grid spanning two ‘medium order’ conductances (g_3 and g_4). For each value of $g_{3,4}$, the $g_{1,2}$ plot is repeated for the respective values. This process is repeated to represent the two ‘high order’ conductances (g_5 and g_6). (B) Example showing a random stack order (left), versus an optimised stack order (right) for the same variable.

continuously slicing the dimensional space iteratively reduces the dimensionality of the space until it can be visualised in two dimensions.

The general form of projection, to give each entry in an n dimensional space (represented by (x_1, \dots, x_n)) a unique point (represented by x'_i) in 1D space, is given by

$$x'_i = \sum_{i=1}^n \left((x_i - 1) \prod_{j=i-1}^i N_j \right) + 1, \quad (4.1)$$

which returns a value between 1 and N , where N is the total number of data points; the number of data points in each dimension is given by N_i . A two dimensional representation can be constructed by splitting the total number of dimensions in two, and treating each separately as above.

A visual representation of this projection process, ending in a two dimensional space, is given in Fig. 4.1A—the process thus illustrated is referred to as *dimensional stacking*. In the instance illustrated, two of the conductances being varied are chosen at random (g_1 and g_2), and with all other parameters set to their minimum value, the effect of the variation of g_1 and g_2 on a particular output metric of interest is plotted using a contour plot; this is Level 1, and is referred to as the lowest level in the dimensional stack. Next, two other conductances are chosen (g_3 and g_4), and the original Level 1 plot is repeated for each combination of these two parameters. Each of these plots is arranged in a manner reflecting the variation in g_3 and g_4 to form Level 2 of the stack, *i.e.* the Level 1 plot that has g_3 and g_4 at their minimum values is at the bottom left of the Level 2 grid, and the Level 1 plot that has g_3 and g_4 at their maximum values is at the top right of the Level 2 grid. This process was then repeated for the last two conductances.

However, the so-called ‘stack order’ (which conductances are plotted as low order and which conductances are plotted as high order) is initially a random choice. The next stage in CBDR is the optimisa-

tion of the stack order. This is done by minimising the absolute difference between each point and its four neighbours in the x and y planes; in more general terms, it is those points that are separated by one step in one dimension. An alternative definition of ‘neighbour’ is those that are separated by one step in multiple dimensions—in two dimensions, this would thus include the diagonally connected points. However, Taylor et al. (2006) demonstrated that the connectivity of the space is not adversely affected by using the more restrictive definition. This will be expanded upon further in §5.4.2. This process of minimisation is done by comparing the score of the current stack order with the score of the neighbouring stack orders (which are those stack orders that are identical save for the swapping of two conductances). If one of the neighbouring stack orders has a lower score than the current stack order, the neighbour’s order is adopted, and the process is repeated. While this would technically lead only to a local minima in the stack order space, in practice it is rare for the global minimum to be found (this is confirmed by performing multiple searches, each for a different start order).

The results of such an optimisation process is to ‘smooth’ the image, as shown in Fig. 4.1B. This means that those parameters with a lesser effect on the measured biomarker are assigned as ‘lower order’ conductances (Level 1), while those that have a greater effect are ‘higher order’ (Level 3). By rearranging the stack order to this optimum stack order, it is thus easier to discern the patterns within the data, both in terms of which parameters have the greatest effect, and also (by virtue of the complete representation of the parameter space) details of the interactions between the parameters.

4.2 Computational Models & Simulation Techniques

Two models were used in this thesis: both are designed to utilise biophysically detailed formulations of key currents to reproduce the action potential of rabbit epicardial myocytes. The first is presented in Shannon et al. (2004) (henceforth referred to as the Shannon model/framework), and the second is that presented in Mahajan et al. (2008) (or the Mahajan model/framework).¹ The Mahajan framework is itself based on the Shannon framework, with alterations made to the L-type Ca^{2+} current, intracellular Ca^{2+} cycling, $\text{Na}^+-\text{Ca}^{2+}$ exchanger and channel distributions; these alterations were made to allow the model to better fit the provided training data for AP and Ca^{2+} -handling dynamics at rapid pacing rates.

The frameworks for both models were downloaded from the CellML repository (Lloyd et al., 2008)), with the Shannon framework corrected according to Shannon et al. (2012). These CellML files were then converted to C++ using the Cellular Open Resource software (Garny et al., 2003, 2009), and all simulations were performed using an ordinary differential equation solver with adaptive time-stepping (CVODE), with relative and absolute tolerances set to 10^{-7} and 10^{-9} , respectively. Both frameworks, in describing the AP of ventricular epicardial myocytes, require stimulation by an external source for the development of an AP. This is provided by a stimulus current (I_{stim}), applied appropriately to pace the cell at a given cycle length (CL). This takes the form of a 3 ms step function current, and is initially the same as is provided with the CellML file.

4.2.1 Nimrod Distributed Computing Grid

While the CVODE solver dramatically reduces simulation time when compared to a Forward Euler ODE solver, when investigating parameter spaces, the sheer number of simulations that have to be run can quickly escalate dramatically. However, parameter space investigation is an embarrassingly parallelisable problem, *i.e.* there is no communication between each individual simulation used to

¹It should be noted that, according to the previous dominant modelling paradigm, these are individual models. However, as it is one of the main driving forces of this thesis to replace a single model with a population of models, it is useful in the context of this dissertation to think of these two papers as providing *frameworks* on which to base model populations, rather than as individual models.

```

parameter x float range from 1 to 10 step 1;

task main
    copy param-search.exe node:./
    copy param_var.sub node:./
    node:substitute inputfile.sub inputfile
    node:execute param-search.exe
    copy node:output.dat output.${x}
endtask

```

Code Excerpt 4.1: *Example of plan file used from the Nimrod ‘root’ to determine Nimrod execution. In this instance, after copying the executable param-search.exe and the substitution file inputfile.sub to the node, the Nimrod/G platform performs the substitution and the execution, before copying the resulting output file output.dat from the node back to the root.*

```

// Declare the file parameter to read the data
std::ifstream params;
// Open the file
params.open("inputfile");
// Check the file is open
assert(params.is_open());
// Push the value that it reads from file into the variables
params >> x;

```

Code Excerpt 4.2: *Excerpt of C++ code required for resulting executable program to be able to perform substitution as per the plan file shown in Code Excerpt 4.1.*

investigate the space, and thus, given the correct tools, it is a relatively simple matter to parallelise the search. To this end, the Nimrod/G distributed computing grid (Abramson et al., 2000, 2010) is used. Developed by the Monash eScience and Grid Engineering Laboratory, this system permits a correctly written program to be run in parallel across multiple resources. While the use of this tool will be expanded upon only insofar as it furthers the goal of this thesis, it must be remembered that this presents a powerful option for many possible problems (Abramson et al., 2011, 2009).

Of note for this dissertation is the ability to copy an executable program from the ‘root’ to one of several ‘nodes’—the exact number of nodes available depends entirely on the resources available to user. The results of the simulation are then copied from the node back to the root, and saved according to instructions provided in a given *plan file*, an example of which is given in Code Excerpt 4.1. To perform the substitution in the manner described in this way, the executable must be prepared to accept this input—an example of C++ code that produces such an executable is shown in Code Excerpt 4.2.

It should be noted that there are many ways to skin a cat, and it is possible to pass parameter values directly to the executable using the appropriate command line syntax.

The Nimrod/G platform is a powerful tool, but it must be remembered that it provides only a tool, and the means of analysis are still within the hands of the user. With regards this thesis, this presents itself in the choice of the parameters being varied. It can be noted from other analyses of variation and variability in §?? that the extent of variation that has been proposed can vary across a huge range. However, in performing the comprehensive parameter sweep proposed in this work the sheer volume of data generated must be borne in mind. To that end, the number of parameters to be varied, and the extent of their variation, is chosen to reflect the best trade-off between:

- Resolution of the parameter space,
- Breadth of the parameter space,
- Number of varied parameters,
- Volume of data generated.

The volume of data being generated in itself is not an issue *per se*, but rather an indication of how many data can be *usefully* generated. The dimensional stacking mentioned earlier is of use only in so far as the visual representation remains comprehensible—a dimensional stack loses utility when it is not possible to keep some mental track of what the relevance of each parameter is.

4.2.2 Parameter Space Simulations

The first stage in this thesis is to (a) examine the effects of simultaneous variation in multiple parameters on model output, and (b) determine which of those models amongst those simulated produce output that matches the experimental literature, thus producing a population of models to reproduce the experimental variation.

Internal K⁺ concentration ($[K^+]_i$) was unclamped, and variables introduced to alter the peak conductances of six different ion channels (the reasons for varying these parameters specifically will be given in §5.2).

The equations representing ion flow through ion channels (and the associated current) is mostly given according to Eq. (3.2). However, even when the formulation of the model is more complicated, *e.g.* a Markov model, an important consideration at this stage is the *compartmentalisation* of the model, which refers to whether there is a spatial subdivision of the ion channel distribution in the cell (see also §??). Both Shannon and Mahajan frameworks are, for the main part, non-compartmentalised models. The reason this is of note here is due to the consequent physiological meaning of altering the peak ion channel conductance (g_X). As there is no spatial distinction in the cell model, any changes in g_X can be thought of as a change in (a) the peak conductance of an individual ion channel, or (b) a reduction in the total number of ion channels within the cell; mathematically, the two are equivalent.

Among the ion channel conductances being varied is the for the transient outward current (I_{to}). However, in both Shannon and Mahajan frameworks, I_{to} is composed of two components: a fast and slow activating component ($I_{to,f}$ and $I_{to,s}$, respectively)—for further details, see §??. To thus model variation of I_{to} within these frameworks, a scaling factor not present in either framework was introduced (g_{to}), which was applied to the summation of $I_{to,f}$ and $I_{to,s}$. Individual references to $I_{to,f}$ and $I_{to,s}$ (beyond those equations required to directly calculate the current) are not present, and thus replacing references to ($I_{to,f} + I_{to,s}$) with I_{to} makes no difference to the end result.

The purpose of the simulations examining the parameter space was to elucidate the model’s ‘steady state’ behaviour. As such, it was felt that an extended simulation time was appropriate, to allow the model to fully ‘relax’ to the behaviour that would characterise the framework’s response to a given parameter set. Initial simulations conducted using COR and the original CellML file of the Mahajan framework indicated that changes to the AP would be complete within 750 s of simulation, given changes in the parameter set that be included in the eventual search. On this basis, initial simulation time was set to 1,000 s, with data recorded for the last two stimulated APs. Each model output was checked for steady state by comparing corresponding data points for the last two data points: the cell was considered to be in steady state if the difference for each data point in the AP was less than 5% of the difference between the maximum and minimum AP values for the last AP. In common with the preliminary tests, steady state was often reached within the initial simulation time. For those models where steady state was not reached, and yet cell excitation was present, simulation was continued until steady state was reached.

	g_{to}	$g_{\text{Ca,L}}$	g_{Kr}	g_{Ks}	g_{Ki}	g_{NaK}
Shannon	+30%	+0%	+0%	-15%	-30%	+15%
Mahajan	+0%	+75%	+30%	+75%	+15%	-30%

Table 4.1: Details of the variations in given peak ion channel conductances from originally provided values for the model for the Shannon and Mahajan populations that produce APD_{90} closest to the population mean for CLs of 400 ms, 600 ms, and 1,000 ms.

4.2.3 Ischæmia Simulations

The model populations determined using the methodology described in the previous cell were entirely appropriate for their task—reproduction of the normal, electrophysiological AP. Consequently, to investigate the changes involved in using model populations in studying ischæmia, adaptations must be made. As was mentioned in §2.4.1, much work has been done to allow accurate computational assessment of ischæmia, and thus the frameworks were adapted to allow the models to reproduce the symptoms of ischæmia.

The first stage was to define a new ‘model’ model with which to train the new adjustments (the original models were not in the defined populations—for further details, see the results presented in §5.4.1). To this end, the model within the populations that produced the value for APD_{90} closest to the population mean at all previously simulated CLs (400 ms, 600 ms and 1,000 ms) was selected. All subsequent single model simulation and analysis was performed using this model (Table 4.1). Using this new model, the value of I_{stim} is then retrained—Sutton et al. (2000) demonstrated the possible important implications for I_{stim} on calculated ERP. The new value of I_{stim} is designed to be 1.5 times greater than the minimum value that causes cell excitation (after 3 ms application). Finally, the cell is simulated for an extended previous time period, with the resulting model parameters (for such details as ion concentrations) then being fixed. This was done to try and ensure that the population, prior to ischæmic conditions, would have conditions that would be most appropriate for the defined population, rather than for a model that is no longer included in the population.

With these considerations complete, the model was subsequently adapted to recreate ischæmic conditions. The mechanisms used were mostly in common with those from Rodríguez et al. (2006), with the addition of alterations in the Na^+ -handling system of the cell. The changes associated with ischæmia are summarised in §??, and are here modelled according to:

Anoxia: Activation of $I_{\text{K-ATP}}$ channels to 0.8% full activation, and inhibition of I_{NaK} by 30%.

Hyperkalæmia: Increase in extracellular K^+ concentration ($[\text{K}^+]_{\text{o}}$). Associated with this is an increase in $[\text{Na}^+]_{\text{i}}$.

Acidosis: Decrease in peak conductance of I_{Na} and $I_{\text{Ca,L}}$ by $f_{\text{inhib}} = 25\%$.

For all conditions, their values are varied independently to allow exploration of the ischæmic parameter space. In addition to this, the values are varied linearly from their ‘normal’ conditions to their ‘ischæmic’ conditions to allow approximation of evolution of the population response during ischæmia; this is in common with Rodríguez et al. (2004).

The model of $I_{\text{K-ATP}}$ used here is common in its overall structure to that used in Michailova et al. (2007), itself inherited from Michailova et al. (2005), and is expressed according to:

$$I_{\text{K-ATP}} = f_{\text{K-ATP}} g_{\text{K-ATP}} \left(\frac{[\text{K}^+]_{\text{o}}}{[\text{K}^+]_{\text{o,normal}}} \right)^{0.24} (V_m - E_{\text{K}}), \quad (4.2)$$

where $f_{\text{K-ATP}}$ represents the fraction of $I_{\text{K-ATP}}$ channels activated, $g_{\text{K-ATP}}$ represents the peak ion channel conductance and $[\text{K}^+]_{\text{o,normal}}$ represents the pre-ischæmic value of $[\text{K}^+]_{\text{o}}$ (which is considered to be 5.4 mM); the other values in the equation are as defined previously. It should be noted that this is a simplified version of the Michailova formulation; for simplicity, terms regarding the regulation

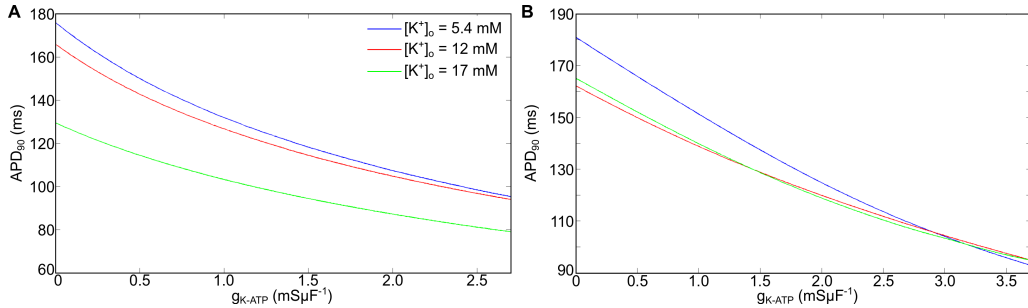


Figure 4.2: The effect of varying the value of $g_{K\text{-ATP}}$ (with $f_{K\text{-ATP}} = 0.8\%$) on APD_{90} for Shannon (A) and Mahajan (B) models. The effect is charted against normal conditions, and two possible ischaemic concentrations of $[K^+)_o$.

of the channel by changing concentrations of ATP and ADP are implicitly included in the value for $g_{K\text{-ATP}}$.

As has been mentioned in §??, the ‘spare channel hypothesis’ suggests that full activation of $I_{K\text{-ATP}}$ is not necessary, and does not occur, during ischaemia, with $f_{K\text{-ATP}} = 0.8\%$ being suggested as a reasonable degree of activation. Coupled with this degree of activation is the value assigned to $g_{K\text{-ATP}}$, which is thus trained to produce a similar value to other forms of the current at equivalent degrees of ischaemia. Further to this, preliminary analysis was performed to examine the effects of varying values of $g_{K\text{-ATP}}$ on both different models—the results are shown in Fig. 4.2. As can be seen, the models respond differently to the value of $g_{K\text{-ATP}}$ used. On the basis of this result, and in the interests of maintaining consistency with prior work, a value of $g_{K\text{-ATP}} = 2.61 \text{ mS}\mu\text{F}^{-1}$ was used.

The extent of increase in $[K^+)_o$ due to ischaemic hyperkalæmia is subject to debate—prior work tends to put the increase to a value of $\sim 12 \text{ mM}$. However, $[K^+)_o$ is a remarkably variable quantity, not only with regards its ‘ischaemic’ value, but also with regards its ‘normal’ value. As such, while $[K^+)_o, \text{normal}$ is set to 5.4 mM and $[K^+)_o, \text{ischæmia}$ is set to 17 mM , the parameter space for $[K^+)_o$ is also explored.

The value for $[Na^+)_i$ is clamped, and the change (with fully ischaemic conditions representing a 30% increase) imposed at the start of the simulation. Inhibition of ion currents (I_{Na} , $I_{Ca,L}$ and I_{NaK}) is achieved in the same manner as in the earlier parameter space search: direct reduction of the peak conductance g_X .

The simulation protocol is to (i) impose the relevant conditions directly to the model, (ii) stimulate the cell at a CL of 600 ms for 10 APs, (iii) record the data for the last AP, and use these data to calculate the required biomarkers. While preliminary simulations with the Shannon model indicated that the broad strokes of the model response are achieved within this timeframe, it can be noted that some models are sensitive to simulation duration, especially within the Mahajan population. However, to consider further simulation time worthwhile would be misleading. It must be remembered that these models, and the changes imposed upon them to reproduce ischaemia, are approximations, and they are most suited to short-term simulations—neither model framework is designed to reproduce the complicated effects of the medium- to long-term effects of ischaemia. As such, the simulation duration is designed to reproduce most faithfully the short-term impacts of ischaemia.

4.3 Biomarker Calculation

Biomarkers represent a means of quantitatively comparing different APs, and with the large volumes of data generated by parameter searches and model populations, a means of automating the analysis of model response is vital. For this reason, biomarkers present a valuable tool to compare data with previous experimental data from the literature. While many biomarkers are common throughout the

literature, some are poorly defined. As such, the following defines the terms as used in this dissertation.

V_{rest} is defined as the value of V_m immediately prior to application of I_{stim} —due to the lack of any leak current in these models (due to being ventricular myocyte models), this is synonymous with the minimum/diastolic value of V_m during the AP. Similarly, V_{max} is defined as the maximum value of V_m during the AP. (dV_m/dt) is the rate of maximum membrane depolarisation, and corresponds to a measure of the rapidity of the upstroke of the AP. It should be noted that (dV_m/dt) is directly proportional to the square of the conduction velocity of the AP in tissue (Hodgkin, 1954; Kléber and Rudy, 2004; Walton and Fozzard, 1983; Tasaki and Hagiwara, 1957).

The plateau membrane potential (V_{plat}) is defined as the point at which (dV_m/dt) reaches its maximum value (while still remaining greater than 0) after the initial upstroke. Thus, in an AP with a spike and dome morphology, it corresponds to the maximum value of V_m after the initial upstroke. AP duration (APD_X) is one of the more common AP biomarkers, but suffers from being relatively poorly defined, at least to the extent that there can be confusion about the specific definition while the broad strokes of the definition are agreed upon. Here, APD_X is defined as the time interval between the point of $(dV_m/dt)_{\text{max}}$ and the point at which V_m is repolarised by $X\%$ (*i.e.* where V_m is less than or equal to $V_{\text{rest}} + X(V_{\text{max}} - V_{\text{rest}})$).

The effective refractory period (ERP) and post-repolarisation refactoriness (PRR) are also measured, where PRR is defined as $\text{ERP} - \text{APD}_{90}$. In tissue, ERP is defined as the length of time required for the tissue to become excitable after excitation; however, such a definition is not able to be used in ventricular cell models where a stimulus current is applied. As such, the method used to calculate ERP here is the same used in Tice et al. (2007); Romero et al. (2009b); Trénor et al. (2007); Pandit and Jalife (2013), where the time interval between activation and the product of the h and j inactivation gates of I_{Na} equalling 0.012 ($h \cdot j_{\text{crit}}$) is used as a proxy. This method is used due to the importance of I_{Na} during the upstroke of the AP, with the rationale that while I_{Na} is still inactivated, the cell can still be regarded as refractory. $h \cdot j_{\text{crit}}$ is corroborated as being a valid value by confirming that $t(h \cdot j_{\text{crit}} = 0.012) \approx t(\text{APD}_{90})$ under normal conditions, *i.e.* under normal conditions, $\text{ERP} \approx \text{APD}_{90}$.

Biomarkers for $[\text{Ca}^{2+}]_i$ were also calculated. $[\text{Ca}^{2+}]_i^{\text{sys}}$ and $[\text{Ca}^{2+}]_i^{\text{dia}}$ were the systolic and diastolic values of $[\text{Ca}^{2+}]_i$, respectively, and the difference between these two values is referred to as the calcium transient (CaT). Finally, the calcium transient duration (CTD_X) was defined in an analogous manner to APD_X .

For reasons detailed in the results presented in §??, biomarkers were also required that used the total data available from the AP. To this end, a normalised root mean square deviation measure was defined according to

$$M_{\text{NRMSD}} = \frac{1}{M_{\text{max}} - M_{\text{min}}} \sqrt{\frac{\sum_{j=1}^N (M_{\text{combination}}(j) - M_{\text{original}}(j))^2}{N}}, \quad (4.3)$$

where M_{max} and M_{min} are the maximum and minimum V_m or $[\text{Ca}^{2+}]_i$ values for the original model, $M_{\text{combination}}(j)$ and $M_{\text{original}}(j)$ are the data points for V_m or $[\text{Ca}^{2+}]_i$ for a given parameter set and the original model, and N is the number of data points. Importantly, the normalisation step in this equation allowed AP_{NRMSD} and $\text{Ca}^{2+}_{\text{NRMSD}}$ to be directly compared. By using data from the entire AP or Ca^{2+} transient, this method is a robust measure of goodness-of-fit; however, it is computationally expensive and poorly suited for comparison of model output with noisy experimental data. Furthermore, a comparison using such a metric requires the totality of recorded data to be available for all subsequent comparisons, in contrast to the other biomarkers, where comparison can be made on the basis of a single number.

PARAMETER SPACE EXPLORATION



I sometimes ponder on variation form and it seems to me it ought to be more restrained, purer.
(Johannes Brahms)

The rationale for using parameter space variation as a means to model physiological variation is presented, with caveats appropriate for this thesis given. Details of which parameters are varied are given, with reasons for their choice. An examination of the efficacy of various different commonly used biomarkers as a measure of goodness-of-fit is presented, with a view to determining which biomarkers are most suited under conditions that may include experimental noise. The results of parameter variation for two separate computational model frameworks are explored, and models that reproduce experimentally observed variation are isolated, with patterns amongst the parameters that contribute to these populations being discussed.

5.1 Reproduction of Experimental Variation

As was elaborated on in §??, variation is a constant companion in the experimentalist's world. As computational models of biological processes become more complex, with advancing technology allowing us to discard earlier assumptions made for the sake of computational tractability, and further advances in experimental results allow greater understanding of the system being modelled, variation is now increasingly becoming the computational modeller's companion as well. It is to be noted that this variability includes the so-called experimental variation, the 'noise' that can get in the way of the 'true' data, but also includes the variation that is a normal, and perhaps essential, component of physiological symptoms.

However, exactly *how* this variation is to be modelled is a question left to the modeller—there are many possible alternatives. Which of these alterantives is to be used depends on the exact question being asked: what system is being modelled, how its output is being assessed, and so forth. It depends further on the available resources, and the demands being made of those resources. Were resources and capabilities infinite and on demand, a fully stochastic, molecular model, subject to multiple simulations, would accurately and precisely model the system—indeed, for all intents and purposes, it would *be* the system. However, not only are resources finite, such a model would be drastic overkill for most research questions regarding cardiac physiology. Instead, much like the research question

being posed drives the model choice, it also drives the methodology for reproduction of variability, if it is required—it should be as complex as required, but it need not be any more so.

It is the main drive of this thesis to demonstrate a method for reproducing the observed experimental variation that is

- biophysically detailed,
- computationally tractable, and
- easily scalable.

To this end, we utilise the population level approach used previously in neuron modelling (Marder and Taylor, 2011). As compared to stochastic simulations, such a methodology is computationally simpler—due to their complexity and the requirement for multiple simulations for their statistical properties to be refined, stochastic models are often limited to phenomenological, small scale models. This thus ties in to the other advantage of the model population approach: the biophysical detail that can be applied via such a process. In prescribing variation to certain biophysically specific properties, and observing the consequences, specific output variation effects can be attributed to specific input variation effects. It should be noted, however, that Heijman et al. (2013) recently demonstrated the feasibility of using a biophysically-detailed stochastic model, although it is still restricted to small-scale simulations.

Using parallelisation available by means of the Nimrod/G distributed computing grid and its various alternatives, a population model approach is also computationally tractable—each individual simulation can be computationally simple, and correct distribution can ensure that non-specialised computing resources are sufficient to the task. Finally, it is also easily scalable. By this, it is meant that not only is it a simple process to introduce variation to further parameters of interest, but also that the methodology is trivially applicable to multiple models (indeed, this thesis is based on investigations using two different models).

5.1.1 Comparison with Alternative Methods

It should be noted that the complete, multi-dimensional parameter sweep method used here provides significant benefits compared to other possible methods, insofar as the goals of this thesis are concerned. By this, it is meant that alternative methods for examining the effect of multiple parameter variation are not appropriate for this thesis. For the purposes of comparison, we may consider three alternative methods:

1. Stochastic Models (Heijman et al., 2013)
2. Multi-variable regression analysis (Sobie, 2009; Sobie and Sarkar, 2011; Sarkar and Sobie, 2010, 2011),
3. Sampling from the multi-dimensional parameter space (Britton et al., 2013),

Further details of these methods can be found in §???. It should be noted that significant work has been achieved using single parameter variation, both in deterministic studies (Romero et al., 2009a, 2011) and in stochastic studies (Pueyo et al., 2011; Hashambhoy et al., 2011; Sato et al., 2009; Tanskanen et al., 2005), but this thesis is explicitly multi-dimensional in scope.

The advantages for this thesis of the population approach over stochastic approaches depends, precisely, on what stochastic approach is being used. In most cases, however, stochastic models are far less computationally tractable, especially for large simulations. This presents limits on the scale of the model that can be simulated using stochastic means. If one applies stochasticity to multiple parameters (to provide an analogy to the goal of this thesis), the spatial scale of the simulation is curtailed (Heijman et al., 2013). It can also be noted that some studies apply stochasticity within a phenomenological model, but this prevents analysis on the biophysical source of the variability (Walmsley et al., 2010).

Multi-variable regression analysis samples from a given parameter space, and uses this to return the effect matrix \mathbf{B} that approximates the effect each parameter has on a given biomarker (Sobie, 2009; Sobie and Sarkar, 2011; Sarkar and Sobie, 2010, 2011). This methodology is limited by not only sampling from a limited number of models from the total parameter space, but also reduces the analysis to a pseudo-single dimensional one—the entries in \mathbf{B} provide insight to the effect of a single parameter on a single output, and it has been demonstrated that the overall effect is relatively accurately approximated by the linear summation of the effects. However, it provides little insight into the interactions between parameters, and especially how these interactions can vary given changes in other parameters (*i.e.* parameters X and Y are correlated in a particular manner when parameters $\{A, B, C\}$ have these values, but are correlated in a different manner when $\{A, B, C\}$ have different values).

Methodologically, the most similar method to the current is to sample from the multi-dimensional space to generate a population. This was done by (Davies et al., 2012), but only generated a population of 19 models for a canine ventricular AP. The work previously mentioned by Britton et al. (2013) presents the most comprehensive study in cardiac studies. However, sampling from the multi-dimensional space likely gives an incomplete picture, and is thus less suited to analyse the effects of multiple parameter variation. While it does present a computationally efficient means of population production, it should be noted that (a) it may be unable to give a comprehensive account of the parameter variation within the space and (b) Gemmell et al. (2010) suggests that there may be ‘islands’ within the population, and insufficient sampling will either miss these islands, or falsely connect them with nearby groups in the parameter space; further consideration of these problems is given in §5.4.2).

5.1.2 Caveats

It should be noted that constructing a population of models based on a single framework (replacing the initial parameter set with a parameter space) allows for a biophysically realistic method of reproducing physiological variation which remains computationally tractable. However, there are several key points that must be remembered that represent the limitations of this, and many related, approach.

1. The underlying assumptions regarding the original model still apply. As such, any inaccurate assumptions remain present in derived populations Noble and Rudy (2001); Quinn and Kohl (2013).
2. The populations derived using experimental data rely on these data remaining appropriate for the considered task. The populations used in this thesis are derived using ‘healthy’ data. As such, without further adaptation, the populations are unsuitable for assessing some experimental situations without appropriate alterations made to the framework, *e.g.* where cardiac remodelling has occurred (Walmsley et al., 2013).
3. Related to the point above is the fact that the model populations are united by the data used to create them. As such, if the training data used include differences such as gender, the models cannot then be used to address specific questions regarding gender—these differences are now implicitly encoded within the population.

For this dissertation, cell models are being used, but tissue data are being used for training the population. Moving from cell to tissue represents a large computational task, for two reasons. Firstly, the simple matter of simulating tissue is more computationally intensive, though preliminary simulations using the original Shannon model indicated little difference between the AP generated using cell simulations and those from tissue simulations (performed using the Chaste software (Mirams et al., 2013)). Secondly, and more pertinent for this thesis, is the problem of cell coupling (which itself is a likely candidate for variation). Heijman et al. (2013) predict that cell coupling works to reduce variation between two different cells—by this token, it is likely that any cell model population trained using tissue data is likely to represent an underestimate of the actual variation possible within a cell population. However, to exhaustively test this is computationally challenging. Consider the following: suppose it is wished to test just 20 different cells. To exhaustively examine every possible

combination of this population in a 2 cell chain, it would be required to perform 20^2 . It is simple to abstract this—for a possible cell population of n , in a tissue sample of size m , the number of simulations that would have to be run would be n^m . While there are many possible ways to reduce the search space, it is beyond the scope of this thesis to consider them.

Finally, there is a caveat common to almost all attempts to reproduce variation; indeed, it can be applied to most models as well. Walmsley et al. (2013) demonstrated little correlation between AP and Ca^{2+} biomarkers—this will be expanded upon in §5.5.

5.2 Construction of the Parameter Space

The computational tools involved in investigating the effects of multiple parameter variation were described in the previous chapter—the specific methods used to that end and biological reasons for these methods are described here.

Parameters describing the peak conductance for six different ion channels were varied in this study. The currents considered (with their conductance given in parentheses) were: the transient outward current (g_{to}), the rapid delayed rectifier K^+ current (g_{Kr}), the slow delayed rectifier K^+ current (g_{Ks}), the inward rectifying K^+ current (g_{Ki}), the L-type Ca^{2+} current ($g_{\text{Ca,L}}$), and the Na^+/K^+ pump current (g_{NaK}). These currents were picked in preference to other possible choices based on their perceived impact on the repolarisation of the AP, which has been noted as an indicator of impact on beat-to-beat variability of repolarisation duration (BVR); a longer plateau implies greater BVR (Heijman et al., 2013). Furthermore, the dynamics of these currents were not changed on the basis that (a) it was expected that AP variability is primarily a result of differences in the relative magnitude of the currents rather than the dynamics, and (b) conductance is often the most poorly defined variable within the equations defining these currents in the models. This difficulty in parameter estimation comes from both the inherent experimental difficulties in measuring peak conductance, and the variation in the experimental techniques used to define these values (with methods sometimes being poorly defined) (Quinn et al., 2011).

The conductances were varied by 0%, $\pm 15\%$, and 30%, resulting in 15,625 different models for each framework. This variation is in line with the extent of variation used in previous studies (Romero et al., 2009a, 2011; Walmsley et al., 2013), and is also consistent with the range of experimentally observed variation (Fülöp et al., 2004; Iost et al., 1998; Li et al., 1999; Szentandrásy et al., 2005; Verkerk et al., 2005; Sims et al., 2008) (for further detail, see §??). While some computational studies have used greater degrees of variation, it was decided the variation applied here provided the best compromise between scale and resolution of the parameter space. Furthermore, variation of such scale is not often seen in experimental literature.

Simulations were conducted at three different cycle lengths (CLs) of 400 ms, 600 ms and 1,000 ms to constrain the population of models further—Syed et al. (2005) has demonstrated the importance of considering multiple CLs in order to accurately fit restitution curves. Furthermore, this methodology allows examination of rate-dependent effects, *e.g.* changing parameter importance, changing degrees of output variation.

5.3 Accuracy of Biomarkers in Defining Model Fit

One of the goals of this thesis is to measure the efficacy of commonly used biomarkers in assessing goodness-of-fit for populations. With a parameter sweep providing a population of models, and thus a population of data, that is free from experimental noise, this provides an opportunity for an assessment of such a question. Without having to consider the problems of experimental noise, the entire

range of recorded data can be used to compare a given model output to given training data. The goodness-of-fit by this comprehensive measure can then be compared to the goodness-of-fit given by other biomarkers.

In this specific case, the NRMSD metrics defined in §4.3 were used to compare the output of any given model to the output of the original, unaltered model (*i.e.* the model with 0% variation for all parameters). As previously stated, M_{NRMSD} is unsuited to situations with experimental noise, but in situations where there is no computational noise (as in this parameter search), it provides a comprehensive measure of goodness-of-fit. On the assumption that, due to its involving the totality of available data, it provides the ‘best’ measure of goodness-of-fit, it is then possible to assess how closely other biomarkers come to agreeing with this new gold standard; those biomarkers that come closest to defining the same models as the NRMSD metrics as ‘matching’ training data will then be considered accurate measures of goodness-of-fit in their own right.¹ This process uses multiple biomarkers in unison, *e.g.* APD_{50} and APD_{90} , rather than individual biomarkers in isolation.

The ~ 250 models most closely matching the original model output were determined, based on the minimum values of M_{NRMSD} . Similarly, the ~ 250 models that match original model output was determined based on minimum percentage difference according to groups of biomarkers. The degree of overlap between these two groups (those determined by NRMSD metrics and those determined by biomarkers) was then calculated.

The results of the comparison for some biomarker groups is shown in Fig. 5.1. When $[\text{Ca}^{2+}]_i$ data is available, and thus Ca^{2+} biomarkers can be used in assessing the goodness-of-fit, the accuracy (judged by percentage overlap) is increased overall. The degree of overlap for groups of metrics is not identical between the Shannon and Mahajan populations. However, overall, a combination of APD_{50} , APD_{90} and CaT (or APD_{50} and APD_{90} where $[\text{Ca}^{2+}]_i$ data are not available), is the most accurate measure of goodness-of-fit compared to NRMSD metrics. Consequently, these combinations were used for the remainder of this thesis.

5.4 Defining a Population of Models to Reproduce Physiological Variation

5.4.1 Variation within the Population

In order to constrain the populations of models to those representing physiological variability, only parameter sets that produced APD_{50} and APD_{90} values that fell within the normal range for rabbit epicardium were included. APD_{90} for rabbit epicardium has been well documented and a physiological range was readily established for all CLs (Biagetti and Quinteiro, 2006; Chen et al., 2006; Eckardt et al., 1998; Goldhaber et al., 2005; Jung et al., 2011; Kirchhof et al., 2003; Kurz et al., 1993; McIntosh et al., 2000; Szigligeti et al., 1996; Wu et al., 2011; Yan et al., 2001). Reports of APD_{50} values sufficient to derive a normal range, however, were not available at all CLs. Thus, values from the literature were used to establish a mean value for APD_{50} (Eckardt et al., 1998; Kirchhof et al., 2003). It was then assumed that the percentage variation from mean for APD_{50} is the same as the percentage variation from mean for APD_{90} . By this assumption, an assumed range for APD_{50} that is similar to the range for APD_{90} is calculated, and used in subsequent analysis. The resulting values are shown in Table 5.1.

By using these values, it was possible to constrain the tested parameter space to a population of models that reproduces experimentally measured variability at each CL. The number of models in each

¹It can be noted that, for cells with a long diastolic interval, small differences in V_{rest} would increase AP_{NRMSD} to a great degree, while the rest of the AP may provide an excellent fit to data. Fortunately, both Shannon and Mahajan populations show little variation in V_{rest} , so this problem is not realised

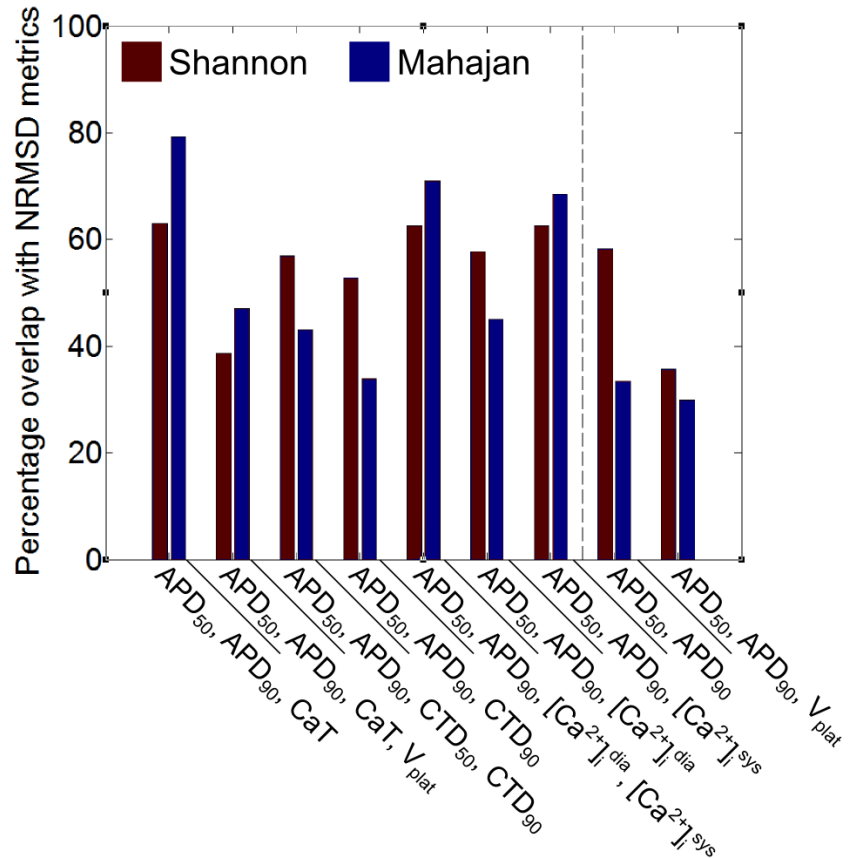


Figure 5.1: Percentage overlap of matches between original model output and model output generated using the ~ 250 parameter sets determined by the NRMSD metrics ($[AP_{NRMSD} \text{ and } Ca_{NRMSD}^{2+}]$) and by combinations of biomarkers. While all combinations of biomarkers were tested, those shown represent the combinations with the highest percentage overlap. Combinations to the left of the dashed line include information about both V_m and $[Ca^{2+}]_i$, while those to the right include only V_m data.

Biomarker	CL (ms)		
	400	600	1,000
APD ₅₀ (ms)	104 – 135	116 – 159	137 – 188
APD ₉₀ (ms)	142 – 185	160 – 220	167 – 230

Table 5.1: Normal range of rabbit epicardial APD₅₀ and APD₉₀ used to define physiological parameter sets. Values are derived from previously reported studies, as described in the text.

Model	CL (ms)							
	400	600	1,000	400 \cap 600	400 \cap 1,000	600 \cap 1,000	400 \cap 600 \cap 1,000	
Shannon	1,691	2,631	5,352	1,384	1,511	2,526	1,352	
Mahajan	3,946	1,031	0	577	0	0	0	
Expanded Mahajan	9,447	11,229	5,650	6,797	779	4,331	779	

Table 5.2: Number of parameter sets producing both APD_{50} and APD_{90} values within the physiological range. Parameter values were varied by $\pm 30\%$ from the original parameter set, and then further for the Mahajan model ('Expanded Mahajan') as explained in the text. $x \cap y$ and $x \cap y \cap z$ represent parameter sets that produce physiological values at a CL of x and y , or a CL of x , y , and z , respectively.

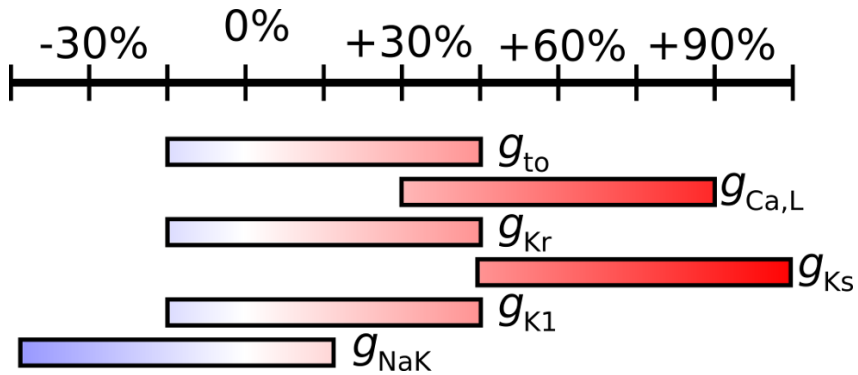


Figure 5.2: Parameter ranges used for 'Expanded Mahajan' search.

population at each CL is given in Table 5.2. Those models that produce output within the physiological range are defined to be in the model population that can reproduce given variation at all CLs; the minimum, mean and maximum values of all computed biomarkers for the Shannon and Mahajan populations thus defined are shown in Table ??.

With the Shannon framework, there existed at least one parameter set that produced a physiological output at each CL, with some of these generating a physiological output at all CLs. On the other hand, while a relatively large number of models produced a physiological output at a CL of 400 ms with the Mahajan framework (the CL for which the original Mahajan model was designed), fewer parameter sets matched at a CL of 600 ms, and none at a CL of 1,000 ms (the increase in APD with increasing CL was disproportionately large).

In order to address the failure of the Mahajan framework in finding parameter sets that generated a physiological output with increased CL, the range of conductance variation was expanded. To determine the direction of this expansion, the first step was to increase the ranges of APD_{50} and APD_{90} by $\pm 10\%$, and the parameter space was compared to this new range. This expanded range of APD resulted in 'matches' being found at all CLs. Based on the trends in the conductances evident amongst these matches, the parameter ranges were altered and a new parameter space was explored. The new ranges are shown in Fig. 5.2, and resulted in an additional 15,625 models being simulated. However, even with this expanded search, the number of parameter sets that matched at all CLs was approximately half of that with the Shannon model.

The parameter sets producing a physiological output with the Shannon framework are shown using a dimensional stack in Fig. 5.3, along with the generated V_m and $[Ca^{2+}]_i$ profiles at a CL of 400 and 1,000 ms, and the associated distribution of conductance values. The most obvious trend is that parameter sets producing a physiological output generally had a simultaneous reduction in both $g_{Ca,L}$ and g_{K1} . This is evident in both Fig. 5.3A, demonstrated by a clustering of the valid models at the bottom left of the dimensional stack, and from the associated distribution of conductances, shown in Fig. 5.3D. It also appears that the distribution of the other conductances was fairly even; however, a closer examination of the dimensional stack in Fig. 5.3A reveals trends between the parame-

Biomarker	CL (ms)	Model	Minimum	Mean	Maximum
$(dV_m/dt)_{\max} (\text{Vs}^{-1})$	400	Shannon	233	302	329
	1,000	Mahajan	200	230	252
	400	Shannon	278	327	352
	1,000	Mahajan	248	279	311
$V_{\text{rest}} (\text{mV})$	400	Shannon	-92	-88	-82
	1,000	Mahajan	-88	-86	-85
	400	Shannon	-88	-86	-81
	1,000	Mahajan	-89	-88	-87
$\text{APD}_{50} (\text{ms})$	400	Shannon	112	126	135
	1,000	Mahajan	104	108	117
	400	Shannon	137	155	181
	1,000	Mahajan	165	182	188
$\text{APD}_{90} (\text{ms})$	400	Shannon	143	154	169
	1,000	Mahajan	142	155	185
	400	Shannon	167	186	217
	1,000	Mahajan	207	223	230
$[\text{Ca}^{2+}]_{\text{i}}^{\text{dia}} (\mu\text{M})$	400	Shannon	1.24	1.29	1.32
	1,000	Mahajan	0.29	0.37	0.47
	400	Shannon	0.82	0.84	0.86
	1,000	Mahajan	0.15	0.16	0.18
$[\text{Ca}^{2+}]_{\text{i}}^{\text{sys}} (\mu\text{M})$	400	Shannon	4.49	4.92	5.22
	1,000	Mahajan	1.43	2.78	4.46
	400	Shannon	3.13	3.33	3.68
	1,000	Mahajan	0.41	0.59	0.76
$\text{CaT} (\mu\text{M})$	400	Shannon	3.25	3.63	3.91
	1,000	Mahajan	1.14	2.41	4.00
	400	Shannon	2.30	2.49	2.82
	1,000	Mahajan	0.26	0.42	0.58
$\text{CTD}_{50} (\text{ms})$	400	Shannon	123	130	134
	1,000	Mahajan	133	139	147
	400	Shannon	139	150	157
	1,000	Mahajan	208	231	268
$\text{CTD}_{90} (\text{ms})$	400	Shannon	263	267	271
	1,000	Mahajan	245	249	260
	400	Shannon	382	394	404
	1,000	Mahajan	460	510	585

Table 5.3: Minimum, mean, and maximum values of all computed biomarkers produced with the physiological parameter sets.

ters (demonstrating the power of the clutter-based dimension reordering technique for visualisation of multi-dimensional parameter spaces). For instance, within the $g_{\text{NaK}}/g_{\text{Kr}}$ surfaces (Level 2 of the stack), the matching parameter sets are spread in an approximately diagonal line from top left to bottom right, indicating that when g_{NaK} was increased, this was offset by a decrease in g_{Kr} , and *vice versa*. As $g_{\text{Ca,L}}$ and g_{Ki} decrease, this diagonal line moves further to the bottom left corner, indicating that a further reduction of g_{NaK} and g_{Kr} was required to continue to produce a physiological output.

The effect of g_{to} is more complicated. When $g_{\text{Ca,L}}$ and g_{Ki} were reduced by 30%, and g_{NaK} was also reduced, matching parameter sets then included those with an increased g_{to} . The opposite was true when g_{NaK} was increased, as in these cases a decrease in g_{to} was necessary (square A1 in Fig. 5.3A). As g_{Ki} was increased, fewer parameter sets with an increased g_{NaK} were valid, such that an increase in g_{to} was observed (squares B1, C1, and D1 in Fig. 5.3). However, in all cases where $g_{\text{Ca,L}}$ was not reduced by 30%, the opposite was true: parameter sets included reduced g_{NaK} and increased g_{to} were no longer valid (squares A2 and A3 in Fig. 5.3). Finally, in all valid parameter sets as g_{Ki} was increased, g_{to} decreased. On the other hand, there appeared to be no pattern to the values of g_{Ks} within the model population.

For the expanded Mahajan search, the parameter sets producing a physiological output, the generated cellular profiles, and the distribution of valid conductance values are shown in Fig. 5.4. There are some differences compared to the Shannon framework. For instance, with the Shannon framework, g_{Ks} appeared to have no effect in determining the validity of parameter sets, while with the Mahajan framework it had a strong influence, as most matching parameter sets included the largest conductance variation (+105%). The opposite was true for g_{Ki} : while it had a large influence with the Shannon framework, it was relatively unimportant with the Mahajan framework. Similarly, with the Shannon framework, g_{to} and g_{NaK} generally varied in the opposite direction, while with the Mahajan framework they changed in the same direction.

With the Mahajan model, there was also a strong correlation between g_{NaK} and g_{Ks} , such that when g_{NaK} was increased, g_{Ks} also increased (demonstrated by a shift of matching parameter sets from the predominantly lower left corner to the upper right corner of the level two plots in Fig. 5.4A; for instance, compare the distribution within E1 and E3). On the other hand, there appeared to be no limitations on the values of g_{Kr} .

It is of note that the original model for both frameworks is not included in the final model populations. This does not in any way remove the validity of these models—they are entirely valid for the CLs for which they were designed. It can also be compared to Sato et al. (2009), in which different parameters had to be used within the model to generate the required behaviour. However, this does demonstrate the limitations of any given model, and the requirement to be careful of any applications for which the model/framework was not explicitly designed. On a related note, it can be observed that there is little variation observed in V_{rest} in both populations. While this is almost to be expected (none of the varied parameters would be expected to have a great effect on this biomarker), it should be noted that, in experimental data, V_{rest} is rarely so well-behaved.

While the results presented here suggest that variation in current conductances over a wide range of values may account for normal variability in rabbit ventricular AP repolarisation, other factors may be involved. One of the underlying assumptions of this thesis is that AP variability is primarily a result of differences in the relative magnitude of the currents, rather than underlying current dynamics, which were not varied. Changes in channel properties other than conductance could result in similar changes in AP biomarkers, and also account for some of the experimentally observed variability. Romero et al. (2011) presented a one-dimensional sensitivity analysis of the rabbit-specific frameworks used in this thesis with a similar range of parameter variation, and showed that along with repolarisation currents, APD was significantly modified by changes in the activation and inactivation rates of the associated channels. At the same time, further constraints to the model populations (*e.g.* matching of rate-adaptation of restitution properties), as well as consideration of additional biomarkers (for instance, relating to intracellular ion concentration), may be necessary to ensure their applicability to additional physiological states. This has been recently demonstrated in Walmsley et al. (2013), in which populations of failing and non-failing human ventricular myocytes with variation in current conductances were compared using various biomarkers at numerous CLs to investigate which currents drive variability in the two cell populations. Finally, as the range and resolution of parameter

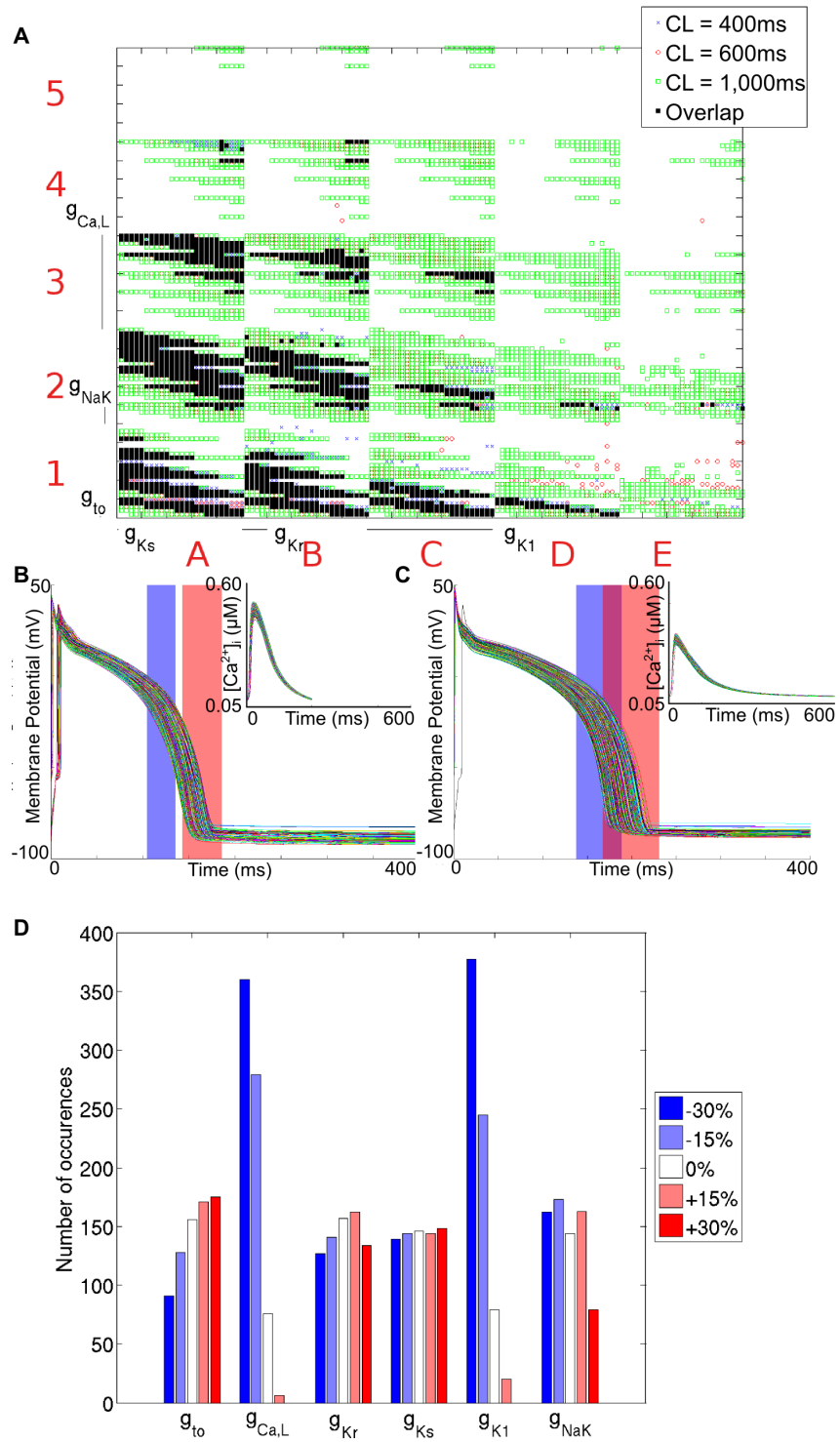


Figure 5.3: Model population for the Shannon framework that produces values of both APD_{50} and APD_{90} that fall within the experimentally derived range. (A) Dimensional stack image showing the location of matching parameter sets for each CL and their overlap. (B) V_m and $[Ca^{2+}]_i$ (inset) profiles for the matching parameter sets at a CL of 400 ms. (C) V_m and $[Ca^{2+}]_i$ (inset) profiles for the matching parameter sets at a CL of 1,000 ms. (D) Distribution of conductance values for the valid parameter sets. For both (B) and (C), the physiological ranges of APD_{50} and APD_{90} are represented by the blue and red rectangles, respectively.

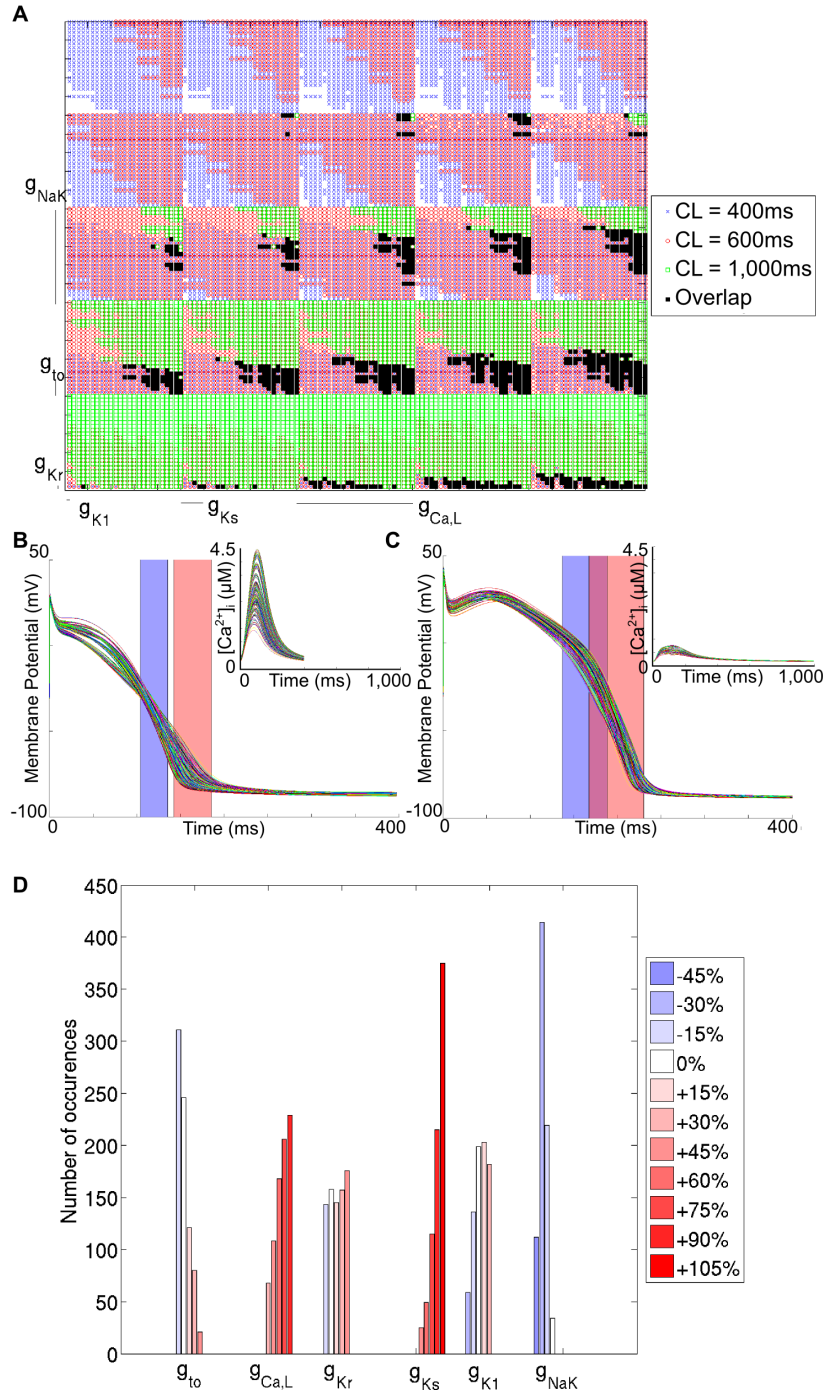


Figure 5.4: Model population for the expanded Mahajan framework that produces values of both APD_{50} and APD_{90} that fall within the experimentally derived range. (A) Dimensional stack image showing the location of matching parameter sets for each CL and their overlap. (B) V_m and $[Ca^{2+}]_i$ (inset) profiles for the matching parameter sets at a CL of 400 ms. (C) V_m and $[Ca^{2+}]_i$ (inset) profiles for the matching parameter sets at a CL of 1,000 ms. (D) Distribution of conductance values for the valid parameter sets. For both (B) and (C), the physiological ranges of APD_{50} and APD_{90} are represented by the blue and red rectangles, respectively.

space sampling in the present study was limited by computational tractability, there may be additional influences and interactions of current conductances important for ventricular AP variability that were not appreciated. As mentioned earlier, it is difficult to properly assess the true physiological ranges of the current conductances considered in this study, so that they may be related to the values included in the calibrated populations of models. We initially varied all conductances by $\pm 30\%$, yet it was necessary with the Mahajan framework to expand this range to generate a physiological output. Other computational studies have used a larger range of conductances than presented here (Sobie, 2009; Britton et al., 2013; Davies et al., 2012), possibly representing the true physiological range of values, and supporting the expanded range used with the Mahajan framework..

5.4.2 Connectivity within the Parameter Space

Of note is the question which has been touched upon earlier, both in this study and others: are the populations generated here ‘connected’, by which it is asked whether or not one can connect all models in the population with a single parameter space, or does the population consist of several separate populations within the population space. The answer to this is irritatingly dependent on how, exactly, one defines ‘connected’. If one requires connection only by one step in multiple dimensions, then the populations derived here are connected. However, if one adopts a stricter definition of connection (two models are connected only if they are one step away from each other in a single dimension), then the populations are not connected—this is shown in a dimensional stack in Fig. 5.5.

It is beyond the scope of this thesis to determine whether the two definitions of connectivity can be reconciled—whether by increased resolution, or by inclusion of alternative parameters, those semi-connected regions will become connected. However, if we work on the (somewhat reasonable) assumption that either they can, or the looser definition of connectivity is a reasonable approximation, this has significant implications for population construction, in that it implies that, once a ‘valid’ model has been found, the search for other ‘valid’ models can be directed, and thus the computational task of searching the entire parameter space is reduced.

5.5 Effects of Parameter Variation

Using the biomarkers thus defined as providing measures of goodness-of-fit, it is now possible to assess the effects of parameter variation on the model populations; it also allows judgement of how these different biomarkers are affected by these different parameters, and how these differences are altered based on CL. The dimensional stack images showing these effects are presented in Fig. 5.6 (for the Shannon population) and Fig. ?? (for the Mahajan population). In addition, the optimum stack orders are shown in Table 5.4.

These results demonstrate how the relative importance of the varied current conductances was dependent on both the CL, and on the biomarker being considered. In considering this, it should be noted that the non-linear interactions between currents and ion concentrations often resulted in different changes in the current magnitudes that might be expected from the change in current conductance. For instance, when g_{K_s} was subject to $\pm 30\%$ variation at a CL of 1,000 ms, the amplitude of I_{K_s} varied from -99% to $+386\%$ for the Mahajan population. (TODO: CHECK THE DETAILS OF THIS MORE PRECISELY).

The optimum stack order, which is an indication of both the relative importance of the individual conductances on the biomarker and the inter-relation between parameters, changes with CL. The extent of this change is unpredictable, and can be dramatic. This is best demonstrated with the Shannon framework, and the change in influence of g_{to} on APD_{50} and APD_{90} . At a CL of 400 ms, g_{to} was a low-order conductance (reflecting a low importance), while at a CL of 1,000 ms, it became a high-order conductance. The relative importance of g_{K_i} decreases at the same time. However, this degree

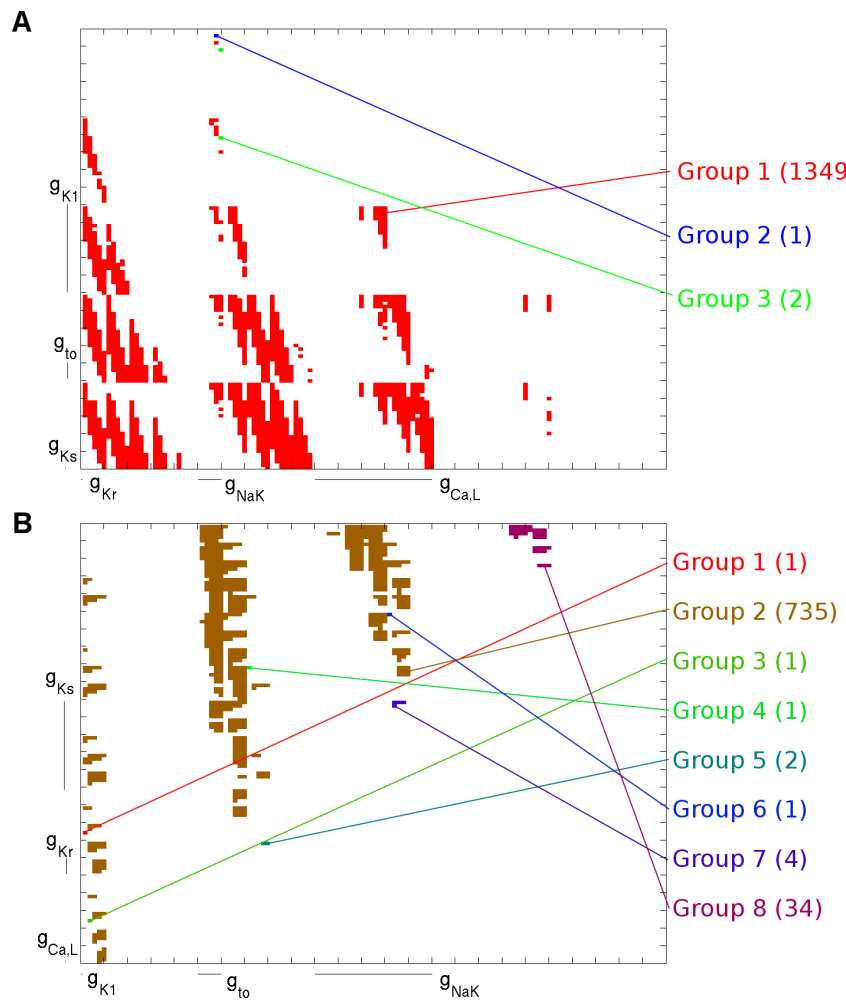


Figure 5.5: Dimensional stack images showing connectivity within model populations for the Shannon (A) and Mahajan (B) frameworks, with a space defined as being connected if two points are connected only if they are one step away from each other in a single dimension.

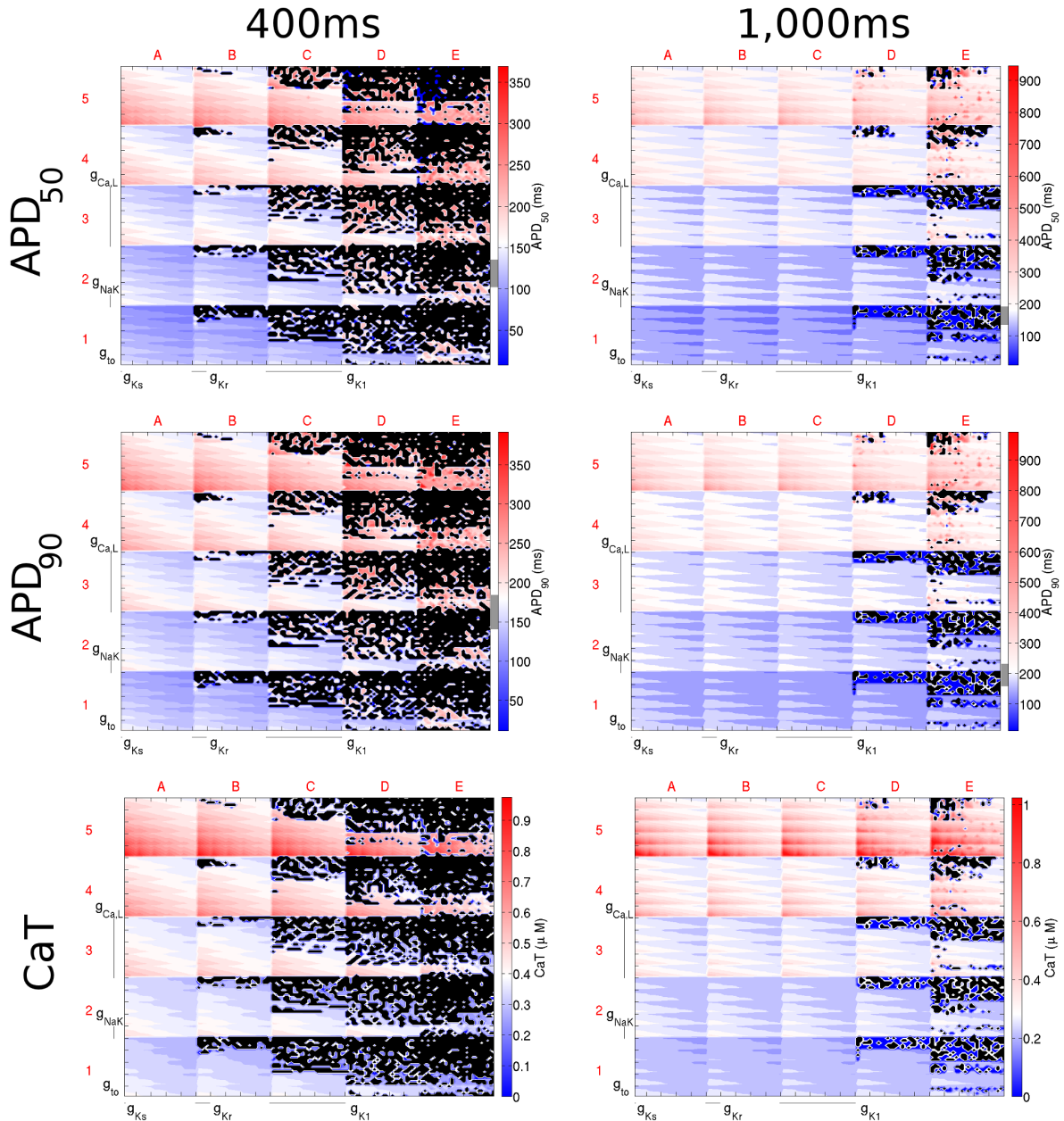


Figure 5.6: Dimensional stack images demonstrating the effect of simultaneously varying the magnitude of six repolarising current conductances in the Shannon model. The top, middle, and bottom rows show the effects on APD_{50} , APD_{90} , and CaT , respectively. The left column is based on simulations with a CL of 400 ms and the right with a CL of 1,000 ms. In the contour plots, red represents an increase from the initial parameter value, blue a decrease, and white no change. The physiological range determined from the literature (see §5.4 for details) is represented by the grey region next to the colour bars in each panel. Black dots represent parameter sets with which the model did not reach steady state. In this case the optimum stack orders are not displayed; instead the order before optimisation has been used, which allowed direct comparison of the stacks to reveal differences in effects on each biomarker.

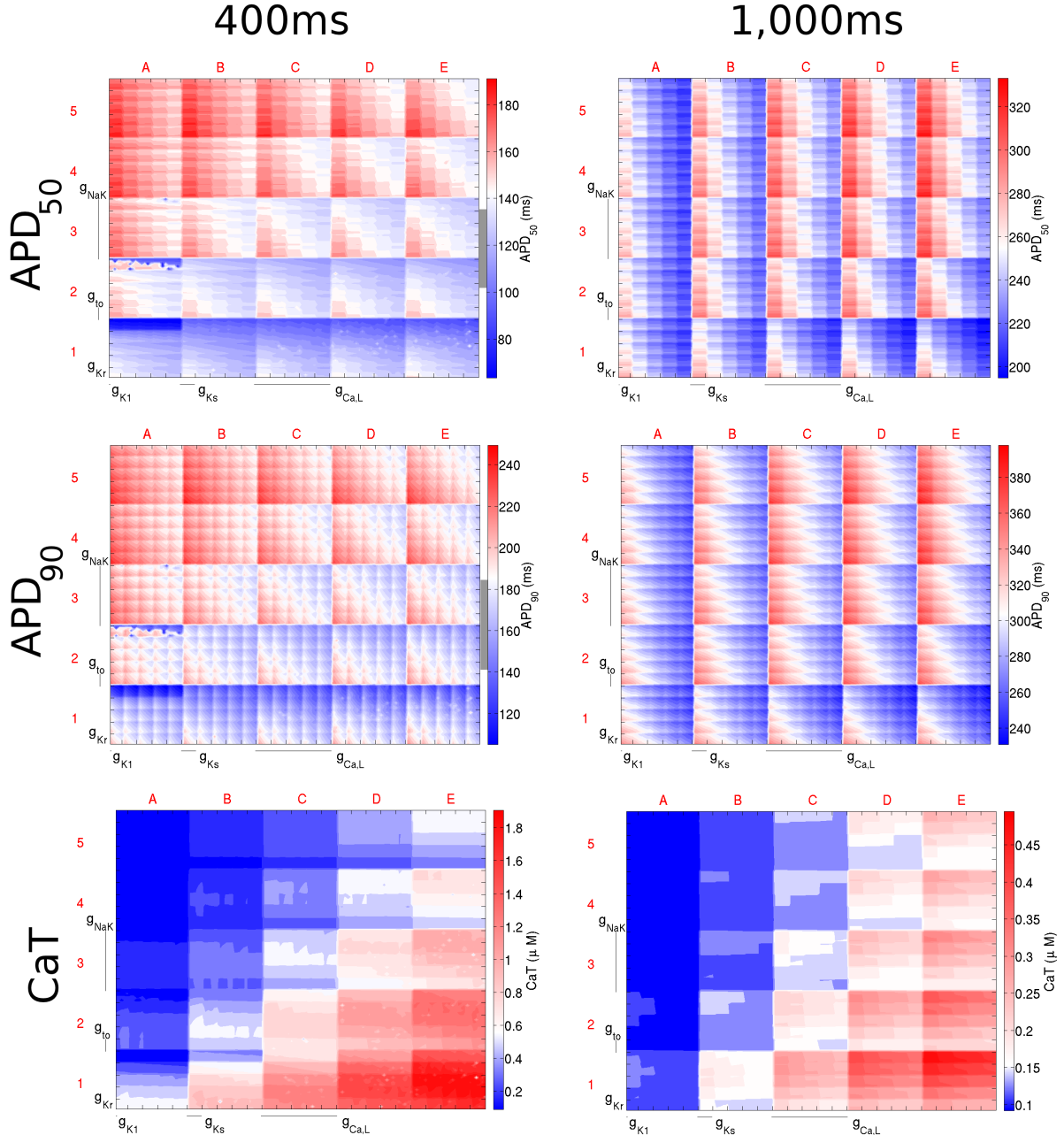


Figure 5.7: Dimensional stack images demonstrating the effect of simultaneously varying the magnitude of six repolarising current conductances in the Mahajan model. The top, middle, and bottom rows show the effects on APD_{50} , APD_{90} , and CaT , respectively. The left column is based on simulations with a CL of 400 ms and the right with a CL of 1,000 ms. In the contour plots, red represents an increase from the initial parameter value, blue a decrease, and white no change. The physiological range determined from the literature for a CL of 400 ms is represented by the grey region next to the colour bars in each panel (the grey region is absent for a CL of 1,000 ms as the APD values fell outside of the physiological range). In this case the optimum stack orders are not displayed; instead the order before optimisation has been used, which allows direct comparison of the stacks to reveal differences in effects on each biomarker.

Framework	Biomarker	CL (ms)	Optimum Stack Order (x, y)		
			Low Order \rightarrow High Order		
Shannon	APD ₅₀	400	($g_{\text{to}}, g_{\text{Ks}}$)	($g_{\text{NaK}}, g_{\text{Kr}}$)	($g_{\text{Ca,L}}, g_{\text{Ki}}$)
		1,000	($g_{\text{Ki}}, g_{\text{Ks}}$)	($g_{\text{NaK}}, g_{\text{Kr}}$)	($g_{\text{Ca,L}}, g_{\text{to}}$)
	APD ₉₀	400	($g_{\text{to}}, g_{\text{Ks}}$)	($g_{\text{NaK}}, g_{\text{Kr}}$)	($g_{\text{Ca,L}}, g_{\text{Ki}}$)
		1,000	($g_{\text{Ki}}, g_{\text{Ks}}$)	($g_{\text{NaK}}, g_{\text{Kr}}$)	($g_{\text{Ca,L}}, g_{\text{to}}$)
Mahajan	CaT	400	($g_{\text{Ki}}, g_{\text{Ks}}$)	($g_{\text{NaK}}, g_{\text{to}}$)	($g_{\text{Ca,L}}, g_{\text{Kr}}$)
		1,000	($g_{\text{Ki}}, g_{\text{Ks}}$)	($g_{\text{NaK}}, g_{\text{Kr}}$)	($g_{\text{Ca,L}}, g_{\text{to}}$)
	APD ₅₀	400	($g_{\text{Kr}}, g_{\text{Ki}}$)	($g_{\text{Ks}}, g_{\text{Ca,L}}$)	($g_{\text{to}}, g_{\text{NaK}}$)
		1,000	($g_{\text{Kr}}, g_{\text{Ki}}$)	($g_{\text{to}}, g_{\text{Ca,L}}$)	($g_{\text{Ks}}, g_{\text{NaK}}$)
	APD ₉₀	400	($g_{\text{Kr}}, g_{\text{Ca,L}}$)	($g_{\text{Ki}}, g_{\text{Ks}}$)	($g_{\text{to}}, g_{\text{NaK}}$)
		1,000	($g_{\text{Kr}}, g_{\text{Ki}}$)	($g_{\text{Ks}}, g_{\text{to}}$)	($g_{\text{Ca,L}}, g_{\text{NaK}}$)
	CaT	400	($g_{\text{Kr}}, g_{\text{Ki}}$)	($g_{\text{to}}, g_{\text{Ks}}$)	($g_{\text{NaK}}, g_{\text{Ca,L}}$)
		1,000	($g_{\text{Kr}}, g_{\text{Ki}}$)	($g_{\text{Ks}}, g_{\text{to}}$)	($g_{\text{NaK}}, g_{\text{Ca,L}}$)

Table 5.4: Optimum stack order for APD₅₀, APD₉₀, and CaT for the Shannon and Mahajan frameworks, at CLs of 400 and 1,000 ms. Each pair of parameters represents low, medium, or high order current conductances. For each pair, the first component is plotted on the x-axis and the second component on the y-axis. The (x, y) order can be reversed without affecting the result, though only if all (x, y) pairs are reversed.

of change does not always occur— $g_{\text{Ca,L}}$ was consistently of high-order and g_{Ks} of low-order, while g_{Kr} and g_{NaK} were generally of medium-order.

For the Mahajan framework, as CL increased, the relative importance of g_{to} decreased. This is opposite to the response seen with the Shannon framework. At the same time, g_{Ks} becomes more influential, despite little change in its position in the optimum stack order. This can be seen by examining the difference between the dimensional stacks with CLs of 400 and 1,000 ms shown in Fig. 5.7. At a CL of 400 ms, the greatest effect on APD (represented by deep red and blue) is seen at the edges of the dimensional stack image (squares A1, A5, E1 and E5), indicating an extreme increase/decrease in $g_{\text{Ca,L}}$ and g_{NaK} is required for such effects. However, with an increase in CL, the maximum effect of the change in seen throughout the dimensional stack image, as a result of the increased importance of g_{Ks} . In contrast, the relative importance of g_{NaK} and g_{Kr} were independent of CL, being consistently one of the highest and lowest order conductances, respectively.

The same optimum stack order is rarely shared between APD₅₀/APD₉₀ and CaT; moreover, there are instances where even the APD biomarkers have different optimum stack orders (see the Mahajan framework results). This point becomes more evident with inspection of the dimensional stack images—the distribution of changes is drastically different between AP and $[\text{Ca}^{2+}]_i$ biomarkers, and subtly different between the AP biomarkers themselves. This emphasises the folly, already noted elsewhere (Walmsley et al., 2013), of the thinking of ‘parameter X ’ is very influential. Rather, the conditions under which parameter X is important, and by which metric it is important, must always be added as caveats to such sweeping statements.

These results can be contrasted with the results presented in Heijman et al. (2013), which indicated I_{Na} and I_{Kr} as the most influential for affecting BVR. While the obvious differences between these studies, both in terms of methods and in terms of goals, should be remembered, it is instructive to note the common themes, and the implications of these works on the current results. For example, Heijman et al. demonstrated little stochastic effects of pumps and exchangers due to their low throughput and high expression rate ‘smoothing out’ stochastic effects. This is compared the results presented here, and in the work from Sobie et al., which noted the effect of I_{NaK} and I_{NaCa} —while they may be noted as having little stochastic effect, their interactions with other components reinforces their importance in their own right. Furthermore, it is implied that their effects are mediated via their effect on ion concentrations and the like rather than direct effect on the AP, as these do not affect BVR directly.

The results presented in this section serve as an illustration of the importance of considering (1) the independence of the relative importance of parameters on the different biomarkers, and (2) the effect of CL when determining the effects of current conductance variability on biomarkers. It is also worth noting the differences that exist between the two frameworks when subjected to identical degrees of parameter variation, with the consideration that the Mahajan framework is based in large part on the Shannon framework. However, the non-linear nature of the interactions between the components that make up a biophysically detailed cell model mean that, even with these common elements, the response can be drastically different.

5.6 Rate Dependence of Biomarkers

Related to the changes in parameter importance varying with rate is variability of the biomarker distribution itself with changes in CL. Histograms showing the variability of APD₅₀, APD₉₀ and CaT across all combinations of current conductances are shown in Fig. 5.8. Both frameworks demonstrated similar distributions for both APD₅₀ and APD₉₀ (upper and middle panels). They differed, however, in that the Mahajan framework demonstrated more narrow distributions than the Shannon framework, while the Shannon framework generated more APD values that fell within the physiological range (discussed in §5.4.1). For the Shannon framework, the shape of the APD₅₀ and APD₉₀ distributions were relatively well conserved between a CL of 400 and 1,000 ms, other than an increase in the number of matching parameter sets. In contrast, the Mahajan framework demonstrated a widening of the APD₅₀ and APD₉₀ distributions, as well as an increase in their mean. In the case of simulations with a CL of 1,000 ms, the increase in APD was such that the entire distribution fell outside of the physiological range. The change in CaT distribution with a change in CL was more dramatic (lower panels in Fig. 5.8). For the Shannon framework, the distribution narrowed with an increase in CL. The distribution with the Mahajan framework followed a similar pattern, however with an even larger change. At a CL of 400 ms, the range of CaT was very broad ($\sim 0.1\mu\text{M}$ to $\sim 1.9\mu\text{M}$), indicating that CaT was relatively poorly constrained within the parameter space. When CL was increased, however, the range was greatly reduced ($\sim 0.1\mu\text{M}$ to $\sim 0.5\mu\text{M}$)

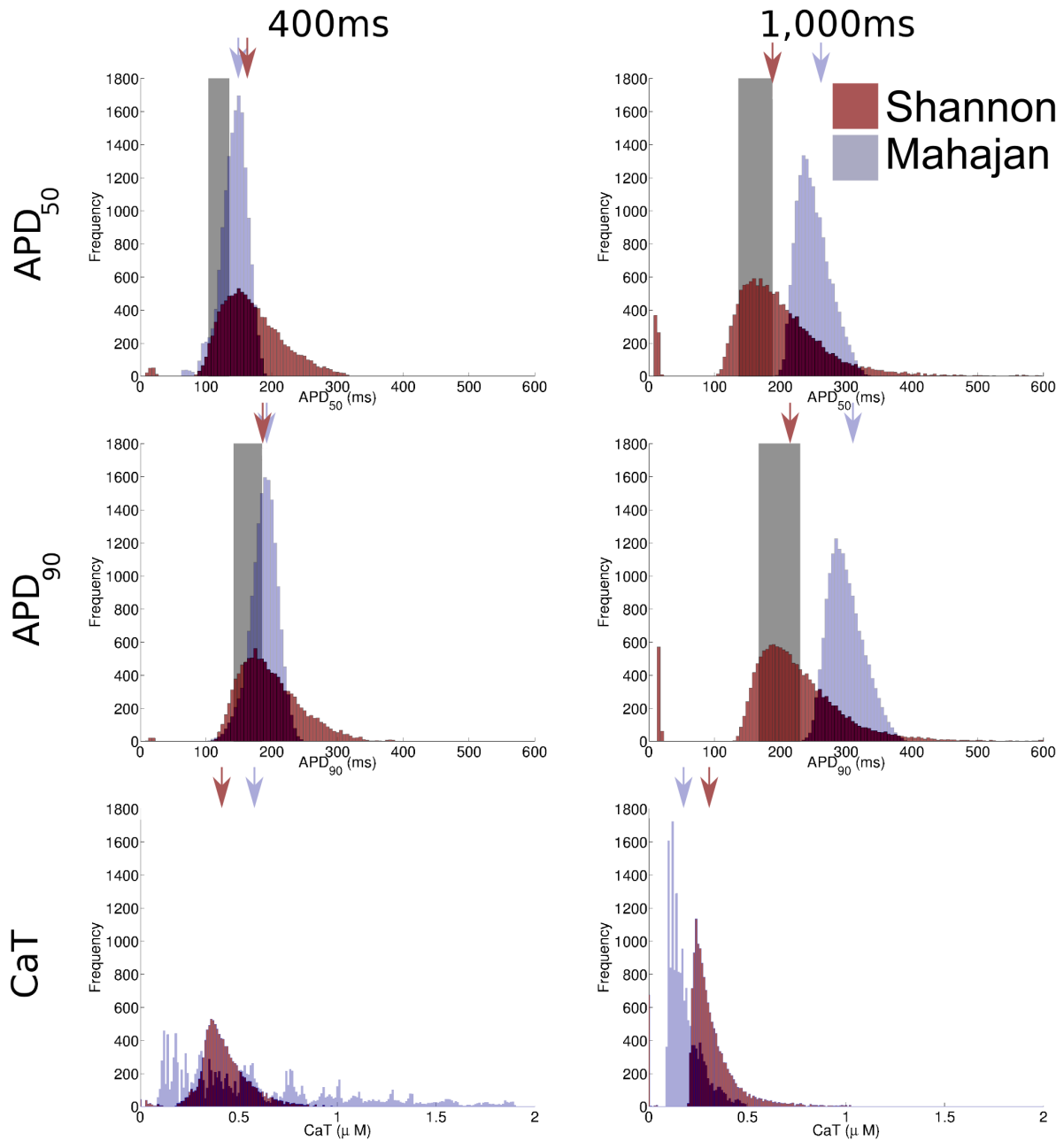


Figure 5.8: Histograms showing the range of APD₅₀, APD₉₀, and CaT in the model populations. The value generated with the initial parameter set for each framework is indicated by the arrow. The physiological range of APD₅₀ and APD₉₀ derived from the literature are represented by the boxed area.

ISCHÆMIC VARIATION

6

Quotation

(Source)

This chapter presents insights into the ischæmic parameter space. A brief introduction is given to the work, and the justification behind the methodology used here. The changes of the parameter space defined in the previous chapter are discussed, followed by an analysis of the effects of the ischæmic parameter space itself. The possible consequences of model failure are discussed.

6.1 Variation Within Ischæmia

As has previously been commented upon, computational modelling of variation is promising new insights into the causes and consequences of variation. Coupled to this progress in computational modelling are the benefits when investigating ischæmia: due to the rapidly changing nature of the ischæmic milieu, comprehensive experimental validation of hypotheses is difficult. Computational modelling allows a rapid, flexible manner with which to test hypotheses regarding ischæmia. This is especially useful for assessing the import of factors that are difficult to constrain and control experimentally.

This work presents the first time, to the author's knowledge, where a comprehensive model population approach has been applied to the ischæmic environment. Furthermore, the parameter space methodology is applied to the ischæmic environment itself. This provides two important possible benefits. First of all, in the same way that the previous chapter postulated variation in the model itself as being partly responsible for natural variation, it is reasonable to extend this same postulate of variability, and thus the methodology used, to the environment itself. Secondly, it can be remembered that ischæmia rarely exists in isolation, and that there is commonly a 'border zone' that exists between the central ischæmic zone and the surrounding healthy tissue. As was commented upon in §2.4.1, the changes in environmental conditions associated with ischæmia do not vary in a spatially uniform manner—Fig.2.6 in that section (originally from Tice et al. (2007)) demonstrates that it can be expected that hyperkalæmic conditions can exist while other environmental changes associated with ischæmia are not present. Performing a parameter space search allows us to examine this spatial variation.

The inclusion of variation in ischæmia modelling is of potentially key importance. It is already known through significant previous literature (see §?? for a review) that ischæmia provides an arrhythmogenic substrate. It has also been demonstrated that arrhythmogenesis is favoured in heterogeneous substrate—indeed, Tice et al. (2007) demonstrated that the heterogeneity introduced by changes

Time (min PO)	0	2	4	6	8	10
$[K^+]_o$ (mM)	5.40	7.72	10.04	12.36	14.68	17.00
$f_{K\text{-ATP}}$ (%)	0.00	0.16	0.32	0.48	0.64	0.80
f_{inhib} (%)	0	5	10	15	20	25
f_{Na} (%)	0	6	12	18	24	30

Table 6.1: Table showing what parameters are used in simulation to approximate a given time post-occlusion. $f_{K\text{-ATP}}$ represents the degree of activation of $I_{K\text{-ATP}}$, f_{inhib} represents the degree of inhibition applied to I_{Na} and $I_{Ca,L}$, and f_{Na} represents the percentage increase/decrease in $[Na^+]_i$ and I_{NaK} , respectively.

from the central ischæmic zone, to the border zone, to normal tissue, can provide the substrate for arrhythmias.

It is based on these observations that the primary hypothesis being tested here is: does the application of ischæmic conditions lead to an increase in heterogeneity within the population that could, in tissue, be arrhythmogenic? To put it another way, one could ask whether the benign variation that is being modelled by the population then transitions to malign variation under ischæmic conditions. It should be remembered that the results presented in this work cannot be said to imply arrhythmogenesis, which is a super-cellular behaviour. However, there is a silver lining to the simulation of ischæmia—since it has been noted that ischæmia reduces the extent of cell-coupling, it is implied that the results presented here will be ameliorated to a lesser degree by any cell-coupling.

In this chapter, it must be remembered that the term 'x minutes post-occlusion (PO)' is used as shorthand, and it is wise to consider the data presented with such a label in terms of the underlying conditions instead; the corresponding values are given in Table 6.1.

As a further matter of nomenclature in this chapter, two different measures of variation are used in this chapter: the variance and the range (defined as the difference between the maximum and the minimum values found amongst the population for a given set of environmental conditions. When both measures demonstrate the same trend, the term variation shall be used directly. It must also be considered that it is not always sufficient to use simply these measures, but sometimes to examine the data directly—such measures will be used in the following analysis.

6.2 Population Response to Ischæmia

The APs for the population at various discrete points during ischæmia are shown in Fig. 6.1, with histograms representing the APD_{90} values for the populations also shown. Associated data for the mean, standard deviation and range responses for common biomarkers for both populations are shown in Table 6.2.

Both populations show a qualitative and quantitative (based on mean population response) agreement with expected AP response (increase in V_{rest} , decrease in $(dV_m/dt)_{max}$ and APD_{90}). However, the AP morphology of the two populations, while initially similar, shows different population-level responses to ischæmia. The Shannon population demonstrates secondary depolarisation as ischæmia progresses, *i.e.* beyond 4 min PO, V_{max} is not reached during the initial upstroke, but rather

6.2.1 APD_{90}

For both model populations, progression of ischæmia works to reduce population variation in its early stages (until 4 min PO)—beyond this point, the response is population-dependent, as can be seen in Fig. 6.1 and Table 6.2.

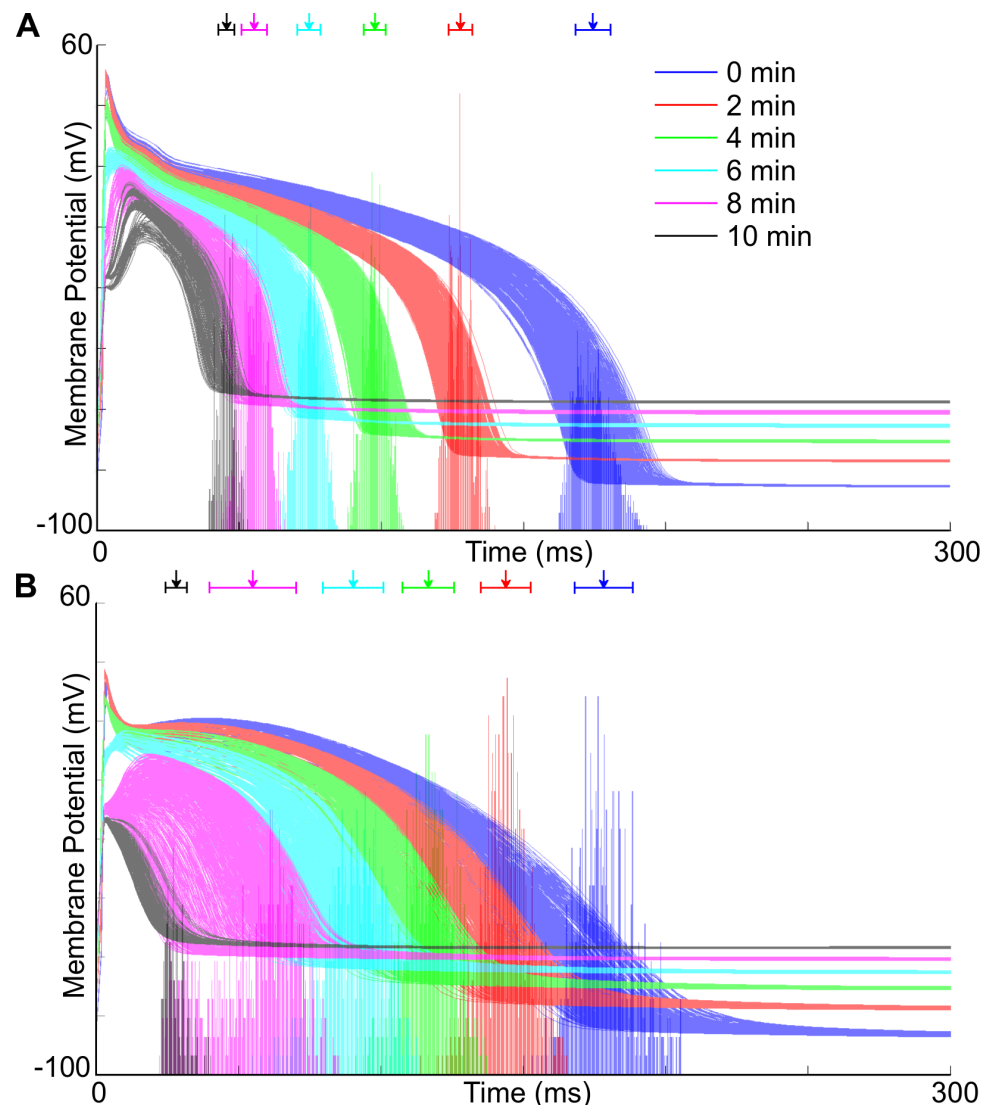


Figure 6.1: Effect of different degrees of ischaemia on the Shannon (A) and Mahajan (B) model populations. The histograms represent the APD_{90} values associated with the populations.

		Time PO (min)						
		0	2	4	6	8	10	
Shannon	APD ₉₀	Mean	174.1	127.4	97.4	74.2	55.0	45.3
		Std	6.23	4.17	3.89	4.14	4.44	2.82
		Range	30.9	20.9	19.7	21.8	23.5	13.5
Mahajan	ERP	Mean	175.9	132.7	107.5	93.2	94.8	182.9
		Std	6.20	4.21	3.85	3.77	2.87	31.47
		Range	30.7	21.3	19.5	19.9	15.5	324.0
	PRR	Mean	1.8	5.3	10.1	19.0	39.8	137.6
		Std	0.09	0.19	0.23	0.49	1.96	31.94
		Range	0.4	1.1	1.1	2.1	8.2	319.9
	APD ₉₀	Mean	177.9	143.6	116.3	90.0	54.7	27.8
		Std	10.20	8.77	9.04	10.64	15.25	3.75
		Range	55.0	51.4	54.0	58.4	62.5	17.4
	ERP	Mean	174.2	148.7	128.0	112.0	100.8	600.0
		Std	9.32	8.82	9.43	11.44	18.31	0.00
		Range	50.2	51.4	56.2	63.3	77.5	0.0
	PRR	Mean	-3.7	5.1	11.7	22.0	46.1	572.2
		Std	1.98	0.32	0.48	0.91	3.17	3.75
		Range	7.9	2.0	2.3	5.0	15.5	17.4

Table 6.2: *Effect of different degrees of ischaemic severity on the population level response for common biomarkers for the Mahajan and Shannon frameworks, according to mean, standard deviation (Std) and range.*

The Shannon population variation never exceeds the variation evident under ‘normal’ conditions.

6.2.2 ERP and PRR

6.2.3 Other Biomarkers

6.3 Model Failure During Ischæmia

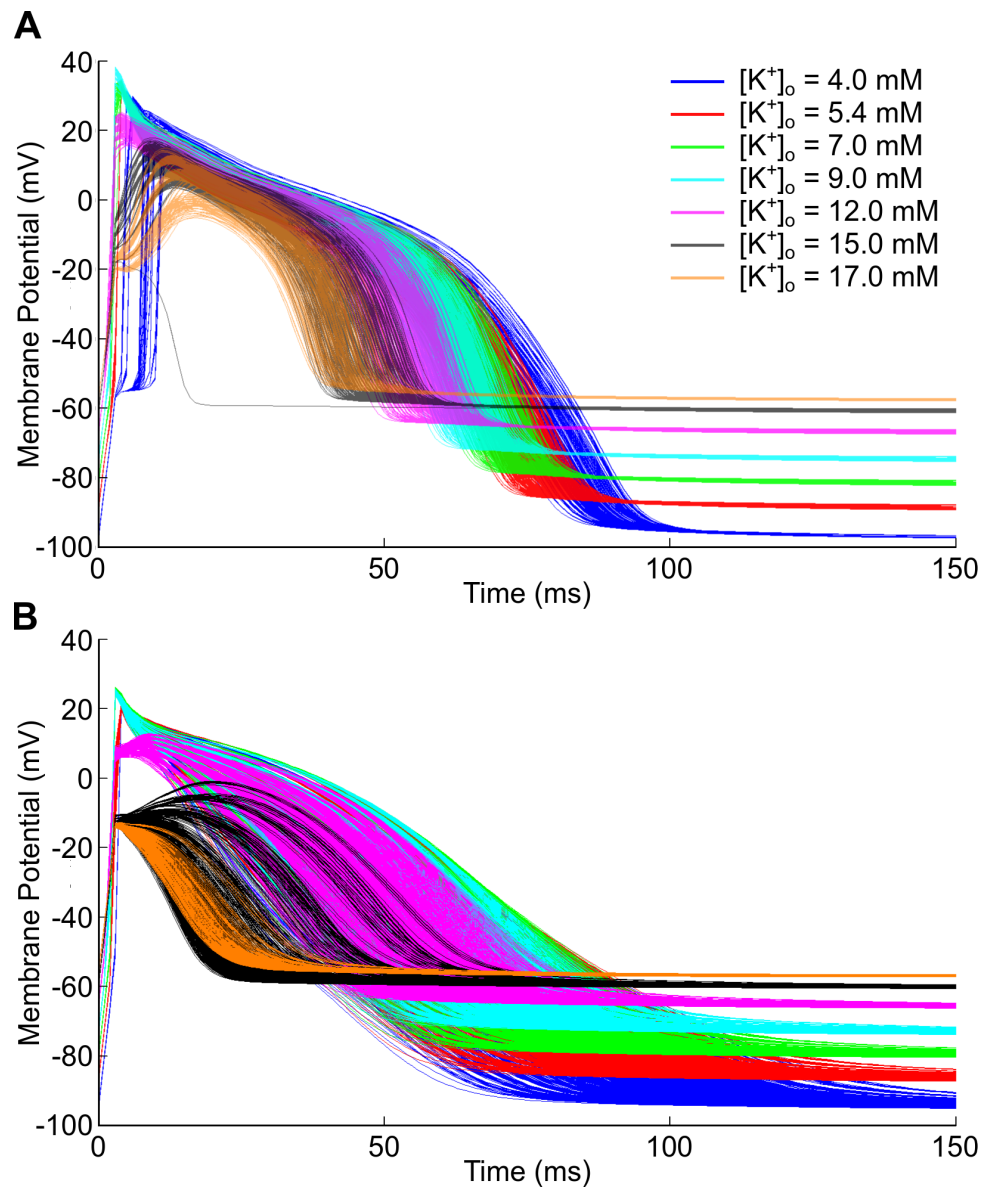


Figure 6.2: Effect of different degrees of ischaemia on the Shannon (A) and Mahajan (B) model populations. The histograms represent the APD_{90} values associated with the populations.

$[K^+]_o$ (mM)	$f_{K\text{-ATP}}$	f_{inhib}	f_{Na}	Shannon		Mahajan	
				Failure	$ERP \geq CL$	Failure	$ERP \geq CL$
5.4	0.00	0	0	0	0	0	0
7.72	0.16	5	6	0	0	0	0
10.04	0.32	10	12	0	0	0	0
12.36	0.48	15	18	0	0	0	0
14.68	0.64	20	24	0	0	0	0
17.0	0.80	25	30	605 (44.7%)	0	613 (78.7%)	166 (100%)
17.0	0.00	0	0	3 (0.0%)	1349 (100%)	0	779 (100%)
5.4	0.80	0	0	0	0	0	0
5.4	0.00	25	0	0	0	0	0
5.4	0.00	0	30	0	0	0	0
5.4	0.80	25	30	0	1349 (100%)	0	779 (100%)
17.0	0.00	25	30	72 (5.3%)	1280 (100%)	183 (23.5%)	596 (100%)
17.0	0.80	0	30	150 (11.1%)	192 (16.0%)	432 (55.5%)	347 (100%)
17.0	0.80	25	0	411 (30.4%)	82 (8.7%)	584 (75.0%)	193 (99.0%)

Table 6.3: Effect of different conditions associated with ischæmia on the number of models within the populations that fail, and of those that do not fail, those which exhibit $ERP \geq CL$. The first group represent those conditions simulating linear progression from normal to ischæmic conditions; the second group represent each individual change in ischæmia applied individually; the third group represent ischæmia when one condition remains ‘normal’.

DIFFUSION

New quote!

(Source)

This appendix gives greater detail about the ionic movement theories, and electric theory properties generally, of the modelling of electrically active cells—note that this applies equally well to both cardiac cells and to neurons.

A.1 Simple Diffusion

By simple diffusion, there is a net movement of particles from a region of high concentration to a region of low diffusion with simple thermal movement. This movement is according to Fick's Law,

$$F_X = -D \frac{\partial C_X}{\partial x}, \quad (\text{A.1})$$

where F_X and C_X represent the flux and concentration of particle X respectively, and D represents the diffusion coefficient. It should be noted that this represents *net* diffusion: there will be movement of particles in both directions. For circumstances where D is constant, this solves to produce

$$F_X = P(C_{X,o} - C_{X,i}), \quad (\text{A.2})$$

where P represents the permeability of the membrane, and is equivalent to D/d , where d represents the thickness of the membrane. $C_{X,o}$ and $C_{X,i}$ represent the extracellular and intracellular concentrations of X , respectively; thus F_X in this form describes flux from the extra- to the intracellular space. It can be noted that for substances that diffuse through the lipid phase of the membrane, the permeability also depends on the oil/water partition coefficient β , according to $P = \beta D/d$.

A.2 Facilitated Diffusion, Michaelis-Menten Kinetics

While Fick's Law can describe the movement of small, uncharged particles and some ions across a membrane very well, it does not serve particularly well for large molecules or charged substances. While ions can move across the membrane via membrane proteins suchs as channels and exchangers, some large molecules such as amino acids and glucose are large enough that pore-based channels would

have no selectivity over what moves through them. Thus, they instead make use of *carrier-mediated diffusion*, also called *facilitated diffusion*, where the molecule binds to a transmembrane protein and causes a conformational change that results in the molecule being translocated across the membrane.

This mechanism obeys Michaelis-Menten kinetics, and can be viewed as a catalysed reaction, where the reaction is not a chemical one, but rather a translation of substance across the membrane.

Briefly, Michaelis-Menten kinetics are used to describe a two-stage reaction, the first stage being reversible, the second stage irreversible:



The above expression uses X_o and X_i to represent the extracellular and intracellular molecule respectively, and C the carrier; CX represents the moment when the molecule and the carrier combine for the transport process. It thus proposes that there is a reversible reaction between the extracellular molecule and the carrier, and that the transport process itself is irreversible. By certain assumptions, including that the number of extracellular molecules is far greater than the number of carriers, the rate of this process can be estimated to be

$$v = \frac{dX_o}{dt} = v_{\max} \frac{[X_o]}{K_m + [X_o]}, \quad (\text{A.3})$$

where v represents the velocity of the reaction (*i.e.*, the rate of translocation of X), v_{\max} represents the maximum velocity at which the translocation can take place, $[X_o]$ the concentration of X outside the cell, K_m represents the so-called Michaelis-Menten constant, which in turn represents the concentration at which the half-maximum speed occurs. It can be noted that v_{\max} is equal to the rate of the final step of the reaction.

Facilitated diffusion shows saturation (the point at which increasing the extracellular concentration further does not lead to an increase in flux), competitive and non-competitive inhibition, stereospecificity and a relatively slow turnover.

A.3 Electrodiffusion

This section deals with the form of transportation that is of most interest for this thesis: the passive movement of charged substances (ions) in the presence of an electrochemical gradient. It should be noted that the content in this section, while being in the appendix, is nonetheless vital for almost all mathematical models of electrically active cellular activity.

A.3.1 The Nernst Equation

A key concept is that of the *Nernst Potential*, derived using the Nernst Equation, which describes the potential difference that is required to oppose the net flow of an ionic species against a specified concentration gradient. The equation shall here be derived in full using statistical mechanics.

Initially, recall that the probability of a system being in a particular state α is given by

$$P(\alpha) = \frac{1}{Z} e^{-\beta E_\alpha}; \quad Z = \sum_i e^{\beta E_i}, \quad (\text{A.4})$$

where E_i is the energy of state i , and $\beta = k_B T$, with T being the temperature of the system.

For a large number of molecules, $[A] \propto P(A)$. Furthermore, if we consider the diffusion of ions from one location to another to be a reversible reaction according to $A \xrightleftharpoons[k_2]{k_1} B$, by applying the law of mass action ($F_{A \rightarrow B} \propto [A]$), at steady state we achieve the following equation, which can be manipulated accordingly:

$$k_1[A] = k_2[B] \quad (\text{A.5})$$

$$\frac{[A]}{[B]} = \frac{k_2}{k_1} \quad (\text{A.6})$$

$$= \frac{\frac{1}{Z}e^{-\beta E_A}}{\frac{1}{Z}e^{-\beta E_B}} \quad (\text{A.7})$$

$$= e^{-\beta(E_A - E_B)} \quad (\text{A.8})$$

$$\Delta E = k_B T \ln \frac{[B]}{[A]} \quad (\text{A.9})$$

At this stage, the electric gradient is introduced to the equation as the reason for the energy difference that maintains the steady state, with $\Delta E = zqV$, where z is the valence of the ionic species being considered, q_e is the charge (in this case equal to the charge of an electron, *i.e.*, the charge of a singly ionised ion), and V is the potential difference.

$$zq_e V = k_B T \ln \frac{[B]}{[A]} \quad (\text{A.10})$$

$$V = \frac{k_B T}{zq_e} \ln \frac{[B]}{[A]} \quad (\text{A.11})$$

$$= \frac{RT}{zF} \ln \frac{[B]}{[A]} \quad (\text{A.12})$$

Equations A.11 and A.12 are equivalent, the only difference being the constants used in the expression. Eq. A.12 is the more common formulation, using the gas constant R and the Faraday constant F in place of the Boltzmann constant k_B and the electron charge q_e respectively. The Nernst potential is, therefore, the potential difference that must be applied to maintain a specified concentration gradient, and is given by either equation.

Bibliography

- Abramson, D., Bernabeu, M. O., Bethwaite, B., Burrage, K., Corrias, A., Enticott, C., Garic, S., Gavaghan, D. J., Peachey, T., Pitt-Francis, J., Pueyo, E., Rodríguez, B., Sher, A., and Tan, J. (2010). High-throughput cardiac science on the Grid. *Philosophical Transactions of the Royal Society A: Mathematical, Physical and Engineering Sciences*, 368(1925):3907–23.
- Abramson, D., Bethwaite, B., Enticott, C., Garic, S., and Peachey, T. (2009). Parameter Space Exploration Using Scientific Workflows. In Allen, G., Nabrzyski, J., Seidel, E., Albada, G. D., Dongarra, J., and Sloot, P. M. A., editors, *Computational Science - ICCS 2009*, volume 5544 of *Lecture Notes in Computer Science*, pages 104–113. Springer Berlin Heidelberg, Berlin, Heidelberg.
- Abramson, D., Bethwaite, B., Enticott, C., Garic, S., and Peachey, T. (2011). Parameter Exploration in Science and Engineering Using Many-Task Computing. *IEEE Transactions on Parallel and Distributed Systems*, 22(6):960–973.
- Abramson, D., Foster, I., Giddy, J., Lewis, A., Sosic, R., Sutherst, R., and White, N. (1997). The Nimrod Computational Workbench : A Case Study in Desktop Metacomputing. In *20th Australasian Computer Science Conference*.
- Abramson, D., Giddy, J., and Kotler, L. (2000). High performance parametric modeling with Nimrod/G: killer application for the global grid? In *14th International Parallel and Distributed Processing Symposium*, pages 520–528, Cancun, Mexico. IEEE Comput. Soc.
- Achard, P. and De Schutter, E. (2006). Complex parameter landscape for a complex neuron model. *PLoS Computational Biology*, 2(7):e94.
- Adeniran, I., McPate, M. J., Witchel, H. J., Hancox, J. C., and Zhang, H. (2011). Increased vulnerability of human ventricle to re-entrant excitation in hERG-linked variant 1 short QT syndrome. *PLoS Computational Biology*, 7(12):e1002313.
- Aistrup, G. L., Kelly, J. E., Kapur, S., Kowalczyk, M., Sysman-Wolpin, I., Kadish, A. H., and Wasserman, J. A. (2006). Pacing-induced heterogeneities in intracellular Ca^{2+} signaling, cardiac alternans, and ventricular arrhythmias in intact rat heart. *Circulation Research*, 99(7):e65–73.
- Allen, D. G. and Orchard, C. H. (1983). Intracellular calcium concentration during hypoxia and metabolic inhibition in mammalian ventricular muscle. *The Journal of Physiology*, 339(1983):107–22.
- Allessie, M. A., Bonke, F. I. M., and Schopman, F. J. G. (1976). Circus movement in rabbit atrial muscle as a mechanism of tachycardia. II. The role of nonuniform recovery of excitability in the occurrence of unidirectional block, as studied with multiple microelectrodes. *Circulation Research*, 39(2):168–77.
- Allessie, M. A., Bonke, F. I. M., and Schopman, F. J. G. (1977). Circus movement in rabbit atrial muscle as a mechanism of tachycardia. III. The "leading circle" concept: a new model of circus movement in cardiac tissue without the involvement of an anatomical obstacle. *Circulation Research*, 41(1):9–18.
- Alvarez-Lacalle, E., Cantalapiedra, I. R., Peñaranda, A., Cinca, J., Hove-Madsen, L., and Echebarria, B. (2013). Dependency of calcium alternans on ryanodine receptor refractoriness. *PloS One*, 8(2):e55042.

- Alwan, A., Armstrong, T., Bettcher, D., Branca, F., Chisholm, D., Ezzati, M., Garfield, R., MacLean, D., Mathers, C., Mendis, S., Poznyak, V., Riley, L., Tang, K. C., and Wild, C. (2011). World Health Organisation Global status report on noncommunicable diseases 2010. Technical report.
- Antzelevitch, C., Sicouri, S., Litovsky, S. H., Lukas, A., Krishnan, S. C., Di Diego, J. M., Gintant, G. A., and Liu, D.-W. (1991). Heterogeneity within the ventricular wall. Electrophysiology and pharmacology of epicardial, endocardial, and M cells. *Circulation Research*, 69(6):1427–1449.
- Applegate, R. J., Walsh, R. A., and O'Rourke, R. A. (1987). Effects of nifedipine on diastolic function during brief periods of flow-limiting ischemia in the conscious dog. *Circulation*, 76(6):1409–21.
- Arevalo, H., Rodríguez, B., and Trayanova, N. A. (2007). Arrhythmogenesis in the heart: Multiscale modeling of the effects of defibrillation shocks and the role of electrophysiological heterogeneity. *Chaos*, 17(1):015103.
- Armstrong, C. M. and Bezanilla, F. (1977). Inactivation of the sodium channel. II. Gating current experiments. *Journal of General Physiology*, 70(5):567–90.
- Auerbach, D. S., GrzÄžda, K. R., Furspan, P. B., Sato, P. Y., Mironov, S., and Jalife, J. (2011). Structural heterogeneity promotes triggered activity, reflection and arrhythmogenesis in cardiomyocyte monolayers. *The Journal of Physiology*, 589(Pt 9):2363–81.
- Avitall, B. (1979). Computer simulation of ventricular tachyarrhythmias during coronary artery ligation and release. *Journal of Electrocardiology*, 12(1):17–22.
- Barrett, T. D., MacLeod, B. A., and Walker, M. J. A. (1997). A model of myocardial ischemia for the simultaneous assessment of electrophysiological changes and arrhythmias in intact rabbits. *Journal of Pharmacological and Toxicological Methods*, 37(1):27–36.
- Bassani, J. W. M., Bassani, R. A., and Bers, D. M. (1994). Relaxation in rabbit and rat cardiac cells: species-dependent differences in cellular mechanisms. *The Journal of Physiology*, 476(2):279–93.
- Bassani, R. A., Altamirano, J., Puglisi, J. L., and Bers, D. M. (2004). Action potential duration determines sarcoplasmic reticulum Ca²⁺ reloading in mammalian ventricular myocytes. *The Journal of Physiology*, 559(Pt 2):593–609.
- Beeler, G. W. and Reuter, H. (1977). Reconstruction of the Action Potential of Ventricular Myocardial Fibres. *The Journal of Physiology*, 268:177–210.
- Behrens, S., Li, C., and Franz, M. R. (1997). Effects of myocardial ischemia on ventricular fibrillation inducibility and defibrillation efficacy. *Journal of the American College of Cardiology*, 29(4):817–24.
- Bers, D. M. and Berlin, J. R. (1995). Kinetics of [Ca]_i decline in cardiac myocytes depend on peak [Ca]_i. *The American Journal of Physiology*, 268(1 Pt 1):C271–7.
- Bers, D. M. and Ellis, D. (1982). Intracellular calcium and sodium activity in sheep heart Purkinje fibres. Effect of changes of external sodium and intracellular pH. *Pflügers Archiv: European Journal of Physiology*, 393(2):171–8.
- Bezanilla, F. (2000). The voltage sensor in voltage-dependent ion channels. *Physiological Reviews*, 80(2):555–92.
- Bezanilla, F. and Armstrong, C. M. (1977). Inactivation of the sodium channel. I. Sodium Current Experiments. *Journal of General Physiology*, 70(5):549–66.
- Bhargava, A., Lin, X., Novak, P., Mehta, K., Khorchev, Y., Delmar, M., and Gorelik, J. (2013). Super-Resolution Scanning Patch-Clamp Reveals Clustering of Functional Ion Channels in the Adult Ventricular Myocyte. *Circulation Research*, pages 1112–1120.
- Biagiotti, M. O. and Quinteiro, R. A. (2006). Gender differences in electrical remodeling and susceptibility to ventricular arrhythmias in rabbits with left ventricular hypertrophy. *Heart Rhythm: the Official Journal of the Heart Rhythm Society*, 3(7):832–9.

- Blanchard, E. M. and Solaro, R. J. (1984). Inhibition of the activation and troponin calcium binding of dog cardiac myofibrils by acidic pH. *Circulation Research*, 55(3):382–91.
- Bourdillon, P. D. and Poole-Wilson, P. A. (1982). The effects of verapamil, quiescence, and cardio-plegia on calcium exchange and mechanical function in ischemic rabbit myocardium. *Circulation Research*, 50(3):360–8.
- Britton, O. J., Bueno-Orovio, A., Van Ammel, K., Lu, H. R., Towart, R., Gallacher, D. J., and Rodríguez, B. (2013). Experimentally calibrated population of models predicts and explains inter-subject variability in cardiac cellular electrophysiology. *Proceedings of the National Academy of Sciences of the United States of America*.
- Cabo, C., Pertsov, A. M., Davidenko, J. M., Baxter, W. T., Gray, R. A., and Jalife, J. (1996). Vortex shedding as a precursor of turbulent electrical activity in cardiac muscle. *Biophysical journal*, 70(3):1105–11.
- Caldwell, J., Burton, F. L., Smith, G. L., and Cobbe, S. M. (2007). Heterogeneity of ventricular fibrillation dominant frequency during global ischemia in isolated rabbit hearts. *Journal of Cardiovascular Electrophysiology*, 18(8):854–61.
- Camacho, S. A., Brandes, R., Figueredo, V. M., and Weiner, M. W. (1994). Ca²⁺ transient decline and myocardial relaxation are slowed during low flow ischemia in rat hearts. *The Journal of Clinical Investigation*, 93(3):951–7.
- Camacho, S. A., Figueredo, V. M., Brandes, R., and Weiner, M. W. (1993). Ca(2+)-dependent fluorescence transients and phosphate metabolism during low-flow ischemia in rat hearts. *The American Journal of Physiology*, 265(1 Pt 2):H114–22.
- Carmeliet, E. (1961). Chloride ions and the membrane potential of Purkinje fibres. *The Journal of Physiology*, 156:375–388.
- Carmeliet, E. (1999). Cardiac ionic currents and acute ischemia: from channels to arrhythmias. *Physiological Reviews*, 79(3):917–1017.
- Carmeliet, E. (2006). Repolarization Reserve in Cardiac Cells. *Journal of Medical and Biological Engineering*, 26(3):97–105.
- Carmeliet, E. and Vereecke, J. (2002). *Cardiac Cellular Electrophysiology*. Springer.
- Ch'en, F. F.-T., Vaughan-Jones, R. D., Clarke, K., and Noble, D. (1998). Modelling myocardial ischaemia and reperfusion. *Progress in Biophysics and Molecular Biology*, 69(2-3):515–38.
- Chen, W., Wasserstrom, J. A., and Shiferaw, Y. (2009). Role of coupled gating between cardiac ryanodine receptors in the genesis of triggered arrhythmias. *American Journal of Physiology - Heart and Circulatory Physiology*, 297(1):H171–80.
- Chen, X., Cordes, J. S., Bradley, J. A., Sun, Z., and Zhou, J. (2006). Use of arterially perfused rabbit ventricular wedge in predicting arrhythmogenic potentials of drugs. *Journal of Pharmacological and Toxicological Methods*, 54(3):261–72.
- Cherry, E. M. and Fenton, F. H. (2007). A tale of two dogs: analyzing two models of canine ventricular electrophysiology. *American Journal of Physiology - Heart and Circulatory Physiology*, 292(1):H43–55.
- Cherry, E. M., Fenton, F. H., and Gilmour, R. F. (2012). Mechanisms of ventricular arrhythmias: a dynamical systems-based perspective. *American Journal of Physiology - Heart and Circulatory Physiology*, 302(12):H2451–63.
- Chou, C.-C., Zhou, S., Hayashi, H., Nihei, M., Liu, Y.-B., Wen, M.-S., Yeh, S.-J., Fishbein, M. C., Weiss, J. N., Lin, S.-F., Wu, D., and Chen, P.-S. (2007). Remodelling of action potential and intracellular calcium cycling dynamics during subacute myocardial infarction promotes ventricular arrhythmias in Langendorff-perfused rabbit hearts. *The Journal of Physiology*, 580(Pt.3):895–906.

- Chudin, E., Goldhaber, J. I., Garfinkel, A., Weiss, J. N., and Kogan, B. (1999). Intracellular Ca(2+) dynamics and the stability of ventricular tachycardia. *Biophysical Journal*, 77(6):2930–41.
- Clancy, C. E. and Kass, R. S. (2005). Inherited and acquired vulnerability to ventricular arrhythmias: cardiac Na⁺ and K⁺ channels. *Physiological Reviews*, 85(1):33–47.
- Clancy, C. E. and Rudy, Y. (1999). Linking a genetic defect to its cellular phenotype in a cardiac arrhythmia. *Nature*, 400(6744):566–9.
- Cleemann, L., Wang, W., and Morad, M. (1998). Two-dimensional confocal images of organization, density, and gating of focal Ca₂₊ release sites in rat cardiac myocytes. *Proceedings of the National Academy of Sciences of the United States of America*, 95(18):10984–9.
- Clusin, W. T. (1983). Caffeine induces a transient inward current in cultured cardiac cells. *Nature*, 301(5897):248–50.
- Clusin, W. T. (2003). Calcium and cardiac arrhythmias: DADs, EADs, and alternans. *Critical Reviews in Clinical Laboratory Sciences*, 40(3):337–75.
- Coetzee, W. A. and Opie, L. H. (1987). Effects of components of ischemia and metabolic inhibition on delayed afterdepolarizations in guinea pig papillary muscle. *Circulation Research*, 61(2):157–65.
- Colquhoun, D., Neher, E., Reuter, H., and Stevens, C. F. (1981). Inward current channels activated by intracellular Ca in cultured cardiac cells. *Nature*, 294(5843):752–4.
- Cook, D. L., Satin, L. S., Ashford, M. L. J., and Hales, C. N. (1988). ATP-sensitive K⁺ channels in pancreatic beta-cells. Spare-channel hypothesis. *Diabetes*, 37(5):495–8.
- Cooper, J., Mirams, G. R., and Niederer, S. A. (2011). High-throughput functional curation of cellular electrophysiology models. *Progress in Biophysics and Molecular Biology*, 107(1):11–20.
- Coronel, R., Janse, M. J., Ophof, T., Wilde, A. A. M., and Taggart, P. (2012). Postrepolarization refractoriness in acute ischemia and after antiarrhythmic drug administration: action potential duration is not always an index of the refractory period. *Heart Rhythm : the Official Journal of the Heart Rhythm Society*, 9(6):977–82.
- Coronel, R., Wilms-Schopman, F. J. G., Ophof, T., and Janse, M. J. (2009). Dispersion of repolarization and arrhythmogenesis. *Heart Rhythm : the Official Journal of the Heart Rhythm Society*, 6(4):537–43.
- Corrias, A., Giles, W. R., and Rodríguez, B. (2011). Ionic mechanisms of electrophysiological properties and repolarization abnormalities in rabbit Purkinje fibers. *American Journal of Physiology - Heart and Circulatory Physiology*, 300(5):H1806–13.
- Cross, H. R., Lu, L., Steenbergen, C., Philipson, K. D., and Murphy, E. (1998). Overexpression of the cardiac Na⁺/Ca₂₊ exchanger increases susceptibility to ischemia/reperfusion injury in male, but not female, transgenic mice. *Circulation Research*, 83(12):1215–23.
- Dangerfield, C. E., Kay, D., and Burrage, K. (2012). Modeling ion channel dynamics through reflected stochastic differential equations. *Physical Review E, Statistical, Nonlinear, and Soft Matter Physics*, 85(5 Pt 1):051907.
- Davies, M. R., Mistry, H. B., Hussein, L., Pollard, C. E., Valentin, J.-P., Swinton, J., and Abi-Gerges, N. (2012). An in silico canine cardiac midmyocardial action potential duration model as a tool for early drug safety assessment. *American Journal of Physiology - Heart and Circulatory Physiology*, 302(7):H1466–80.
- Dhalla, N. S., Panagia, V., Singal, P. K., Makino, N., Dixon, I. M. C., and Eyolfson, D. A. (1988). Alterations in heart membrane calcium transport during the development of ischemia-reperfusion injury. *Journal of Molecular and Cellular Cardiology*, 20 Suppl 2(Supplement II):3–13.

- DiFrancesco, D. and Noble, D. (1985). A Model of Cardiac Electrical Activity Incorporating Ionic Pumps and Concentration Changes. *Philosophical Transactions of the Royal Society B: Biological Sciences*, 307(1133):353–398.
- Downar, E., Janse, M. J., and Durrer, D. (1977). The effect of acute coronary artery occlusion on subepicardial transmembrane potentials in the intact porcine heart. *Circulation*, 56(2):217–224.
- Dumaine, R., Wang, Q., Keating, M. T., Hartmann, H. A., Schwartz, P. J., Brown, A. M., and Kirsch, G. E. (1996). Multiple mechanisms of Na⁺ channel-linked long-QT syndrome. *Circulation Research*, 78(5):916–24.
- Eckardt, L., Haverkamp, W., Göttker, U., Madeja, M., Johna, R., Borggrefe, M., and Breithardt, G. (1998). Divergent effect of acute ventricular dilatation on the electrophysiologic characteristics of d,l-sotalol and flecainide in the isolated rabbit heart. *Journal of Cardiovascular Electrophysiology*, 9(4):366–83.
- Edelman, G. M. and Gally, J. A. (2001). Degeneracy and complexity in biological systems. *Proceedings of the National Academy of Sciences of the United States of America*, 98(24):13763–8.
- Eisner, D. A., Choi, H. S., Díaz, M. E., O'Neill, S. C., and Trafford, A. W. (2000). Integrative analysis of calcium cycling in cardiac muscle. *Circulation Research*, 87(12):1087–94.
- Eisner, D. A. and Sipido, K. R. (2004). Sodium calcium exchange in the heart: necessity or luxury? *Circulation Research*, 95(6):549–51.
- Esumi, K., Nishida, M., Shaw, D., Smith, T. W., and Marsh, J. D. (1991). NADH measurements in adult rat myocytes during simulated ischemia. *The American Journal of Physiology*, 260(6 Pt 2):H1743–52.
- Fabiato, A. (1992). Two kinds of calcium-induced release of calcium from the sarcoplasmic reticulum of skinned cardiac cells. *Advances in Experimental Medicine and Biology*, 311:245–62.
- Fauconnier, J., Meli, A. C., Thireau, J., Roberge, S., Shan, J., Sassi, Y., Reiken, S. R., Rauzier, J.-M., Marchand, A., Chauvier, D., Cassan, C., Crozier, C., Bideaux, P., Lompré, A.-M., Jacotot, E., Marks, A. R., and Lacampagne, A. (2011). Ryanodine receptor leak mediated by caspase-8 activation leads to left ventricular injury after myocardial ischemia-reperfusion. *Proceedings of the National Academy of Sciences of the United States of America*, 108(32):13258–63.
- Fauconnier, J., Roberge, S., Saint, N., and Lacampagne, A. (2013). Type 2 ryanodine receptor: a novel therapeutic target in myocardial ischemia/reperfusion. *Pharmacology & Therapeutics*, 138(3):323–32.
- Fedorov, V. V., Glukhov, A. V., and Chang, R. (2012). Conduction barriers and pathways of the sinoatrial pacemaker complex: their role in normal rhythm and atrial arrhythmias. *American Journal of Physiology - Heart and Circulatory Physiology*, 302(9):H1773–83.
- Feher, J. J., LeBolt, W. R., and Manson, N. H. (1989). Differential effect of global ischemia on the ryanodine-sensitive and ryanodine-insensitive calcium uptake of cardiac sarcoplasmic reticulum. *Circulation Research*, 65(5):1400–8.
- Ferrero, J. M., Sáiz, N. V., and Thakor, N. V. (1996). Simulation of Action Potentials From Metabolically Impaired Cardiac Myocytes. *Circulation Research*, 79(2):208–221.
- Ferrero, J. M., Trénor, B., Rodríguez, B., and Sáiz, J. (2003a). Electrical Activity and Reentry During Regional Myocardial Ischemia: Insights From Simulations. *International Journal of Bifurcation and Chaos*, 13(12):3703–3715.
- Ferrero, J. M., Trénor, B., Sáiz, J., Montilla, F., and Hernandez, V. (2003b). Electrical activity and reentry in acute regional ischemia: insights from simulations. In *Annual International Conference of the IEEE Engineering in Medicine and Biology Society*, pages 17–20. IEEE.

- Ferrier, G. R., Moffat, M. P., and Lukas, A. (1985). Possible mechanisms of ventricular arrhythmias elicited by ischemia followed by reperfusion. Studies on isolated canine ventricular tissues. *Circulation Research*, 56(2):184–94.
- Fink, M., Noble, D., Virág, L., Varró, A., and Giles, W. R. (2008). Contributions of HERG K⁺ current to repolarization of the human ventricular action potential. *Progress in Biophysics and Molecular Biology*, 96(1-3):357–76.
- Fitzhugh, R. (1960). Thresholds and plateaus in the Hodgkin-Huxley nerve equations. *Journal of General Physiology*, 43:867–96.
- Fitzhugh, R. (1961). Impulses and Physiological States in Theoretical Models of Nerve Membrane. *Biophysical Journal*, 1(6):445–66.
- Franzini-Armstrong, C., Protasi, F., and Tijskens, P. (2005). The assembly of calcium release units in cardiac muscle. *Annals of the New York Academy of Sciences*, 1047:76–85.
- Fülöp, L., Bányász, T., Magyar, J., Szentandrassy, N., Varró, A., and Nánási, P. P. (2004). Reopening of L-type calcium channels in human ventricular myocytes during applied epicardial action potentials. *Acta Physiologica Scandinavica*, 180(1):39–47.
- Gaborit, N., Le Bouter, S., Szuts, V., Varró, A., Escande, D., Nattel, S., and Demolombe, S. (2007). Regional and tissue specific transcript signatures of ion channel genes in the non-diseased human heart. *The Journal of Physiology*, 582(Pt 2):675–93.
- Garfinkel, A., Kim, Y.-H., Voroshilovsky, O., Qu, Z., Kil, J. R., Lee, M.-H., Karagueuzian, H. S., Weiss, J. N., and Chen, P.-S. (2000). Preventing ventricular fibrillation by flattening cardiac restitution. *Proceedings of the National Academy of Sciences of the United States of America*, 97(11):6061–6.
- Garny, A., Kohl, P., and Noble, D. (2003). Cellular Open Resource (COR): A Public CellML Based Environment For Modeling Biological Function. *International Journal of Bifurcation and Chaos*, 13(12):3579–3590.
- Garny, A., Noble, D., Hunter, P. J., and Kohl, P. (2009). CELLULAR OPEN RESOURCE (COR): current status and future directions. *Philosophical transactions. Series A, Mathematical, physical, and engineering sciences*, 367(1895):1885–905.
- Gasser, R. N. A. and Vaughan-Jones, R. D. (1990). Mechanism of potassium efflux and action potential shortening during ischaemia in isolated mammalian cardiac muscle. *The Journal of Physiology*, 431:713–41.
- Gemmell, P., Burrage, K., Rodríguez, B., and Quinn, T. A. (2010). Exploring the parameter space of a rabbit ventricular action potential model to investigate the effect of variation on action potential and calcium transients. *Annual International Conference of the IEEE Engineering in Medicine and Biology Society*, 2010:2662–5.
- Giles, W. R. and Imaizumi, Y. (1988). Comparison of potassium currents in rabbit atrial and ventricular cells. *The Journal of Physiology*, 405:123–45.
- Girod, S. and Becker, A. (2006). Cardiac muscle.
- Goaillard, J.-M., Taylor, A. L., Schulz, D. J., and Marder, E. (2009). Functional consequences of animal-to-animal variation in circuit parameters. *Nature Neuroscience*, 12(11):1424–30.
- Goldhaber, J. I., Xie, L.-H., Duong, T., Motter, C., Khuu, K., and Weiss, J. N. (2005). Action potential duration restitution and alternans in rabbit ventricular myocytes: the key role of intracellular calcium cycling. *Circulation Research*, 96(4):459–66.
- Gough, W. B., Mehra, R., Restivo, M., Zeiler, R. H., and El-Sherif, N. (1985). Reentrant ventricular arrhythmias in the late myocardial infarction period in the dog. 13. Correlation of activation and refractory maps. *Circulation Research*, 57(3):432–42.

- Gray, R. A., Pertsov, A. M., and Jalife, J. (1998). Spatial and temporal organization during cardiac fibrillation. *Nature*, 392(6671):75–8.
- Greenstein, J. L. and Winslow, R. L. (2002). An integrative model of the cardiac ventricular myocyte incorporating local control of Ca²⁺ release. *Biophysical Journal*, 83(6):2918–45.
- Haïssaguerre, M., Jaïs, P., Shah, D. C., Takahashi, A., Hocini, M., Quiniou, G., Garrigue, S., Le Mouroux, A., Le Métayer, P., and Clémenty, J. (1998). Spontaneous initiation of atrial fibrillation by ectopic beats originating in the pulmonary veins. *The New England Journal of Medicine*, 339(10):659–66.
- Hall, A. E., Hutter, O. F., and Noble, D. (1963). Current-Voltage Relations of Purkinje Fibres in Sodium Deficient Solutions. *The Journal of Physiology*, 166:225–240.
- Harris, A. S., Bisteni, A., Russell, R. A., Brigham, J. C., and Firestone, J. E. (1954). Excitatory factors in ventricular tachycardia resulting from myocardial ischemia; potassium a major excitant. *Science*, 119(3085):200–3.
- Hashambhoy, Y. L., Winslow, R. L., and Greenstein, J. L. (2011). CaMKII-dependent activation of late INa contributes to cellular arrhythmia in a model of the cardiac myocyte. *Conference proceedings : ... Annual International Conference of the IEEE Engineering in Medicine and Biology Society. IEEE Engineering in Medicine and Biology Society. Conference*, 2011:4665–8.
- Haverkamp, W., Breithardt, G., Camm, A. J., Janse, M. J., Rosen, M. R., Antzelevitch, C., Escande, D., Franz, M., Malik, M., Moss, A. J., and Shah, R. (2000). The potential for QT prolongation and pro-arrhythmia by non-anti-arrhythmic drugs: clinical and regulatory implications. Report on a Policy Conference of the European Society of Cardiology. *Cardiovascular Research*, 47(2):219–33.
- Heijman, J., Zaza, A., Johnson, D. M., Rudy, Y., Peeters, R. L. M., Volders, P. G. A., and Westra, R. L. (2013). Determinants of Beat-to-Beat Variability of Repolarization Duration in the Canine Ventricular Myocyte: A Computational Analysis. *PLoS Computational Biology*, 9(8):e1003202.
- Henderson, S. A., Goldhaber, J. I., So, J. M., Han, T., Motter, C., Ngo, A., Chantawansri, C., Ritter, M. R., Friedlander, M., Nicoll, D. A., Frank, J. S., Jordan, M. C., Roos, K. P., Ross, R. S., and Philipson, K. D. (2004). Functional adult myocardium in the absence of Na⁺-Ca²⁺ exchange: cardiac-specific knockout of NCX1. *Circulation Research*, 95(6):604–11.
- Hiraoka, M., Sunami, A., Fan, Z., and Sawanobori, T. (1992). Multiple ionic mechanisms of early afterdepolarizations in isolated ventricular myocytes from guinea-pig hearts. *Annals of the New York Academy of Sciences*, 644:33–47.
- Hodgkin, A. L. (1954). A note on conduction velocity. *The Journal of Physiology*, 125(1):221–4.
- Hodgkin, A. L. and Huxley, A. F. (1952). A quantitative description of membrane current and its application to conduction and excitation in nerve. *The Journal of Physiology*, 117:500–544.
- Hoefen, R., Reumann, M., Goldenberg, I., Moss, A. J., O-Uchi, J., Gu, Y., McNitt, S., Zareba, W., Jons, C., Kanters, J. K., Platonov, P. G., Shimizu, W., Wilde, A. A. M., Rice, J. J., and Lopes, C. M. B. (2012). In silico cardiac risk assessment in patients with long QT syndrome: type I: clinical predictability of cardiac models. *Journal of the American College of Cardiology*, 60(21):2182–91.
- Huang, C., Bao, M., Jiang, H., Liu, J., Yang, B., and Wang, T. (2004). Differences in the changing trends of monophasic action potential duration and effective refractory period of the ventricular myocardium after myocardial infarction in vivo. *Circulation Journal : Official Journal of the Japanese Circulation Society*, 68(12):1205–9.
- Hund, T. J., Kucera, J. P., Otani, N. F., and Rudy, Y. (2001). Ionic charge conservation and long-term steady state in the Luo-Rudy dynamic cell model. *Biophysical Journal*, 81(6):3324–31.
- Hutter, O. F. and Noble, D. (1960). Rectifying properties of heart muscle. *Nature*, 188:495.

- Ichihara, K., Haga, N., and Abiko, Y. (1984). Is ischemia-induced pH decrease of dog myocardium respiratory or metabolic acidosis? *The American Journal of Physiology*, 246(5 Pt 2):H652–7.
- Inoue, R., Jensen, L. J. r., Shi, J., Morita, H., Nishida, M., Honda, A., and Ito, Y. (2006). Transient receptor potential channels in cardiovascular function and disease. *Circulation Research*, 99(2):119–31.
- Iost, N., Virág, L., Opincariu, M., Szécsi, J., Varró, A., and Papp, J. G. (1998). Delayed rectifier potassium current in undiseased human ventricular myocytes. *Cardiovascular Research*, 40(3):508–15.
- Isoyama, S., Apstein, C. S., Wexler, L. F., Grice, W. N., and Lorell, B. H. (1987). Acute decrease in left ventricular diastolic chamber distensibility during simulated angina in isolated hearts. *Circulation Research*, 61(6):925–33.
- Jalife, J. (2003). Rotors and spiral waves in atrial fibrillation. *Journal of Cardiovascular Electrophysiology*, 14(7):776–80.
- Jalife, J. (2009). Inward rectifier potassium channels control rotor frequency in ventricular fibrillation. *Heart Rhythm : the Official Journal of the Heart Rhythm Society*, 6(II Suppl):S44–8.
- Janse, M. J., Vermeulen, J. T., Ophof, T., Coronel, R., Wilms-Schopman, F. J. G., Rademaker, H. M. E., Baartscheer, A., and Dekker, L. R. C. (2001). Arrhythmogenesis in heart failure. *Journal of Cardiovascular Electrophysiology*, 12(4):496–9.
- John, R. M., Tedrow, U. B., Koplan, B. A., Albert, C. M., Epstein, L. M., Sweeney, M. O., Miller, A. L., Michaud, G. F., and Stevenson, W. G. (2012). Ventricular arrhythmias and sudden cardiac death. *Lancet*, 380(9852):1520–9.
- Jons, C., O-Uchi, J., Moss, A. J., Reumann, M., Rice, J. J., Goldenberg, I., Zareba, W., Wilde, A. A. M., Shimizu, W., Kanters, J. K., McNitt, S., Hofman, N., Robinson, J. L., and Lopes, C. M. B. (2011). Use of mutant-specific ion channel characteristics for risk stratification of long QT syndrome patients. *Science Translational Medicine*, 3(76):76ra28.
- Jost, N., Virág, L., Bitay, M., Takács, J., Lengyel, C., Biliczki, P., Nagy, Z., Bogáts, G., Lathrop, D. A., Papp, J. G., and Varró, A. (2005). Restricting excessive cardiac action potential and QT prolongation: a vital role for IKs in human ventricular muscle. *Circulation*, 112(10):1392–9.
- Jou, C. J., Barnett, S. M., Bian, J.-T., Weng, H. C., Sheng, X., and Tristani-Firouzi, M. (2013). An In Vivo Cardiac Assay to Determine the Functional Consequences of Putative Long QT Syndrome Mutations. *Circulation Research*, pages 826–830.
- Jung, B.-C., Lee, S.-H., Cho, Y.-K., Park, H.-S., Kim, Y.-N., Lee, Y.-S., and Shin, D.-G. (2011). Role of the alternans of action potential duration and aconitine-induced arrhythmias in isolated rabbit hearts. *Journal of Korean Medical Science*, 26(12):1576–81.
- Jurkat-Rott, K. and Lehmann-Horn, F. (2005). Muscle channelopathies and critical points in functional and genetic studies. *Journal of Clinical Investigation*, 115(8):2000–9.
- Kagiyama, Y., Hill, J. L., and Gettes, L. S. (1982). Interaction of acidosis and increased extracellular potassium on action potential characteristics and conduction in guinea pig ventricular muscle. *Circulation Research*, 51(5):614–23.
- Kannankeril, P., Roden, D. M., and Darbar, D. (2010). Drug-induced long QT syndrome. *Pharmacological Reviews*, 62(4):760–81.
- Kaplan, P., Hendrikx, M., Mattheussen, M., Mubagwa, K., and Flameng, W. (1992). Effect of ischemia and reperfusion on sarcoplasmic reticulum calcium uptake. *Circulation Research*, 71(5):1123–1130.
- Kherlopian, A. R., Ortega, F. A., and Christini, D. J. (2011). Cardiac myocyte model parameter sensitivity analysis and model transformation using a genetic algorithm. In *13th Annual Conference*

- Companion on Genetic and Evolutionary Computation*, page 755, New York, New York, USA. ACM Press.
- Kihara, Y., Grossman, W., and Morgan, J. P. (1989). Direct measurement of changes in intracellular calcium transients during hypoxia, ischemia, and reperfusion of the intact mammalian heart. *Circulation Research*, 65(4):1029–1044.
- Kirchhof, P., Degen, H., Franz, M. R., Eckardt, L., Fabritz, L., Milberg, P., Läer, S., Neumann, J., Breithardt, G., and Haverkamp, W. (2003). Amiodarone-induced postrepolarization refractoriness suppresses induction of ventricular fibrillation. *Journal of Pharmacology and Experimental Therapeutics*, 305(1):257–263.
- Kléber, A. G. (1987). Conduction of the impulse in the ischemic myocardium—implications for malignant ventricular arrhythmias. *Experientia*, 43(10):1056–61.
- Kléber, A. G., Rieger, C. B., and Janse, M. J. (1987a). Electrical uncoupling and increase of extracellular resistance after induction of ischemia in isolated, arterially perfused rabbit papillary muscle. *Circulation Research*, 61(2):271–279.
- Kléber, A. G., Rieger, C. B., and Janse, M. J. (1987b). Extracellular K⁺ and H⁺ shifts in early ischemia: mechanisms and relation to changes in impulse propagation. *Journal of Molecular and Cellular Cardiology*, 19 Suppl 5(Supplement V):35–44.
- Kléber, A. G. and Rudy, Y. (2004). Basic mechanisms of cardiac impulse propagation and associated arrhythmias. *Physiological Reviews*, 84(2):431–88.
- Krause, H., Antoni, H., and Fleckenstein, A. (1966). [An electronic model for the formation of local and transmitted stimuli on the myocardium fibers based upon variable current-voltage characteristics for potassium and sodium ions]. *Pflügers Archiv für die gesamte Physiologie des Menschen und der Tiere*, 289(1):12–36.
- Krause, S. and Hess, M. L. (1984). Characterization of cardiac sarcoplasmic reticulum dysfunction during short-term, normothermic, global ischemia. *Circulation Research*, 55(2):176–84.
- Kuo, C.-S., Munakata, K., Reddy, C. P., and Surawicz, B. (1983). Characteristics and possible mechanism of ventricular arrhythmia dependent on the dispersion of action potential durations. *Circulation*, 67(6):1356–1367.
- Kurokawa, J., Kodama, M., Furukawa, T., and Clancy, C. E. (2012). Sex and gender aspects in antiarrhythmic therapy. *Handbook of Experimental Pharmacology*, (214):237–63.
- Kurz, R. W., Mohabir, R., Ren, X. L., and Franz, M. R. (1993). Ischaemia induced alternans of action potential duration in the intact-heart: dependence on coronary flow, preload and cycle length. *European Heart Journal*, 14(10):1410–20.
- Laurita, K. R. and Rosenbaum, D. S. (2008). Cellular mechanisms of arrhythmogenic cardiac alternans. *Progress in Biophysics and Molecular Biology*, 97(2-3):332–47.
- LeBlanc, J., Ward, M. O., and Wittels, N. (1990). Exploring N-Dimensional Databases. In *Proceedings of the 1st Conference on Visualization*, pages 230–237.
- Lee, H.-C., Mohabir, R., Smith, N., Franz, M. R., and Clusin, W. T. (1988). Effect of ischemia on calcium-dependent fluorescence transients in rabbit hearts containing indo 1. Correlation with monophasic action potentials and contraction. *Circulation*, 78(4):1047–59.
- Lee, K. S., Ladinsky, H., and Stuckey, J. H. (1967). Decreased Ca²⁺ Uptake by Sarcoplasmic Reticulum after Coronary Artery Occlusion for 60 and 90 Minutes. *Circulation Research*, 21(4):439–444.
- Lemay, M., de Lange, E., and Kucera, J. P. (2011). Effects of stochastic channel gating and distribution on the cardiac action potential. *Journal of Theoretical Biology*, 281(1):84–96.
- Lengyel, C., Iost, N., Virág, L., Varró, A., Lathrop, D. A., and Papp, J. G. (2001). Pharmacological block of the slow component of the outward delayed rectifier current (I(Ks)) fails to lengthen

- rabbit ventricular muscle QT(c) and action potential duration. *British Journal Of Pharmacology*, 132(1):101–10.
- Levitsky, D. O., Benevolensky, D. S., Ikemoto, N., Syrbu, S. I., and Watras, J. (1989). Monoclonal antibodies to dog heart sarcoplasmic reticulum as markers of endoplasmic reticulum. *Journal of Molecular and Cellular Cardiology*, 21 Suppl 1(Supplement 1):55–8.
- Li, G.-R., Yang, B., Feng, J., Bosch, R. F., Carrier, M., and Nattel, S. (1999). Transmembrane ICa contributes to rate-dependent changes of action potentials in human ventricular myocytes. *American Journal of Physiology*, 276(1 Pt 2):H98–H106.
- Lloyd, C. M., Lawson, J. R., Hunter, P. J., and Nielsen, P. F. (2008). The CellML Model Repository. *Bioinformatics*, 24(18):2122–3.
- Lukas, A. and Antzelevitch, C. (1996). Phase 2 reentry as a mechanism of initiation of circus movement reentry in canine epicardium exposed to simulated ischemia. *Cardiovascular Research*, 32(3):593–603.
- Luo, C.-H. and Rudy, Y. (1991). A Model of the Ventricular Cardiac Action Potential: Depolarization, Repolarization and Their Interaction. *Circulation Research*, 68:1501–1526.
- Luo, C.-H. and Rudy, Y. (1994a). A dynamic model of the cardiac ventricular action potential. I. Simulations of ionic currents and concentration changes. *Circulation Research*, 74(6):1071–96.
- Luo, C.-H. and Rudy, Y. (1994b). A dynamic model of the cardiac ventricular action potential. II. Afterdepolarizations, triggered activity, and potentiation. *Circulation Research*, 74(6):1097–113.
- Mahajan, A., Shiferaw, Y., Sato, D., Baher, A., Olcese, R., Xie, L.-H., Yang, M.-J., Chen, P.-S., Restrepo, J. G., Karma, A., Garfinkel, A., Qu, Z., and Weiss, J. N. (2008). A rabbit ventricular action potential model replicating cardiac dynamics at rapid heart rates. *Biophysical Journal*, 94(2):392–410.
- Malloy, C. R., Buster, D. C., Castro, M. M. C. A., Gerald, C. F. G. C., Jeffrey, F. M. H., and Sherry, A. D. (1990). Influence of global ischemia on intracellular sodium in the perfused rat heart. *Magnetic Resonance in Medicine : Official Journal of the Society of Magnetic Resonance in Medicine / Society of Magnetic Resonance in Medicine*, 15(1):33–44.
- Mandapati, R., Skanes, A., Chen, J., Berenfeld, O., and Jalife, J. (2000). Stable microreentrant sources as a mechanism of atrial fibrillation in the isolated sheep heart. *Circulation*, 101(2):194–9.
- Marder, E. and Taylor, A. L. (2011). Multiple models to capture the variability in biological neurons and networks. *Nature Neuroscience*, 14(2):133–8.
- McAllister, R. E., Noble, D., and Tsien, R. W. (1975). Reconstruction of the electrical activity of cardiac Purkinje fibres. *The Journal of Physiology*, 251(1):1–59.
- McIntosh, M. A., Cobbe, S. M., and Smith, G. L. (2000). Heterogeneous changes in action potential and intracellular Ca²⁺ in left ventricular myocyte sub-types from rabbits with heart failure. *Cardiovascular Research*, 45(2):397–409.
- McKay, M. D., Beckman, R. J., and Conover, W. J. (1979). Comparison of Three Methods for Selecting Values of Input Variables in the Analysis of Output from a Computer Code. *Technometrics*, 21(2):239–245.
- Meech, R. W. and Standen, N. B. (1975). Potassium activation in Helix aspersa neurones under voltage clamp: a component mediated by calcium influx. *The Journal of Physiology*, 249(2):211–39.
- Michailova, A., Lorentz, W., and McCulloch, A. D. (2007). Modeling transmural heterogeneity of K(ATP) current in rabbit ventricular myocytes. *American Journal of Physiology - Cell Physiology*, 293(2):C542–57.

- Michailova, A., Saucerman, J., Belik, M. E., and McCulloch, A. D. (2005). Modeling regulation of cardiac KATP and L-type Ca^{2+} currents by ATP, ADP, and Mg^{2+} . *Biophysical Journal*, 88(3):2234–49.
- Mirams, G. R., Arthurs, C. J., Bernabeu, M. O., Bordas, R., Cooper, J., Corrias, A., Davit, Y., Dunn, S.-J., Fletcher, A. G., Harvey, D. G., Marsh, M. E., Osborne, J. M., Pathmanathan, P., Pitt-Francis, J., Southern, J., Zemzemi, N., and Gavaghan, D. J. (2013). Chaste: an open source C++ library for computational physiology and biology. *PLoS Computational Biology*, 9(3):e1002970.
- Miura, M., Boyden, P. A., and ter Keurs, H. E. (1998). Ca^{2+} waves during triggered propagated contractions in intact trabeculae. *The American Journal of Physiology*, 274(1 Pt 2):H266–76.
- Mohabir, R., Lee, H.-C., Kurz, R. W., and Clusin, W. T. (1991). Effects of ischemia and hypercarbic acidosis on myocyte calcium transients, contraction, and pHi in perfused rabbit hearts. *Circulation Research*, 69(6):1525–1537.
- Mubagwa, K. (1995). Sarcoplasmic reticulum function during myocardial ischaemia and reperfusion. *Cardiovascular Research*, 30(2):166–75.
- Nattel, S., Frelin, Y., Gaborit, N., Louault, C., and Demolombe, S. (2010). Ion-channel mRNA-expression profiling: Insights into cardiac remodeling and arrhythmic substrates. *Journal of Molecular and Cellular Cardiology*, 48(1):96–105.
- Neely, J. R., Whitmer, J. T., and Rovetto, M. J. (1975). Effect of coronary blood flow on glycolytic flux and intracellular pH in isolated rat hearts. *Circulation Research*, 37(6):733–41.
- Nekouzadeh, A. and Rudy, Y. (2011). Continuum molecular simulation of large conformational changes during ion-channel gating. *PLoS One*, 6(5):e20186.
- Niederer, S. (2013). Regulation of ion gradients across myocardial ischemic border zones: a biophysical modelling analysis. *PLoS One*, 8(4):e60323.
- Niederer, S. A., Fink, M., Noble, D., and Smith, N. P. (2009). A meta-analysis of cardiac electrophysiology computational models. *Experimental Physiology*, 94(5):486–95.
- Noble, D. (1960). Cardiac Action and Pacemaker Potentials based on the Hodgkin-Huxley Equations. *Nature*, 4749:495–497.
- Noble, D. (1962). A modification of the Hodgkin-Huxley equations applicable to Purkinje fibre action and pace-maker potentials. *The Journal of Physiology*, 160:317–52.
- Noble, D. (2002). Simulation of Na/Ca exchange activity during ischemia. *Annals of the New York Academy of Sciences*, 976:431–7.
- Noble, D. (2011). Successes and failures in modeling heart cell electrophysiology. *Heart Rhythm : the Official Journal of the Heart Rhythm Society*, 8(11):1798–803.
- Noble, D., Garny, A., and Noble, P. J. (2012). How the Hodgkin-Huxley equations inspired the Cardiac Physiome Project. *The Journal of Physiology*, 590(Pt 11):2613–28.
- Noble, D. and Rudy, Y. (2001). Models of cardiac ventricular action potentials: iterative interaction between experiment and simulation. *Philosophical Transactions of the Royal Society A: Mathematical, Physical and Engineering Sciences*, 359(1783):1127–1142.
- Nolasco, J. B. and Dahlen, R. W. (1968). A graphic method for the study of alternation in cardiac action potentials. *Journal of Applied Physiology*, 25(2):191–6.
- Noujaim, S. F., Berenfeld, O., Kalifa, J., Cerrone, M., Nanthakumar, K., Atienza, F., Moreno, J., Mironov, S., and Jalife, J. (2007). Universal scaling law of electrical turbulence in the mammalian heart. *Proceedings of the National Academy of Sciences of the United States of America*, 104(52):20985–9.

- Nygren, A., Fiset, C., Firek, L., Clark, J. W., Lindblad, D. S., Clark, R. B., and Giles, W. R. (1998). Mathematical model of an adult human atrial cell: the role of K⁺ currents in repolarization. *Circulation Research*, 82(1):63–81.
- Pandit, S. V. and Jalife, J. (2013). Rotors and the Dynamics of Cardiac Fibrillation. *Circulation Research*, 112(5):849–862.
- Panfilov, A. V. (2006). Is heart size a factor in ventricular fibrillation? Or how close are rabbit and human hearts? *Heart Rhythm : the Official Journal of the Heart Rhythm Society*, 3(7):862–4.
- Peng, W. (2005). *Clutter-Based Dimension Reordering in Multi-Dimensional Data Visualization*. Msc (computer science), Worcester Polytechnic Institute.
- Peng, W., Ward, M. O., and Rundensteiner, E. A. (2004). Clutter Reduction in Multi-Dimensional Data Visualization Using Dimension Reordering. In Ward, M. and Munzner, T., editors, *IEEE Symposium on Information Visualization*, pages 89–96. IEEE.
- Pike, M. M., Luo, C. S., Clark, M. D., Kirk, K. A., Kitakaze, M., Madden, M. C., Cragoe, E. J., and Pohost, G. M. (1993). NMR measurements of Na⁺ and cellular energy in ischemic rat heart: role of Na(+)-H⁺ exchange. *The American Journal of Physiology*, 265(6 Pt 2):H2017–26.
- Pitt-Francis, J., Pathmanathan, P., Bernabeu, M. O., Bordas, R., Cooper, J., Fletcher, A. G., Mirams, G. R., Murray, P., Osborne, J. M., Walter, A., Chapman, S. J., Garny, A., van Leeuwen, I. M., Maini, P. K., Rodríguez, B., Waters, S. L., Whiteley, J. P., Byrne, H. M., and Gavaghan, D. J. (2009). Chaste: A test-driven approach to software development for biological modelling. *Computer Physics Communications*, 180(12):2452–2471.
- Pollard, A. E., Cascio, W. E., Fast, V. G., and Knisley, S. B. (2002). Modulation of triggered activity by uncoupling in the ischemic border. A model study with phase 1b-like conditions. *Cardiovascular Research*, 56(3):381–92.
- Ponard, J. G. C., Kondratyev, A. A., and Kucera, J. P. (2007). Mechanisms of intrinsic beating variability in cardiac cell cultures and model pacemaker networks. *Biophysical Journal*, 92(10):3734–52.
- Pozzan, T., Rizzuto, R., Volpe, P., and Meldolesi, J. (1994). Molecular and cellular physiology of intracellular calcium stores. *Physiological Reviews*, 74(3):595–636.
- Prinz, A. A., Billimoria, C. P., and Marder, E. (2003). Alternative to hand-tuning conductance-based models: construction and analysis of databases of model neurons. *Journal of Neurophysiology*, 90(6):3998–4015.
- Pruvot, E. J., Katra, R. P., Rosenbaum, D. S., and Laurita, K. R. (2004). Role of calcium cycling versus restitution in the mechanism of repolarization alternans. *Circulation Research*, 94(8):1083–90.
- Pueyo, E., Corrias, A., Virág, L., Jost, N., Szél, T., Varró, A., Szentandrásy, N., Nánási, P. P., Burrage, K., and Rodríguez, B. (2011). A multiscale investigation of repolarization variability and its role in cardiac arrhythmogenesis. *Biophysical Journal*, 101(12):2892–902.
- Puglisi, J. L. and Bers, D. M. (2001). LabHEART: an interactive computer model of rabbit ventricular myocyte ion channels and Ca transport. *American Journal of Physiology - Cell Physiology*, 281(6):C2049–60.
- Puglisi, J. L., Wang, F., and Bers, D. M. (2004). Modeling the isolated cardiac myocyte. *Progress in Biophysics and Molecular Biology*, 85(2-3):163–78.
- Qian, Y.-W., Clusin, W. T., Lin, S.-F., Han, J., and Sung, R. J. (2001). Spatial Heterogeneity of Calcium Transient Alternans During the Early Phase of Myocardial Ischemia in the Blood-Perfused Rabbit Heart. *Circulation*, 104(17):2082–2087.
- Qu, Z., Garfinkel, A., Chen, P.-S., and Weiss, J. N. (2000). Mechanisms of Discordant Alternans and Induction of Reentry in Simulated Cardiac Tissue. *Circulation*, 102(14):1664–1670.

- Quinn, T. A., Granite, S., Allessie, M. A., Antzelevitch, C., Bollensdorff, C., Bub, G., Burton, R. A. B., Cerbai, E., Chen, P.-S., Delmar, M., DiFrancesco, D., Earm, Y. E., Efimov, I. R., Egger, M., Entcheva, E., Fink, M., Fischmeister, R., Franz, M. R., Garny, A., Giles, W. R., Hannes, T., Harding, S. E., Hunter, P. J., Iribé, G., Jalife, J., Johnson, C. R., Kass, R. S., Kodama, I., Koren, G., Lord, P., Markhasin, V. S., Matsuoka, S., McCulloch, A. D., Mirams, G. R., Morley, G. E., Nattel, S., Noble, D., Olesen, S. P., Panfilov, A. V., Trayanova, N. A., Ravens, U., Richard, S., Rosenbaum, D. S., Rudy, Y., Sachs, F., Sachse, F. B., Saint, D. A., Schotten, U., Solovyova, O., Taggart, P., Tung, L., Varró, A., Volders, P. G. A., Wang, K., Weiss, J. N., Wettwer, E., White, E., Wilders, R., Winslow, R. L., and Kohl, P. (2011). Minimum Information about a Cardiac Electrophysiology Experiment (MICEE): standardised reporting for model reproducibility, interoperability, and data sharing. *Progress in Biophysics and Molecular Biology*, 107(1):4–10.
- Quinn, T. A. and Kohl, P. (2013). Combining wet and dry research: experience with model development for cardiac mechano-electric structure-function studies. *Cardiovascular Research*, 97(4):601–II.
- Restrepo, J. G., Weiss, J. N., and Karma, A. (2008). Calsequestrin-mediated mechanism for cellular calcium transient alternans. *Biophysical Journal*, 95(8):3767–89.
- Riccio, M. L., Koller, M. L., and Gilmour, R. F. (1999). Electrical restitution and spatiotemporal organization during ventricular fibrillation. *Circulation Research*, 84(8):955–63.
- Roden, D. M. (1998). Taking the "idio" out of "idiosyncratic": predicting torsades de pointes. *Pacing and Clinical Electrophysiology : PACE*, 21(5):1029–34.
- Roden, D. M., Balser, J. R., George Jr., A. L., and Anderson, M. E. (2002). Cardiac ion channels. *Annual Review of Physiology*, 64:431–75.
- Rodríguez, B. and Ferrero, J. M. (2001a). Integrated mechanisms of K⁺ loss in myocardial ischemia: a simulation study. In *2001 Conference Proceedings of the 23rd Annual International Conference of the IEEE Engineering in Medicine and Biology Society*, volume 1, pages 48–51. IEEE.
- Rodríguez, B. and Ferrero, J. M. (2001b). Mechanistic investigation of the causes of cellular K⁺ loss during acute myocardial ischemia: a simulation study. In *Computers in Cardiology 2001. Vol.28 (Cat. No.01CH37287)*, pages 361–364. IEEE.
- Rodríguez, B., Ferrero, J. M., and Trénor, B. (2002). Mechanistic investigation of extracellular K⁺ accumulation during acute myocardial ischemia: a simulation study. *American Journal of Physiology - Heart and Circulatory Physiology*, 283(2):H490–500.
- Rodríguez, B., Tice, B. M., Eason, J. C., Aguel, F., and Trayanova, N. A. (2004). Cardiac vulnerability to electric shocks during phase 1A of acute global ischemia. *Heart Rhythm : the Official Journal of the Heart Rhythm Society*, 1(6):695–703.
- Rodríguez, B., Trayanova, N. A., and Noble, D. (2006). Modeling cardiac ischemia. *Annals of the New York Academy of Sciences*, 1080:395–414.
- Romero, L., Carbonell, B., Trénor, B., Rodríguez, B., Sáiz, J., and Ferrero, J. M. (2010). Human and rabbit inter-species comparison of ionic mechanisms of arrhythmic risk: A simulation study. In *Annual International Conference of the IEEE Engineering in Medicine and Biology Society*, volume 2010, pages 3253–6.
- Romero, L., Carbonell, B., Trénor, B., Rodríguez, B., Sáiz, J., and Ferrero, J. M. (2011). Systematic characterization of the ionic basis of rabbit cellular electrophysiology using two ventricular models. *Progress in Biophysics and Molecular Biology*, 107(1):60–73.
- Romero, L., Pueyo, E., Fink, M., and Rodríguez, B. (2009a). Impact of ionic current variability on human ventricular cellular electrophysiology. *American Journal of Physiology - Heart and Circulatory Physiology*, 297(4):H1436–45.

- Romero, L., Trénor, B., Alonso, J. M., Tobón, C., Sáiz, J., and Ferrero, J. M. (2009b). The relative role of refractoriness and source-sink relationship in reentry generation during simulated acute ischemia. *Annals of Biomedical Engineering*, 37(8):1560–71.
- Rosati, B. and McKinnon, D. (2004). Regulation of ion channel expression. *Circulation Research*, 94(7):874–83.
- Rudy, Y. and Silva, J. R. (2006). Computational biology in the study of cardiac ion channels and cell electrophysiology. *Quarterly Reviews of Biophysics*, 39(1):57–116.
- Saffitz, J. E., Kanter, H. L., Green, K. G., Tolley, T. K., and Beyer, E. C. (1994). Tissue-specific determinants of anisotropic conduction velocity in canine atrial and ventricular myocardium. *Circulation Research*, 74(6):1065–1070.
- Sanguinetti, M. C. and Jurkiewicz, N. K. (1990). Two components of cardiac delayed rectifier K⁺ current. Differential sensitivity to block by class III antiarrhythmic agents. *Journal of General Physiology*, 96(1):195–215.
- Sanguinetti, M. C. and Jurkiewicz, N. K. (1992). Role of external Ca²⁺ and K⁺ in gating of cardiac delayed rectifier K⁺ currents. *Pflügers Archiv: European Journal of Physiology*, 420(2):180–6.
- Sarkar, A. X., Christini, D. J., and Sobie, E. A. (2012). Exploiting mathematical models to illuminate electrophysiological variability between individuals. *The Journal of Physiology*, 212:2555–2567.
- Sarkar, A. X. and Sobie, E. A. (2010). Regression analysis for constraining free parameters in electrophysiological models of cardiac cells. *PLoS Computational Biology*, 6(9):e1000914.
- Sarkar, A. X. and Sobie, E. A. (2011). Quantification of repolarization reserve to understand interpatient variability in the response to proarrhythmic drugs: a computational analysis. *Heart Rhythm: the Official Journal of the Heart Rhythm Society*, 8(11):1749–55.
- Sato, D., Shiferaw, Y., Garfinkel, A., Weiss, J. N., Qu, Z., and Karma, A. (2006). Spatially discordant alternans in cardiac tissue: role of calcium cycling. *Circulation Research*, 99(5):520–7.
- Sato, D., Xie, L.-H., Nguyen, T. P., Weiss, J. N., and Qu, Z. (2010). Irregularly appearing early afterdepolarizations in cardiac myocytes: random fluctuations or dynamical chaos? *Biophysical Journal*, 99(3):765–73.
- Sato, D., Xie, L.-H., Sovari, A. A., Tran, D. X., Morita, N., Xie, F., Karagueuzian, H., Garfinkel, A., Weiss, J. N., and Qu, Z. (2009). Synchronization of chaotic early afterdepolarizations in the genesis of cardiac arrhythmias. *Proceedings of the National Academy of Sciences of the United States of America*, 106(9):2983–8.
- Schulz, D. J., Goaillard, J.-M., and Marder, E. (2006). Variable channel expression in identified single and electrically coupled neurons in different animals. *Nature Neuroscience*, 9(3):356–62.
- Serizawa, T., Momomura, S.-i., Kohmoto, O., Ohya, T., Sato, H., Takahashi, T., Mochizuki, T., Iizuka, M., and Sugimoto, T. (1987). Mechanisms of abnormal myocardial relaxation induced by ischemia: comparison of low flow ischemia and hypoxia in isolated rabbit heart. *Japanese Circulation Journal*, 51(1):90–7.
- Serizawa, T., Vogel, W. M., Apstein, C. S., and Grossman, W. (1981). Comparison of acute alterations in left ventricular relaxation and diastolic chamber stiffness induced by hypoxia and ischemia. Role of myocardial oxygen supply-demand imbalance. *The Journal of Clinical Investigation*, 68(1):91–102.
- Severi, S., Cavalcanti, S., Mancini, E., and Santoro, A. (2002). Effect of electrolyte and pH changes on the sinus node pacemaking in humans. *Journal of Electrocardiology*, 35(2):115–24.
- Shannon, T. R., Wang, F., Puglisi, J. L., Weber, C., and Bers, D. M. (2004). A mathematical treatment of integrated Ca dynamics within the ventricular myocyte. *Biophysical Journal*, 87(5):3351–71.

- Shannon, T. R., Wang, F., Puglisi, J. L., Weber, C., and Bers, D. M. (2012). Correction. *Biophysical Journal*, 102(8):1996–2001.
- Sharma, A. D., Saffitz, J. E., Lee, B. I., Sobel, B. E., and Corr, P. B. (1983). Alpha adrenergic-mediated accumulation of calcium in reperfused myocardium. *The Journal of Clinical Investigation*, 72(3):802–18.
- Shaw, R. M. and Rudy, Y. (1997a). Electrophysiologic effects of acute myocardial ischemia. A mechanistic investigation of action potential conduction and conduction failure. *Circulation Research*, 80(1):124–38.
- Shaw, R. M. and Rudy, Y. (1997b). Electrophysiologic effects of acute myocardial ischemia: a theoretical study of altered cell excitability and action potential duration. *Cardiovascular Research*, 35(2):256–72.
- Shaw, R. M. and Rudy, Y. (1997c). Ionic mechanisms of propagation in cardiac tissue. Roles of the sodium and L-type calcium currents during reduced excitability and decreased gap junction coupling. *Circulation Research*, 81(5):727–41.
- Shiferaw, Y., Sato, D., and Karma, A. (2005). Coupled dynamics of voltage and calcium in paced cardiac cells. *Physical Review E*, 71(2):021903.
- Shiferaw, Y., Watanabe, M. A., Garfinkel, A., Weiss, J. N., and Karma, A. (2003). Model of intracellular calcium cycling in ventricular myocytes. *Biophysical Journal*, 85(6):3666–86.
- Silva, J. R. and Rudy, Y. (2005). Subunit interaction determines IKs participation in cardiac repolarization and repolarization reserve. *Circulation*, 112(10):1384–91.
- Silverman, H. S., Ninomiya, M., Blank, P. S., Hano, O., Miyata, H., Spurgeon, H. A., Lakatta, E. G., and Stern, M. D. (1991). A cellular mechanism for impaired posthypoxic relaxation in isolated cardiac myocytes. Altered myofilament relaxation kinetics at reoxygenation. *Circulation Research*, 69(1):196–208.
- Sims, C., Reisenweber, S., Viswanathan, P. C., Choi, B.-R., Walker, W. H., and Salama, G. (2008). Sex, age, and regional differences in L-type calcium current are important determinants of arrhythmia phenotype in rabbit hearts with drug-induced long QT type 2. *Circulation Research*, 102(9):e86–100.
- Smaill, B. H., Zhao, J., and Trew, M. L. (2013). Three-Dimensional Impulse Propagation in Myocardium: Arrhythmogenic Mechanisms at the Tissue Level. *Circulation Research*, 112(5):834–848.
- Sobie, E. A. (2009). Parameter sensitivity analysis in electrophysiological models using multivariable regression. *Biophysical Journal*, 96(4):1264–74.
- Sobie, E. A. and Ramay, H. R. (2009). Excitation-contraction coupling gain in ventricular myocytes: insights from a parsimonious model. *The Journal of Physiology*, 587(Pt 6):1293–9.
- Sobie, E. A. and Sarkar, A. X. (2011). Regression methods for parameter sensitivity analysis: applications to cardiac arrhythmia mechanisms. In *Annual International Conference of the IEEE Engineering in Medicine and Biology Society*, volume 2011, pages 4657–60.
- Spach, M. S., Dolber, P. C., and Heidlage, J. F. (1988). Influence of the passive anisotropic properties on directional differences in propagation following modification of the sodium conductance in human atrial muscle. A model of reentry based on anisotropic discontinuous propagation. *Circulation Research*, 62(4):811–32.
- Spector, P. S., Curran, M. E., Zou, A., Keating, M. T., and Sanguinetti, M. C. (1996). Fast inactivation causes rectification of the IKr channel. *Journal of General Physiology*, 107(5):611–9.
- Sperelakis, N. and McConnell, K. (2002). Electric field interactions between closely abutting excitable cells. *IEEE Engineering in Medicine and Biology Magazine : The Quarterly Magazine of the Engineering in Medicine & Biology Society*, 21(1):77–89.

- Stern, M. D. (1992). Theory of excitation-contraction coupling in cardiac muscle. *Biophysical Journal*, 63(2):497–517.
- Sun, Y.-L., Hu, S.-J., Wang, L.-H., Hu, Y., and Zhou, J.-Y. (2005). Effect of beta-blockers on cardiac function and calcium handling protein in postinfarction heart failure rats. *Chest*, 128(3):1812–21.
- Sutton, P. M. I., Taggart, P., Ophof, T., Coronel, R., Trimlett, R., Pugsley, W., and Kallis, P. (2000). Repolarisation and refractoriness during early ischaemia in humans. *Heart (British Cardiac Society)*, 84(4):365–9.
- Syed, Z., Vigmond, E., Nattel, S., and Leon, L. J. (2005). Atrial cell action potential parameter fitting using genetic algorithms. *Medical & Biological Engineering & Computing*, 43(5):561–71.
- Szentandrassy, N., Banyasz, T., Biro, T., Szabo, G., Toth, B. I., Magyar, J., Lazar, J., Varró, A., Kovacs, L., and Nanasi, P. P. (2005). Apico-basal inhomogeneity in distribution of ion channels in canine and human ventricular myocardium. *Cardiovascular Research*, 65(4):851–60.
- Szigligeti, P., Pankucsi, C., Bányász, T., Varró, A., and Nánási, P. P. (1996). Action potential duration and force-frequency relationship in isolated rabbit, guinea pig and rat cardiac muscle. *Journal of Comparative Physiology. B, Biochemical, Systemic, and Environmental Physiology*, 166(2):150–5.
- Taggart, P., Sutton, P. M. I., Boyett, M. R., Lab, M., and Swanton, H. (1996). Human ventricular action potential duration during short and long cycles. Rapid modulation by ischemia. *Circulation*, 94(10):2526–34.
- Talukder, M. A. H., Zweier, J. L., and Periasamy, M. (2009). Targeting calcium transport in ischaemic heart disease. *Cardiovascular Research*, 84(3):345–52.
- Tani, M. and Neely, J. R. (1989). Role of intracellular Na⁺ in Ca²⁺ overload and depressed recovery of ventricular function of reperfused ischemic rat hearts. Possible involvement of H⁺-Na⁺ and Na⁺-Ca²⁺ exchange. *Circulation Research*, 65(4):1045–1056.
- Tanskanen, A. J., Greenstein, J. L., O'Rourke, B., and Winslow, R. L. (2005). The role of stochastic and modal gating of cardiac L-type Ca²⁺ channels on early after-depolarizations. *Biophysical Journal*, 88(1):85–95.
- Tasaki, I. and Hagiwara, S. (1957). Capacity of muscle fiber membrane. *American Journal of Physiology*, 188(3):423–9.
- Taylor, A. L., Goaillard, J.-M., and Marder, E. (2009). How multiple conductances determine electrophysiological properties in a multicompartment model. *Journal of Neuroscience*, 29(17):5573–86.
- Taylor, A. L., Hickey, T. J., Prinz, A. A., and Marder, E. (2006). Structure and visualization of high-dimensional conductance spaces. *Journal of Neurophysiology*, 96(2):891–905.
- Taylor, J. A. and Lipsitz, L. A. (1997). Heart rate variability standards. *Circulation*, 95(1):280–1.
- Temsah, R. M., Netticadan, T., Chapman, D., Takeda, S., Mochizuki, S., and Dhalla, N. S. (1999). Alterations in sarcoplasmic reticulum function and gene expression in ischemic-reperfused rat heart. *The American Journal of Physiology*, 277(2 Pt 2):H584–94.
- Terkildsen, J. R., Crampin, E. J., and Smith, N. P. (2007). The balance between inactivation and activation of the Na⁺-K⁺ pump underlies the triphasic accumulation of extracellular K⁺ during myocardial ischemia. *American Journal of Physiology - Heart and Circulatory Physiology*, 293(5):H3036–45.
- Terkildsen, J. R., Niederer, S. A., Crampin, E. J., Hunter, P. J., and Smith, N. P. (2008). Using Physiome standards to couple cellular functions for rat cardiac excitation-contraction. *Experimental Physiology*, 93(7):919–29.
- Tice, B. M., Rodríguez, B., Eason, J. C., and Trayanova, N. A. (2007). Mechanistic investigation into the arrhythmogenic role of transmural heterogeneities in regional ischaemia phase 1A. *Europace : European Pacing, Arrhythmias, and Cardiac Electrophysiology : Journal of the Working Groups*

- on Cardiac Pacing, Arrhythmias, and Cardiac Cellular Electrophysiology of the European Society of Cardiology, 9 Suppl 6:vi46–58.
- Toba, K., Katagiri, T., and Takeyama, Y. (1978). Studies of the cardiac sarcoplasmic reticulum in myocardial infarction. *Japanese Circulation Journal*, 42(4):447–53.
- Tobón, C., Ruiz, C., Rodríguez, J. F., Hornero, F., Ferrero, J. M., and Sáiz, J. (2010). Vulnerability for reentry in a three dimensional model of human atria: a simulation study. In *Annual International Conference of the IEEE Engineering in Medicine and Biology Society*, volume 2010, pages 224–7.
- Townsend, N., Wickramasinghe, K., Bhatnagar, P., Smolina, K., Nichols, M., Leal, J., Luengo-Fernandez, R., and Rayner, M. (2012). *Coronary Heart Disease Statistics 2012 Edition*. British Heart Foundation: London.
- Trayanova, N. A., Constantino, J., and Gurev, V. (2011). Electromechanical models of the ventricles. *American Journal of Physiology - Heart and Circulatory Physiology*, 301(2):H279–86.
- Trénor, B., Ferrero, J. M., Rodríguez, B., and Montilla, F. (2005). Effects of pinacidil on reentrant arrhythmias generated during acute regional ischemia: a simulation study. *Annals of Biomedical Engineering*, 33(7):897–906.
- Trénor, B., Romero, L., Ferrero, J. M., Sáiz, J., Moltó, G., and Alonso, J. M. (2007). Vulnerability to reentry in a regionally ischemic tissue: a simulation study. *Annals of Biomedical Engineering*, 35(10):1756–70.
- van Echteld, C. J. A., Kirkels, J. H., Eijgelshoven, M. H. J., van der Meer, P., and Ruigrok, T. J. C. (1991). Intracellular sodium during ischemia and calcium-free perfusion: a ^{23}Na NMR study. *Journal of Molecular and Cellular Cardiology*, 23(3):297–307.
- Vandenberg, J. I., Walker, B. D., and Campbell, T. J. (2001). HERG K⁺ channels: friend and foe. *Trends in Pharmacological Sciences*, 22(5):240–6.
- Varró, A. and Baczkó, I. (2011). Cardiac ventricular repolarization reserve: a principle for understanding drug-related proarrhythmic risk. *British Journal Of Pharmacology*, 164(1):14–36.
- Varró, A., Baláti, B., Iost, N., Takács, J., Virág, L., Lathrop, D. A., Csaba, L., Tálosi, L., and Papp, J. G. (2000). The role of the delayed rectifier component IKs in dog ventricular muscle and Purkinje fibre repolarization. *The Journal of Physiology*, 523 Pt 1(2000):67–81.
- Verkerk, A. O., Baartscheer, A., de Groot, J. R., Wilders, R., and Coronel, R. (2011). Etiology-dependency of ionic remodeling in cardiomyopathic rabbits. *International Journal of Cardiology*, 148(2):154–60.
- Verkerk, A. O., Wilders, R., Veldkamp, M. W., de Geringel, W., Kirkels, J. H., and Tan, H. L. (2005). Gender disparities in cardiac cellular electrophysiology and arrhythmia susceptibility in human failing ventricular myocytes. *International Heart Journal*, 46(6):1105–18.
- Virág, L., Acsai, K., Hála, O., Zaza, A., Bitay, M., Bogáts, G., Papp, J. G., and Varró, A. (2009). Self-augmentation of the lengthening of repolarization is related to the shape of the cardiac action potential: implications for reverse rate dependency. *British Journal Of Pharmacology*, 156(7):1076–84.
- Viswanathan, P. C. and Rudy, Y. (1999). Pause induced early afterdepolarizations in the long QT syndrome: a simulation study. *Cardiovascular Research*, 42(2):530–42.
- Viswanathan, P. C. and Rudy, Y. (2000). Cellular Arrhythmogenic Effects of Congenital and Acquired Long-QT Syndrome in the Heterogeneous Myocardium. *Circulation*, 101(10):1192–1198.
- Vogel, W. M., Apstein, C. S., Briggs, L. L., Gaasch, W. H., and Ahn, J. (1982). Acute alterations in left ventricular diastolic chamber stiffness. Role of the "erectile" effect of coronary arterial pressure and flow in normal and damaged hearts. *Circulation Research*, 51(4):465–78.

- Volders, P. G., Kulcsár, A., Vos, M. a., Sipido, K. R., Wellens, H. J., Lazzara, R., and Szabo, B. (1997). Similarities between early and delayed afterdepolarizations induced by isoproterenol in canine ventricular myocytes. *Cardiovascular research*, 34(2):348–59.
- Wagner, M. B., Namiki, T., Wilders, R., Joyner, R. W., Jongsma, H. J., Verheijck, E. E., Kumar, R., Golod, D. A., Goolsby, W. N., and van Ginneken, A. C. G. (1999). Electrical interactions among real cardiac cells and cell models in a linear strand. *American Journal of Physiology - Heart and Circulatory Physiology*, 276:H391–H400.
- Walmsley, J., Mirams, G. R., Bahoshy, M., Bollendorff, C., Rodríguez, B., and Burrage, K. (2010). Phenomenological modeling of cell-to-cell and beat-to-beat variability in isolated Guinea Pig ventricular myocytes. In *Annual International Conference of the IEEE Engineering in Medicine and Biology Society*, volume 2010, pages 1457–60.
- Walmsley, J., Rodríguez, J. F., Mirams, G. R., Burrage, K., Efimov, I. R., and Rodríguez, B. (2013). mRNA Expression Levels in Failing Human Hearts Predict Cellular Electrophysiological Remodeling: A Population-Based Simulation Study. *PloS One*, 8(2):e56359.
- Walton, M. K. and Fozzard, H. A. (1983). The conducted action potential. Models and comparison to experiments. *Biophysical Journal*, 44(1):9–26.
- Wang, C., Liu, N., Luan, R., Li, Y., Wang, D., Zou, W., Xing, Y., Tao, L., Cao, F., and Wang, H. (2013). Apelin protects sarcoplasmic reticulum function and cardiac performance in ischaemia-reperfusion by attenuating oxidation of sarcoplasmic reticulum Ca²⁺-ATPase and ryanodine receptor. *Cardiovascular Research*.
- Watanabe, M. A., Fenton, F. H., Evans, S. J., Hastings, H. M., and Karma, A. (2001). Mechanisms for discordant alternans. *Journal of Cardiovascular Electrophysiology*, 12(2):196–206.
- Weiss, J. N., Karma, A., Shiferaw, Y., Chen, P.-S., Garfinkel, A., and Qu, Z. (2006). From pulsus to pulseless: the saga of cardiac alternans. *Circulation Research*, 98(10):1244–53.
- Weiss, J. N. and Shine, K. I. (1982). [K+]o accumulation and electrophysiological alterations during early myocardial ischemia. *American Journal of Physiology*, 243(2):H318–27.
- Weiss, J. N., Venkatesh, N., and Lamp, S. T. (1992). ATP-sensitive K+ channels and cellular K+ loss in hypoxic and ischaemic mammalian ventricle. *The Journal of Physiology*, 447:649–673.
- Wilde, A. A. M., Peters, R. J. G., and Janse, M. J. (1988). Catecholamine release and potassium accumulation in the isolated globally ischemic rabbit heart. *Journal of Molecular and Cellular Cardiology*, 20(10):887–96.
- Wu, L., Guo, D., Li, H., Hackett, J., Yan, G.-X., Jiao, Z., Antzelevitch, C., Shryock, J. C., and Belardinelli, L. (2008a). Role of late sodium current in modulating the proarrhythmic and antiarrhythmic effects of quinidine. *Heart rhythm : the official journal of the Heart Rhythm Society*, 5(12):1726–34.
- Wu, L., Ma, J., Li, H., Wang, C., Grandi, E., Zhang, P., Luo, A., Bers, D. M., Shryock, J. C., and Belardinelli, L. (2011). Late sodium current contributes to the reverse rate-dependent effect of IKr inhibition on ventricular repolarization. *Circulation*, 123(16):1713–20.
- Wu, L., Rajamani, S., Shryock, J. C., Li, H., Ruskin, J., Antzelevitch, C., and Belardinelli, L. (2008b). Augmentation of late sodium current unmasks the proarrhythmic effects of amiodarone. *Cardiovascular Research*, 77(3):481–8.
- Wu, L., Shryock, J. C., Song, Y., and Belardinelli, L. (2006). An increase in late sodium current potentiates the proarrhythmic activities of low-risk QT-prolonging drugs in female rabbit hearts. *The Journal of Pharmacology and Experimental Therapeutics*, 316(2):718–26.
- Xiao, L., Xiao, J., Luo, X., Lin, H., Wang, Z., and Nattel, S. (2008). Feedback remodeling of cardiac potassium current expression: a novel potential mechanism for control of repolarization reserve. *Circulation*, 118(10):983–92.

- Xie, Y., Hu, G., Sato, D., Weiss, J. N., Garfinkel, A., and Qu, Z. (2007). Dispersion of refractoriness and induction of reentry due to chaos synchronization in a model of cardiac tissue. *Physical Review Letters*, 99(11):118101.
- Xu, A., Hawkins, C., and Narayanan, N. (1993). Phosphorylation and activation of the Ca(2+)-pumping ATPase of cardiac sarcoplasmic reticulum by Ca²⁺/calmodulin-dependent protein kinase. *The Journal of Biological Chemistry*, 268(12):8394–7.
- Xu, K. Y., Zweier, J. L., and Becker, L. C. (1997). Hydroxyl radical inhibits sarcoplasmic reticulum Ca(2+)-ATPase function by direct attack on the ATP binding site. *Circulation Research*, 80(1):76–81.
- Yamazaki, M., Honjo, H., Ashihara, T., Harada, M., Sakuma, I., Nakazawa, K., Trayanova, N., Horie, M., Kalifa, J., Jalife, J., Kamiya, K., and Kodama, I. (2012). Regional cooling facilitates termination of spiral-wave reentry through unpinning of rotors in rabbit hearts. *Heart rhythm : the official journal of the Heart Rhythm Society*, 9(1):107–14.
- Yan, G.-X. and Antzelevitch, C. (1998). Cellular Basis for the Normal T Wave and the Electrocardiographic Manifestations of the Long-QT Syndrome. *Circulation*, 98(18):1928–1936.
- Yan, G.-X., Rials, S. J., Wu, Y., Liu, T., Xu, X., Marinchak, R. A., and Kowey, P. R. (2001). Ventricular hypertrophy amplifies transmural repolarization dispersion and induces early afterdepolarization. *American Journal of Physiology - Heart and Circulatory Physiology*, 281:H1968–H1975.
- Yang, P.-C. and Clancy, C. E. (2012). In silico Prediction of Sex-Based Differences in Human Susceptibility to Cardiac Ventricular Tachyarrhythmias. *Frontiers in Physiology*, 3(September):360.
- Yang, T., Snyders, D. J., and Roden, D. M. (1997). Rapid inactivation determines the rectification and [K+]o dependence of the rapid component of the delayed rectifier K+ current in cardiac cells. *Circulation Research*, 80(6):782–9.
- Zabel, M., Hohnloser, S. H., Behrens, S., Woosley, R. L., and Franz, M. R. (1997a). Differential effects of D-sotalol, quinidine, and amiodarone on dispersion of ventricular repolarization in the isolated rabbit heart. *Journal of Cardiovascular Electrophysiology*, 8(11):1239–45.
- Zabel, M., Woosley, R. L., and Franz, M. R. (1997b). Is dispersion of ventricular repolarization rate dependent? *Pacing and Clinical Electrophysiology : PACE*, 20(10 Pt 1):2405–11.
- Zaniboni, M., Pollard, A. E., Yang, L., and Spitzer, K. W. (2000). Beat-to-beat repolarization variability in ventricular myocytes and its suppression by electrical coupling. *American Journal of Physiology - Heart and Circulatory Physiology*, 278(3):H677–87.
- Zeng, J., Laurita, K. R., Rosenbaum, D. S., and Rudy, Y. (1995). Two Components of the Delayed Rectifier K+ Current in Ventricular Myocytes of the Guinea Pig Type : Theoretical Formulation and Their Role in Repolarization. *Circulation Research*, 77(1):140–152.
- Zhang, H., Wang, J., Yang, L., Wu, R.-J., Mei, X., and Zhao, W. (2011). Vulnerability in simulated ischemic ventricular transmural tissues. *Chinese Journal of Physiology*, 54(6):427–34.
- Zhao, M., Franzen, D., and Eng, C. (1988). The effect of coronary arterial pressure on myocardial distensibility. Absence of a "garden hose" effect during in-vivo conditions. *Basic Research in Cardiology*, 83(6):626–33.
- Zweier, J. L. (1988). Measurement of superoxide-derived free radicals in the reperfused heart. Evidence for a free radical mechanism of reperfusion injury. *The Journal of Biological Chemistry*, 263(3):1353–7.